Exploring the Mutagenic Consequences of Inflammation and DNA Damage

by

Jennifer Elizabeth Kay

B.S., University of Pittsburgh (2011)

Submitted to the Department of Biological Engineering
in partial fulfillment of the requirements for the degree of

Doctor of Philosophy

at the

MASSACHUSETTS INSTITUTE OF TECHNOLOGY

February 2018

Author . . . . . Signature redacted

Department of Biological Engineering
November 20, 2017

Certified by. . . . . Signature redacted

Bevin P. Engelward
Professor of Biological Engineering
Thesis Supervisor

Accepted by . . . . . Signature redacted

Mark Bathe
Chair, Biological Engineering Graduate Program

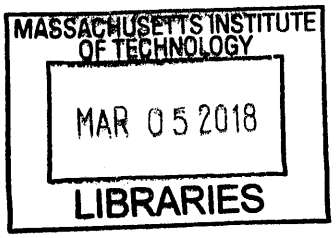

ARCHIVES

This doctoral thesis has been examined by a committee of the Department of Biological Engineering as follows:

Signature redacted

Professor John M. Essigmann

Committee Chair

Professor Bevin P. Engelward

Thesis Supervisor

Signature redacted

Doctor Susan E. Erdman

Thesis Co-Advisor

Professor Leona D. Samson

Dedicated to my pillars of support:

My parents Peg and Jeff Kay

And my wife Kate Bock

You mean everything to me

Preface

The introduction of this thesis is in preparation for submission to *Nature Reviews Cancer*. Experiments using *Apc*$^{Min/+}$ animals discussed in Chapters 2 and 3 are being drafted as manuscripts for submission. We are in the process of designing experiments to elaborate further on observations in *Rag2*$^{-/-}$ pancreas recombination described in Chapter 2 as well as in AagTg recombination described in Chapter 4.

The work presented in this thesis is the product of the author with contributions from many Engelward and Erdman laboratory members and collaborators. Dr. Michelle Sukup-Jackson trained the author on animal husbandry, animal necropsy, RaDR imaging techniques, and flow cytometry. Dr. Sukup-Jackson also assisted with experiment design, execution, and analysis of experiments of *H. hepaticus* infection in *RaDR*;*Rag2*$^{-/-}$ mice. Kunal Tangri, an undergraduate student, assisted in preparation of *RaDR*;*AagTg* tissue samples for flow cytometry. Dr. Takafumi Kimoto, a visiting research scientist from Teijin Pharmaceuticals Ltd., collaborated with the author on RaDR analysis techniques.

The MATLAB-based RaDR foci counting programs were written by Dr. Dushan Wadduwage of Prof. Peter T. So's laboratory. A manuscript detailing the design and efficacy of this program is currently being revised for resubmission to *Scientific Reports*.

Many members of the Division of Comparative Medicine were essential to the work described here. Dr. Susan Erdman co-advised this thesis, and Erdman laboratory members Sheyla Mirabal and Bernard Varian were instrumental in training the author animal handling and necropsy techniques. Dr. Erdman also enabled our collaboration with pathologist Dr. Theofilis Poutahidis of Aristotle University of Thessaloniki.

Profs. John Essigmann and Leona Samson donated their time and expertise as well as laboratory capital. Drs. Supawadee "Apple" Chawanthayatham and Robert Croy of the Essigmann lab trained the author on the Gpt-Δ assay. Prof. Samson donated the AagTg animals used in Chapter 4, and Samson laboratory members Joshua Corrigan and Dr. Jennifer Calvo assisted in genotyping.

We thank the following core facilities for training, guidance and use: Division of Comparative Facilities and Medicine Animal Resource Program; Committee on Animal Care; Center for Environmental Health Sciences Imaging Core; Koch Institute Flow Cytometry; BioMicro Center.

This work was supported by the NIH/NIGMS Interdepartmental Biotechnology Training Program (5 T32 GM008334) MIT Center for Environmental Health Sciences (NIEHS Grant P30-ES002109) and MIT Nitric Oxide Program Project Grant (National Cancer Institute Grant #P01-CA026731)

Acknowledgements

So many wonderful people have contributed time, energy, thought, and effort to the work described here. I would like to begin by thanking Prof. Bevin Engelward for taking me on as a graduate student and guiding me through the past six years. Bevin has instilled in me, as with all her students, a deep appreciation of careful work, detailed records, critical thought, and creative yet logical reasoning. The projects we undertook in this thesis hugely expanded my abilities to design, execute, and interpret experiments, and after many unexpected results, I have learned to take disproven hypotheses in stride, and to focus on what can be learned rather than fixate on what was anticipated originally. I also want to thank Dr. Susan Erdman for coadvising me throughout this thesis, especially for teaching me best practices in conducting animal research and hands-on guidance through many experiments. Professors John Essigmann and Leona Samson were also instrumental to my success, providing excellent insight and suggestions for my research as well as exposing me to a number of career possibilities.

In addition to the professors who facilitated this doctorate, I was fortunate to share workspaces with incredibly intelligent and kind colleagues. I thank our wonderful administrator Kathy Reposa for being a sweetheart, going out of her way to make our days run smoothly, and providing a steady source of midday sugar. I am grateful to all the members of the Engelward lab, especially Marcus Parrish (my dear lab husband), Lizzie Ngo, Ian Tay, Christy Chao, Joshua Corrigan, and Jing Ge, for making the 7th floor a fun place to work. Thanks to Apple Chawanthayatham for her patience in training me and sharing bench space for the Gpt assay. I also want to thank Sheyla Mirabal, BJ Varian, and Ning Thongararm for welcoming me to their lab spaces and later becoming dear friends.

I feel incredibly fortunate to have completed my Ph.D. in MIT's BE department, where I have been surrounded by brilliant minds of all types. The BE students, professors, administrators and support staff make this department the best on campus – our science is great because our people are great, and I'm lucky to count many of you as friends as well as colleagues.

Finally, I want to thank my numerous sources of personal support through this doctorate and the grand challenge of life. Thanks to my wonderful parents, Peg and Jeff, for raising me to ask questions and think critically, to care more about the impact of one's work than the compensation, and to work hard for the greatest good. Thanks to my almost-wife, Kate, for her optimism and faith in me, keeping me grounded when I felt lost, and making me laugh even through tears. Thanks to my sister, Meghan, and my best friends Barbara Fang and Seb Eastham, for your impeccably-suited-to-mine senses of humor and unconditional love. Thanks to my therapist Lynn Bratman for helping me through some of the particularly painful periods of this doctorate. Mom, Dad, Meghan, Kate, Barb and Seb, thank you so very much for caring, believing in me, and supporting me though all this. I mean it literally when I say I could not have gotten here without you. I love you.

Exploring the Mutagenic Consequences of Inflammation and DNA Damage

by

Jennifer Elizabeth Kay

Submitted to the Department of Biological Engineering
On November 20, 2017, in partial fulfillment of the
Requirements for the degree of
Doctor of Philosophy

Abstract

Inflammation is a major risk factor for many types of cancer, and the physiological processes involved in inflammation can contribute to many aspects of cancer development. Inflammation entails reprogramming of cell behaviors that resemble cancer, such as increased proliferation and signals for survival and migration, and it also entails production of reactive chemical species, which can damage DNA to promote genetic instability, another hallmark of cancer. While much research has been dedicated to studying the relationships between inflammation and cancer, it has been difficult to distinguish the relative contributions of modified cell behavior and *de novo* mutagenesis to the development of cancer. Furthermore, few studies have addressed the role(s) inflammation plays in cancer initiation versus promotion. Here, we utilized a transgenic mouse for detecting mutations in a variety of models of inflammation to parse the mechanisms by which inflammation contributes to mutations and cancer.

The RaDR mouse, developed in the Engelward lab, contains a ubiquitously expressed transgene that enables detection of sequence rearrangement mutations following aberrant homologous recombination (HR). These mice also contain the Gpt-Δ transgene for detecting point mutations and deletions, enabling unprecedented breadth and depth of possible mutation analyses in a single tissue. Our studies began by querying whether elements that regulate inflammation protect against mutagenesis in RaDR animals. We then studied RaDR mutagenesis in several models of intestinal inflammation and cancer. Together, these experiments showed that inflammation does not significantly induce *de novo* sequence rearrangement mutations, but it greatly increases the overall burden of mutant cells in a tissue as a result of heightened proliferation and clonal expansion.

We also used the RaDR mouse model to expand upon studies of DNA repair pathway balance. DNA damage is addressed by a network of pathways, each designed to identify and repair specific types of lesions. One of the most important repair pathways for DNA damage caused by inflammation is the Base Excision Repair (BER) pathway, and we have previously found that BER intermediates can increase the frequency of mutagenic HR. Here, we expand upon that

information, showing that acceleration of the BER pathway by increased expression of an initiating enzyme does not increase sequence rearrangement mutations, provided the downstream pathway can be resolved efficiently.

Together, the studies described herein demonstrate that inflammation is unlikely to initiate cancer via sequence rearrangement mutations, but inflammation is a strong promoter of cancer in part through increased clonal expansion of mutant cells.

Thesis Supervisor: Bevin P. Engelward
Title: Professor of Biological Engineering

Contents

List of Figures

List of Tables

List of Abbreviations

5ClC	5-chlorocytosine
5'-dRP	5'-deoxyribophosphate
6TG	6-thioguanine
8oxoG	8-oxoguanine
A	Adenine
AAG	Alkyladenine glycosylase
ALKBH2	AlkB homolog 2
ALKBH3	AlkB homolog 3
AOM	Azoxymethane
AP	Apurinic/Apyrimidinic Site
Apc	Adenomatous polyposis coli
APE1	AP endonuclease 1
ARE	Antioxidant response element
ATM	Ataxia telangiectasia mutated
ATR	Ataxia telangiectasia Rad3-related protein
BER	Base Excision Repair
bp	Base pairs
C	Cytosine
Ca	Cyanuric acid
COX2	Cyclooxygenase-2
DDR	DNA damage response
DNA	Deoxyribonucleic acid
DNA-PK	DNA protein kinase
DNA-PKcs	DNA-PK catalytic subunit
DR	Direct reversal
DSB	Double strand break
DSS	Dextran sodium sulfate
E. coli	*Escherichia coli*
EGFP	Enhanced green fluorescent protein

ER	Endoplasmic reticulum
EXO1	Exonuclease 1
FapyG	2,6-diamino-4-hydroxy-5-formamidopyrimidine
FAP	Familial adenomatous polyposis
Fe^{2+}	Iron II
FEN1	Flap endonuclease 1
FYDR	Fluorescent yellow direct repeat
G	Guanine
GADD34	Growth arrest and DNA damage-inducible protein 34
Gh	Guanidinohydantoin
Gpt	Glutamic-pyruvic transaminase
GSH	Glutathione
GSNO	S-nitrosoglutathione
GSNOR	S-nitrosoglutathione reductase
GST	Glutathione *S*-transferase
H. hepaticus	*Helicobacter hepaticus*
H. pylori	*Helicobacter pylori*
H&E	Hematoxylin & Eosin
H_2O_2	Hydrogen peroxide
HA	Hemagglutinin
HNE	Hydroxynonenal
HOCl	Hypochlorous acid
HOBr	Hypobromous acid
HR	Homologous recombination
Hx	Hypoxanthine
IBD	Inflammatory bowel disease
dI	Inosine
IFNγ	Interferon γ
IL1β	Interleukin 1β
IL10	Interleukin 10
iNOS	Inducible nitric oxide synthase

KEAP1	Kelch like ECH associated protein 1
LPO	Lipid peroxidation
MBD4	Methyl-Cpg-binding domain protein 4
MDA	Malondialdehyde
MGMT	O^6-methylguanine methyltransferase
MMR	Mismatch repair
MMS	Methylmethane sulfonate
MRN	MRE11/RAD50/NBS1
NAD^+	Nicotinamide adenine dinucleotide
NEIL1	Nei-like DNA glycosylase 1
NEIL2	Nei-like DNA glycosylase 2
NER	Nucleotide excision repair
NFκB	Nuclear factor κB
NHEJ	Non-homologous end joining
NO	Nitric oxide
$NO_2^{\bullet}$	Nitrogen dioxide radical
N_2O_3	Nitrous anhydride
NOS	Nitric oxide synthase
NQO1	NADPH quinone oxidoreductase 1
NRF2	Nuclear factor erythroid 2-related factor 2
NT	Non-treated
NTHL1	Nth like DNA glycosylase 1
Oa	Oxaluric acid
$O^{\bullet}{}_2^-$	Superoxide radical
$^{\bullet}OH$	Hydroxyl radical
O^6MeG	O^6-methylguanine
OGG1	8-oxo-guanine glycosylase
$ONOO^-$	Peroxynitrite
$ONOOCO_2^-$	Nitrosoperoxycarbonate
Oz	Oxazolone
PARP1	Poly-ADP ribose polymerase 1

PBS	Phosphate buffered saline
PCNA	Proliferating cell nuclear antigen
PNKP	Polynucleotide kinase phosphatase
POLβ	Polymerase Beta
RaDR	Rosa26 direct repeat
Rag2	Recombination activating gene 2
RONS	Reactive oxygen and nitrogen species
RPA	Replication protein A
SDSA	Synthesis-dependent strand annealing
SMUG1	Sing-strand-selective monofunctional uracil DNA glycosylase 1
SOD	Superoxide dismutase
Sp	Spiroiminodihydantoin
SSB	Single strand break
T	Thymine
TDG	Thymine DNA glycosylase
TLS	Translesion synthesis
TNF	Tumor necrosis factor
U	Uracil
UNG	Uracil DNA glycosylase
WT	Wild type
X	Xanthine
γH2AX	Phosphorylated Serine-139 on Histone H2AX
εA	Ethenoadenine
εC	Ethenocytosine
εG	Ethenoguanine

Chapter 1

Introduction

As early as 1863, Virchow recognized the inextricable connections between the immune system and cancer development. Virchow's prediction that cancer arises at sites of "lymphoreticular infiltrate" has been confirmed many times over, as pancreatitis, hepatitis, colitis, and other chronic inflammatory diseases are now known to be major risk factors for cancer in those tissues [1-6]. In fact, chronic inflammation is often necessary for tumor development [1, 7-9]. The inflammatory environment promotes cellular proliferation and survival, degradation and remodeling of the extracellular matrix, and weakening of vascular barriers to facilitate immune cell migration, all of which enable cancer growth [10, 11]. Inflammation is so pro-tumorigenic that tumors can even generate their own inflammatory microenvironment to facilitate growth [7, 12]. Accordingly, mitigating inflammation is often an effective strategy for slowing or even preventing neoplasia [3, 13, 14]. There are many excellent reviews on a wide range of connections between inflammation and cancer [7, 10, 12, 15]. Here, we will focus on how inflammation and DNA damage contribute to each other as well as to the development of cancer.

Many departures from normal behavior that cancer cells exhibit, such as unchecked proliferation and aberrant migration, can be traced to mutations in DNA that accumulate over time. Mutations generally arise from damaged DNA, and inflammation can cause a great deal of DNA damage. A central component of inflammation is the production of reactive chemicals designed to destroy pathogens, and while these chemicals are essential for protecting the body from infection, they can damage host biomolecules as well, including DNA. Efficient repair of

DNA damage is crucial to prevent mutations in the genetic code. As such, several DNA repair mechanisms have evolved to address the many types of DNA damage. However, DNA repair can be fallible or unable to handle excessive damage, allowing mutations to occur. Since cancer develops from accumulated mutations, it logically follows that DNA damage from inflammation contributes to cancer development by increasing mutagenesis.

It is broadly appreciated that genomic instability is a hallmark of cancer [16-19]. The human haploid genome contains $3.2x10^9$ base pairs, and the spontaneous rate of mutation in normal human cells is estimated to be on the order of $1\text{-}10x10^{-10}$ nucleotides/cell/division [20-22]. Several driver mutations are required within the same cell lineage for it to become malignant, and although the number of necessary mutations has not been defined and likely depends on the type of cancer, the minimum number is around three [23, 24]. The there are approximately $3x10^{13}$ cells in the human body, and the average human lifespan comprises 10^{16} cell divisions (BNIDs 100379, 108562)[25]. According to Loeb, the probability of any one cell acquiring three mutations is approximated by ($1x10^{-10}$ spontaneous mutations/cell/division)^3(10^{16} cell divisions/lifetime) = 10^{-14} potential cancer cells/lifetime [21]. In other words, the prevalence of cancer in the population should be less than one in a trillion people, whereas the actual lifetime probability of developing cancer is ~38.5% [26]. Furthermore, tumor cells contain dozens, sometimes thousands, of mutations. Thus, it is clear that factors such as genetics, environmental exposures, and physiology are required to increase mutation frequency beyond the normal rate to promote cancer, a quality known as a mutator phenotype [21].

Inflammation and genomic instability have a complex relationship (a highly simplified roadmap is shown in Figure 1-1, which will become more detailed throughout this review). Inflammation contributes to mutagenesis through production of reactive oxygen and nitrogen

species (RONS) that can damage DNA, but DNA damage can also exacerbate inflammation. This positive feedback loop is carefully regulated by a network of DNA repair pathways, transcription factors, and cellular signals. Due to the intricacies linking inflammation, DNA damage, and DNA repair, these processes can easily become dysregulated and lead to cancer.

1.1 Inflammation Leads to DNA Damage

The majority of inflammation-induced DNA damage is caused by reactive oxygen and nitrogen species (RONS), which are evolved by immune cells to destroy pathogens, but which can also damage self-biomolecules. One pleiotropic RONS chemical is nitric oxide (NO), which is an essential signaling molecule with functions in the cardiovascular, nervous and immune systems [27, 28]. For most of these processes, the concentration of NO is below 400 nM [29]. During inflammation, however, innate immune cells produce NO at high levels (approaching μM [30, 31]), as well as superoxide and numerous enzymes, leading to a cascade of chemical reactions that produce a range of RONS (Fig 1-2). These reactive species include radicals (e.g., superoxide $O^{\bullet}{}_2^-$, hydroxyl $^{\bullet}OH$, and nitrogen dioxide $NO_2^{\bullet}$), anions (e.g., peroxynitrite $ONOO^-$, and nitrosoperoxycarbonate $ONOOCO_2^-$), anhydrides (e.g., nitrous anhydride N_2O_3), hypohalous acids (e.g., hypochlorous acid HOCl and hypobromous acid HOBr) and hydrogen peroxide (H_2O_2). In addition to the RONS produced by immune cells, pro-inflammatory cytokines can stimulate intracellular RONS production [32-34]. For excellent reviews on RONS and their chemistry, please see [35, 36].

To understand the mutagenic consequences of inflammation, one must first recognize the chemical modifications to DNA and the mechanisms for repair of those lesions. We begin with a

discussion of the DNA damage produced from RONS, including nucleobase oxidation, deamination, halogenation, and alkylation, as well as strand breaks of the phosphodiester backbone. Subsequent sections will review the major repair pathways for these types of damage; the mechanisms that balance DNA damage, DNA repair, and inflammation; and the implications for carcinogenesis.

1.1.1 Oxidation

Many RONS are potent oxidizing agents and can create several kinds of damage to DNA. While there are many potential products of DNA oxidation [37], guanine is the most easily oxidized DNA base [36] and is therefore the primary target for reaction with nucleophilic RONS and the focus of this section. Primary oxidation of guanine by RONS produces 8-oxo-guanine (8oxoG, which is mutagenic) and 8-nitro-guanine (which is unstable and quickly becomes an abasic site) (Fig 1-3). 8oxoG in the normal *anti* conformation pairs with cytosine, but rotation of the glycosidic bond to the *syn* position allows pairing with adenine (Fig 1-3) [38]; thus, 8oxoG can lead to G→T transversions [38-40]. The potential for 8oxoG to cause this mutation depends on the polymerase that encounters it, as will be described in later sections [40-42].

8oxoG is ~1000 times more prone to oxidation than its parent guanine, leading to production of several more stable and mutagenic secondary products. These include spiroiminodihydantoin (Sp), guanidinohydantoin (Gh), oxazolone (Oz), oxaluric acid (Oa), and cyanuric acid (Ca) (see Fig 1-3 for examples). Oz, Oa and Ca have been shown to produce G→T transversions with much higher potency than the parent 8oxoG [43]. Gh primarily leads to G→C mutations, and Sp causes both G→T and G→C mutations, both with frequencies at least an order of magnitude higher than that of 8oxoG [44]. While Gh is relatively easily bypassed (albeit

mutagenically), Sp blocks replication [44] and leads to strand slippage, producing broken replication forks and single base pair deletions in addition to transversions [45, 46]. Until recently, mutagenicity of the secondary oxidation products of 8oxoG had been demonstrated almost exclusively in *E. coli* [43, 44, 47, 48], but studies with mammalian systems in the past decade have yielded similar results [46, 48, 49], suggesting shared mechanisms between species.

In addition to secondary oxidation, 8oxoG can be reduced, opening the imidazole ring to form a 2,6-diamino-4-hydroxy-5-formamidopyrimidine (FapyG). FapyG produces G→T transversions in mammalian cells [50], and some studies suggest it may be more mutagenic than the parent 8oxoG [51].

1.1.2. Deamination

In addition to oxidation, nitrosative RONS can deaminate DNA bases. Deamination products are particularly mutagenic because the chemistry occurs on the functional groups that determine hydrogen bonding, altering the pattern of H-bond donors and acceptors and leading to base mispairing. The chemical primarily responsible for base deamination is thought to be nitrous anhydride [35], generating the products from canonical bases shown in Figure 1-4 (note that Hx is dI in DNA). Indeed, *in vitro* exposure of DNA to nitrosative RONS produces high amounts of X, Hx and U lesions [52, 53].

Deamination of cytosine or its methylated form 5meC changes the base into uracil or thymine, respectively, causing C→T transitions. Recently it has been shown that deamination of adenine to produce hypoxanthine (Hx) can cause either A→G transitions or deletions, depending on the cell type and whether the lesion is on the leading or lagging strand [54]. Finally, guanine deamination to xanthine (X) primarily causes G→A transitions [53], possibly by tautomerization

of X to an enol form that can pair with T. Nitrosative deamination of G or A at the N^7 position can also cause depurination to form an abasic site [55].

Interestingly, while U, Hx and X occur in at high levels in *in vitro* studies [52], these deamination products are rarely observed in cells stimulated with physiological levels of RONS [55]. One possibility for the low cellular levels of these lesions is that repair is very rapid, which is consistent with evolutionary selection for efficient repair of highly mutagenic lesions. Overall, while the chemistry of inflammation probably produces a great deal of deamination, these lesions are rarely observed *in vivo,* possibly due to rapid repair to counterbalance their potent mutagenicity.

1.1.3. Halogenation

Inflammatory chemicals are not limited to oxygen and nitrogen species. Neutrophils secrete the enzyme myeloperoxidase to produce hypochlorous acid (HOCl) [56-58], and eosinophils secrete eosinophil peroxidase to produce hypobromous acid (HOBr) [59, 60] (Fig 1-2). These hypohalous acids readily react with DNA to form the adducts shown in Figure 1-5. Interestingly, the most abundant halogenated nucleobase, 5-chlorocytosine (5ClC) [61, 62], accumulates to a greater degree than oxidative, deamination or LPO (described below) DNA lesions [48, 63]. Due to its significant and persistent accumulation, perhaps a result of inefficient repair, 5ClC has been designated a biomarker for chronic inflammation [48, 63, 64].

The mutagenicity of halogenated DNA has only recently been demonstrated. Halogenation had previously been shown to impact epigenetic modifications [65], but now 5ClC has been shown to cause C→T transitions [64]. These mutations are frequently observed in

tissues under inflammatory stress as well as in inflammation-associated cancers [63, 64, 66], further supporting the designation of 5ClC as a pertinent biomarker for inflammation.

1.1.4. Lipid Peroxidation-Derived Adducts

Oxidative stress can directly damage DNA, as described above, but it can also cause indirect damage by creating reactive species from other biomolecules. Specifically, when RONS encounter polyunsaturated fatty acids, they cause lipid peroxidation (LPO) to generate electrophilic, DNA-reactive aldehyde species. The best-studied of these aldehyde species are 4-hydroxy-2-nonenal (HNE), malondialdehyde (MDA), acrolein, and crotonaldehyde [67], of which HNE and MDA have been directly implicated in carcinogenesis [68]. The resulting LPO-induced DNA adducts are exocyclic additions of two (ε, etheno-) or three (P, propano-) carbons onto a base [67, 69, 70]. Examples of etheno adducts are shown in Figure 1-6. Many studies have demonstrated significant accumulation of etheno adducts as a result of inflammation [48, 69, 71-73].

The most abundant etheno adduct found in DNA is N^2,3-εG [74, 75]. N^2,3-εG is a potent inducer of G→A transitions, and its isomer 1,N^2-εG causes G→T and G→C transversions [74, 76, 77]. 1,N^6-εA causes primarily A→G and A→T mutations [78, 79], and 3,N^4-εC potently induces C→A and C→T mutations [70, 80]. All etheno lesions can block replication to some extent [74, 77, 80], which can lead to larger-scale mutations (discussed below).

1.1.5. Single Strand Breaks (SSBs)

While lesions on nucleobases are an important source of mutations, breakage of the DNA backbone is a far greater threat to genomic integrity. Strand breaks potentiate large-scale

mutations, such as deletions, insertions, and translocations, and they can also cause stress signaling, cell cycle arrest, and cytotoxicity if not efficiently repaired [81-85]. During inflammation, single strand breaks (SSBs) can arise from direct reaction with RONS: for example, radicals can hydrolyze the phosphodiester backbone, and peroxynitrite produces single strand breaks and abasic sites [86]. SSBs also occur naturally as intermediates of some DNA repair pathways.

1.1.6. Double Strand Breaks (DSBs)

Double strand breaks (DSBs) also arise from a variety of sources. Some enzymes, such as endonucleases and topoisomerases, cut the backbone to produce DSBs [87, 88]. SSBs can also potentiate DSBs: for example, two nearby opposed SSBs may reduce the structural integrity of the DNA duplex, and the strand will break apart (Fig 1-7A). Additionally, if a polymerase encounters a SSB during replication, the replication machinery cannot synthesize past the gap, and the replication fork collapses, leaving a one-ended DSB (Fig 1-7B). Similarly, replication-blocking lesions such as εA, εC, and Sp can cause DSBs, possibly because the stress of a replication fork encountering a lesion that cannot be bypassed causes breakage of the backbone, though the exact mechanism(s) for this breakage remains unclear [89, 90]. While both DSBs and SSBs can be mutagenic, DSBs are one of the most deleterious types of DNA damage [91]. Strand breaks potentiate large-scale mutations, including insertions, deletions, translocations, and sequence rearrangements [92-95].

1.2 Repair of Inflammation-Induced DNA Lesions

In order to minimize mutations, multiple mechanisms have evolved to address different types of DNA damage. The simplest way to prevent mutations is through accurate replication of DNA. Polymerases read the template strand and select the correct nucleotide based on the template base's shape and hydrogen bonding pattern to extend the strand being synthesized. When the hydrogen bonding of a base is altered (e.g., by deamination) or blocked (e.g., by etheno adducts), the cell first attempts to synthesize past the lesion (translesion synthesis, or TLS), often using a low-fidelity polymerase, which is only sometimes accurate [51, 96, 97]. However, some lesions cannot be efficiently bypassed by TLS, causing the replication fork to stall [98]. Several mechanisms are capable of restoring stalled replication forks, some of which leave the lesion in place [89], but inefficient fork restoration can cause strand breakage as described above.

Supplementary to polymerase selectivity and proofreading, several DNA repair pathways have evolved to correct lesions before and during replication. The rate of incorrect base incorporation (point mutation) for replicative polymerases is on the order of 10^{-6} to 10^{-8} nucleotides [99], and with 3.2×10^{9} bases in the genome, at least ten point mutations would occur with every cell division. DNA repair processes reduce point mutation frequency to 10^{-10} [21] and also protect against large-scale mutations such as insertions, deletions and rearrangements. DNA repair is of particular importance during inflammation because of (i) the large amount of reactive chemicals produced and (ii) the stimulation of cellular proliferation to regenerate damaged tissue. The combination of damage and cell division synergistically increase mutagenesis [100], and persistent DNA damage signals cell death [83, 101] which may be why deficiencies or imbalance in DNA repair proteins can greatly sensitize animals to inflammation [72, 102-106].

Most DNA damage from inflammation is addressed by the Direct Reversal (DR), Base Excision Repair (BER), and Homologous Recombination (HR) pathways. Here we will briefly describe each pathway and discuss their interactions for robust repair of inflammation-derived damage.

1.2.1. Direct Reversal (DR)

Some DNA alkyl adducts can be directly removed from the base in a process called Direct Reversal, leaving the original base intact. For example, the O^6-methylguanine DNA methyltransferase (MGMT) protein repairs O^6-methylguanine by transferring the methyl group to a cysteine residue in its active site [107]. The other mammalian DR enzymes belong to the ALKBH family, which utilize oxygen, Fe^{2+} and α-ketoglutarate as co-factors for oxidative dealkylation, releasing the alkyl lesion as an aldehyde and restoring the original base [108, 109]. Importantly, ALKBH enzymes can repair etheno adducts, and therefore supplement BER during inflammation [110].

1.2.2. Base Excision Repair (BER)

In general, Base Excision Repair deals with single-base lesions that do not significantly distort the DNA helix; since this encompasses most inflammation-derived lesions, BER is the primary pathway responsible for DNA repair during inflammation. The first step of BER is removal of the damaged base by one of several DNA glycosylases. The second step is to nick the backbone, which can be accomplished by some glycosylases, AP endonuclease-1 (APE1), or AP lyase. The two ends of the single strand break must then be processed to produce a 3'OH (with APE1, Polβ, or PNKP) capable of extension and a 5'PO_4 (with Polβ or PNKP) capable of ligation. The gap is

filled in with Polβ, and ligase seals the nick to complete the process. The elements of BER downstream of the glycosylase can also contribute to repair of SSBs.

Each glycosylase has its own repertoire of substrates, and there is some redundancy in substrate recognition to ensure a robust response. Some of the most important DNA glycosylases for repairing damage from inflammation are 8-oxo-guanine glycosylase (OGG1), which removes 8oxoG and FapyG [111], and alkyladenine glycosylase (AAG, also known as MPG or ANPG), which removes εA, 1,N^2 -εG, Hx, and 8oxoG, among others [72, 112]. AAG also recognizes and binds to εC, but it cannot excise the base, instead blocking replication and contributing to its increased genotoxicity [80]. Damaged pyrimidines may be excised by pyrimidine-specific glycosylases such as MBD4, UNG, TDG, and SMUG1 [112]. The enzyme MYH uniquely protects against 8oxoG mutagenesis, because it specifically recognizes and excises A misincorporated across from 8oxoG during replication [112]. Other BER glycosylases, such as NTHL1, NEIL1, and NEIL2, can recognize a broad range of substrates, including FapyG, hydantoin lesions, 8oxoG, and oxidized pyrimidines [46, 49, 105, 112, 113], providing robust repair of single-base lesions.

Importantly, every intermediate of the BER pathway contains a potentially toxic lesion: either an abasic site or some kind of strand break. Normally, the cell is able to complete BER without toxicity, but this is not always the case. If there is a large amount of damage, there may be simply too few of the molecules necessary for repair, leading to an accumulation of cytotoxic lesions and subsequent apoptosis. Alternatively, if a replication fork encounters a BER intermediate, the fork may break down, creating a DSB. Thus, while BER is essential for repairing DNA damage during inflammation, this pathway can sometimes do more harm than good by generating toxic intermediates.

1.2.3. Double Strand Break Repair

Although DSBs generally arise as secondary lesions during inflammation (e.g., from replication fork breakdown or nearby opposing SSBs) they are one of the most toxic types of DNA damage [91, 93, 95, 114]. Here, we will briefly describe the two major pathways responsible for DSB repair: Non-Homologous End Joining (NHEJ) and Homologous Recombination (HR).

NHEJ, the dominant repair mechanism in G1 phase [115], functions by joining two DSB ends with the Ku70/80 and DNA-PK complexes, and ligating the strands together. This process occurs quickly but is very prone to error. For example, if the two DSB ends are from different chromosomes, translocations occur. However, since DSBs are generally rare in G1, NHEJ sufficiently preserves genomic integrity during this cell cycle phase.

Homologous Recombination repairs DSBs much more accurately than NHEJ, but it acts more slowly and functions mainly during the S and G2 phases of the cell cycle [116]. Since the risk for mutations is highest during replication, and since HR can rescue replication stress, this pathway is of greater importance for inflammation-induced DNA damage. HR comprises multiple subpathways with distinct mechanisms, so here we will provide a basic overview of the major steps. HR begins by recognition of the DSB by CtIP and the MRN complex (consisting of MRE11, NBS1 and RAD50). The 5' end of the DNA is resected by EXO1 to leave a 3' overhang of single stranded DNA, which is stabilized by the protein RPA. BRCA2 displaces the RPA, replacing it with RAD51, and this 3' nucleoprotein filament searches nearby DNA for a homologous sequence. Usually, the cell identifies the correct homologous sequence on the nearby sister chromatid, which it invades and utilizes as a template to resume extension. There are several sub-pathways of HR, but the most common is synthesis-dependent strand annealing

(SDSA) (for more detailed descriptions and digital animations of HR mechanisms, please see [117]). In SDSA, once enough DNA has been synthesized from the template, the overhang will re-hybridize with its original strand, any remaining gaps will be filled, and DNA ligation completes repair of the DSB. A highly simplified diagram of this pathway is shown in Figure 1-8.

Since HR utilizes a homologous region of DNA as a template, this process is mostly error-free as long as the cell identifies the correct sequence in the sister chromatid. However, identification of homology in the homologous chromosome rather than the sister chromatid can lead to loss of heterozygosity, a significant source of tumor suppressor inactivation [118, 119]. Furthermore, a significant portion of the genome has been identified as repetitive or repeat-derived: nearly 10% of the genome consists of Alu repeats [120, 121], and a recent analysis estimates 2/3 of the genome consists of repetitive elements [122]. Thus, there are many opportunities for HR to identify a homologous sequence in the wrong location. Aberrant HR can lead to translocations, deletions, insertions, or sequence rearrangements [94, 123-127]. Some of the mechanisms for HR-derived mutations are illustrated in Figure 1-9. In addition to these large-scale mutations, HR can also produce point mutations, because the polymerases that participate in HR are often error-prone [98, 128-130].

As mentioned earlier, an important source of DSBs during inflammation is broken replication forks, which generate only one DSB end (see Fig 1-7), and thus cannot be accurately repaired by NHEJ. Therefore, lesions that cause replication fork breakdown (including replication blocking lesions and SSBs) necessitate HR to restore the replication fork. Notably, many of the intermediates of the BER pathway are SSBs, so if replication forks encounter these breaks before BER is completed, HR may be initiated as well (Fig 1-8) [101, 131].

1.3 Coordination of DNA Repair During Inflammation

Balance within and among pathways is crucial to genomic maintenance, so we will briefly discuss how the pathways above coordinate for efficient repair.

1.3.1. Intra-Pathway Balance

The importance of balance within a repair pathway has been illustrated with studies of modulated expression of BER proteins. Mice that contain a transgene for increased expression of Aag are more sensitive to alkylation damage, whereas *Aag*$^{-/-}$ mice are more resistant [132]. This varied sensitivity stems from the fact that BER intermediates (abasic sites and SSBs) are often more toxic than the original lesion itself [133]. If the downstream repair proteins do not keep up with glycosylase activity, intermediates accumulate and increase mutagenesis [134, 135] or signal cell death [101]. Accordingly, elevated AAG expression in humans has been associated with lung cancer risk [136, 137] and poor glioma prognosis [138].

1.3.2. Inter-Pathway Redundancy and Crosstalk

To account for potential imbalances or perturbations within repair pathways, there must also be inter-pathway crosstalk, regulation and redundancy. The coordination of multiple DNA repair pathways allows the network to address lesions quickly and compensate with other repair mechanisms if the pathway is not resolved efficiently.

There is often redundancy within and between pathways so that multiple mechanisms can correct the same lesion with equivalent efficacy. For example, supplementary to BER, Direct

Reversal enzymes ALKBH2 and ALKBH3 can repair etheno lesions [72, 139], and nucleotide excision repair (NER) can contribute to repair of the hydantoin lesions Sp and Gh [140, 141]. Redundancy between pathways is so important that mice lacking AAG, ALKBH2 and ALKBH3 are unable to survive even one episode of colonic inflammation [72].

In other cases, potentially redundant repair pathways are coordinated by cell cycle and crosstalk between repair machinery. For example, NHEJ is the dominant mechanism to repair DSBs during G0 and G1 phases of the cell cycle, but during replication, there is a much greater chance that quick ligation of two DSBs will produce a mutation. Thus, NHEJ and HR activities are regulated in part by cell cycle, and many of the proteins that recognize and bind DSBs contribute to the choice of which pathway will complete repair [142-144].

Finally, repair processes may compensate for each other if the pathway that initiated repair is not resolved efficiently. A particularly relevant example is that BER intermediates can cause replication forks to break down, inducing HR for repair (Fig 1-8) [101, 145]. Kiraly *et al.* showed that wild type levels of the BER protein AAG caused a greater accumulation of HR-driven mutations compared to $Aag^{-/-}$ mice [131], indicating that even normal BER glycosylase activity may result in aberrant DSB repair. Further, HR-driven mutations increased synergistically when alkylation damage occurred during proliferation [100, 131]. When Aag activity exceeds the capacity of downstream enzymes, as described above, accumulated BER intermediates can cause stress signaling and apoptosis [132], or they can elicit responses from other pathways, providing the opportunity for different types of mutations than the initial lesion might have created [134, 135, 146]. Of course, there are many ways in which intermediates of some pathways may be substrates for other pathways, but for the scope of this review we confine this example to BER and HR [146].

1.3.3. Fate of the Lesion

To illustrate the interplay among the repair mechanisms described here, let us consider εA (Fig 1-10), a LPO lesion that accumulates during inflammation. Starting from the top, efficient repair of εA can be accomplished with either DR, which removes the etheno lesion and leaves the undamaged base intact, or BER, which excises the entire base and re-synthesizes the DNA properly. However, if εA is encountered during replication, mutagenic consequences can arise. Translesion synthesis by an error-prone polymerase allows the putative development of a point mutation; if the εA lesion is repaired following inaccurate TLS, the mutation will become fixed. εA may also block some polymerases, causing the replication fork to stall. Stalled replication forks can be restarted by several mechanisms [89], some of which leave the lesion intact, but they may also break down to produce a one-ended DSB. Accurate restoration of the replication fork by HR prevents mutagenesis, but aberrant HR or NHEJ causes large-scale mutations, such as translocations, insertions and deletions (some examples are shown in Fig 1-9). DSBs are also highly cytotoxic, so persistence or abundance of DSBs in the cell can signal for it to undergo apoptosis [81, 91, 147]. Thus, a single εA lesion creates the opportunity for many types of mutations through multiple repair pathways.

1.3.4. Transcriptional Regulation of DNA Repair During Inflammation

To cope with the barrage of DNA damage, inflammatory signaling includes upregulation of DNA repair. Indeed, increasing severity of inflammation and precancerous lesions correlates positively with DNA damage response indicators [146, 148, 149]. Elements of BER and HR are promoted in inflammatory environments [148-153], and they have been shown to protect against

inflammation-driven mutations [71, 154-156]. Here we will describe a few major examples of transcription factors that moderate inflammation and their roles in promoting DNA repair.

One of the most important responses to oxidative stress is mediated by NRF2, a transcription factor that regulates the expression of antioxidants and other cytoprotective elements. Briefly, NRF2 is sequestered by KEAP1 in the cytoplasm until stimulation by oxidative stress, whereupon NRF2 translocates to the nucleus to bind antioxidant response elements (AREs) in target gene promoters [157-159]. Target genes of NRF2 include glutathione *S*-transferase (GST), NADPH quinone oxidoreductase 1 (NQO1) and superoxide dismutase (SOD), known collectively as the adaptive response to oxidative and electrophilic damage [158, 160]. Neutralizing RONS to less reactive species protects DNA from much of the deleterious chemistry described earlier.

In addition to antioxidant and metabolic enzymes, AREs have also recently been identified in promoters of several DNA repair genes, including components of HR [150], NHEJ [161], and BER [162]. Indeed, disruption of NRF2 activity has been shown to result in decreased DNA repair activity [150] and increased levels of DNA adducts [163-165]. Thus, when present, NRF2 helps to manage the self-damage from inflammation by increasing expression of genes that neutralize oxidative stressors and promote DNA repair.

Several other transcriptional regulators of inflammation may also play roles in promoting DNA repair. NFκB is a key transcription factor with roles in induction, propagation, and eventual downregulation of inflammation, and DNA damage is one of many signals that can activate it [166-168]. There is also evidence that NFκB enhances HR by stabilizing the CtIP-BRCA1 complex [152]. Similarly, several members of the interferon regulatory factor (IRF) transcription factor family promote DNA repair [169, 170]. For example, recognition of DSBs

can induce IRF1 signaling [169], and some of its target genes include elements of HR and BER [151].

Overall, because inflammation produces a great deal of DNA damage, and the pathogenic insults that cause inflammation also can cause DNA damage, transcriptional regulation of inflammation includes increased DNA repair. Indeed, the only way an organism could evolve to have a self-damaging physiological response like inflammation is to also efficiently repair the damage it causes.

1.4 DNA Damage Promotes Inflammation in a Positive Feedback Loop

Many pathogens can cause DNA damage [153, 171-175], which may be why DNA damage can induce inflammation. Furthermore, proteins that detect and respond to DNA damage can trigger cell cycle arrest, apoptosis, senescence, and necrosis, of which the latter two can promote inflammatory signaling [176-182]. Unfortunately, DNA damage and inflammation can therefore create a positive feedback loop, which can be difficult to regulate. Additionally, response to DNA damage in one cell can induce damage in nearby cells through extracellular signals and epigenetic modifications [183-186]. The propagation of genomic instability to such "bystander" cells, along with systemic inflammatory signals, may contribute to genotoxicity in off-target tissues during inflammation [187-190].

There are many elements of the DNA damage response that promote inflammation. For example, PARP1 (poly(ADP-ribose) polymerase 1) detects and binds SSBs to recruit BER machinery [191-195], and it has been closely linked to inflammation promotion. PARP1 builds branched polymers of ADP-ribose moieties out of NAD^+ (called PARylation) at strand breaks to

help recruit BER proteins and initiate repair. PARP1 is also capable of post-translational PARylation of proteins to modify their activity, notably including the key inflammatory regulator NFκB [166-168, 196]. Indeed, several components of the NFκB complex display increased activity following PARylation [166, 168].

Inhibition of PARP1 has repeatedly been demonstrated to decrease the severity of inflammation in the intestines [197], pancreas [198], heart [199], brain [200], liver [201], and many other tissues and model systems [202-206]. In particular, studies have shown that inhibition of PARP1 results in decreased inflammatory cytokine expression [166, 196, 207] [198, 202, 207, 208] decreased adhesion molecule production [207] [198] [203], decreased inflammation-associated enzyme activity, including iNOS, COX2 and NADPH oxidase [203, 209], and decreased immune cell infiltration [198, 208, 210]. These molecular and cellular alterations all support a model wherein PARP1 activity contributes to increased inflammatory signaling, and its inhibition protects the organism from inflammation-associated damage. Accordingly, PARP inhibitors are experiencing significant clinical success as adjuvants in multiple cancer therapies [211-213].

The BER glycosylase OGG1 can also augment inflammation through NFκB. OGG1 bound to 8oxoG facilitates NFκB binding [214, 215] and increases expression of its pro-inflammatory target genes [216]. Similar to inhibition of PARP1, downregulation or knockout of OGG1 can also reduce inflammation severity [217-219]. Interestingly, the OGG1-8oxoG complex acts as a guanine exchange factor and activates Ras family GTPases, further promoting inflammation through the MEK/ERK pathway [220].

Proteins involved in double strand break repair have also been implicated in pro-inflammatory signaling. DSBs can be recognized and bound by ATM, and RPA-coated single

stranded DNA (an early intermediate of HR) is recognized by ATR. Multiple studies have shown that ATM [152, 177, 178, 221] and ATR [221] can both promote NFκB signaling independent of downstream DNA damage responses. Accordingly, ATM/ATR activity results in increased cytokine production [177-179], and knockdown of ATM or ATR inhibits the production of the immune cell-activating ligand NKG2D [221].

Finally, inflammation can be promoted by generalized DNA damage. For instance, the growth arrest and DNA damage-inducible protein 34 (GADD34) is upregulated in response to multiple types of cellular stress, including DNA damage and ER-stress [181]. In two models of DNA damage-induced cancer, mice knocked out for GADD34 display significantly decreased levels of pro-inflammatory cytokines, immune cell infiltration and malignant lesions [222] [223]. Cytosolic DNA, which can occur from viral infection, can also trigger activation of the pro-inflammatory cytokines IL-1β [224] and IFNγ [225] [226]. Thus, it is not necessary to initiate the BER or HR pathways in the nucleus in order for DNA damage to induce inflammation.

The positive feedback relationship between DNA repair and inflammation is somewhat unexpected, because repair of inflammation-derived lesions can promote inflammation further. This mechanism may have evolved to ensure that inflammation persists long enough to thoroughly remove the perceived insult before down-regulation to baseline levels. However, the processes by which this positive feedback loop is suppressed have yet to be determined.

1.5 Inflammation Impairs Some DNA Repair Processes

In addition to direct damage by RONS, pro-inflammatory cytokines have also been shown to contribute to DNA damage. This signal-induced damage is due in part to the cytokine-stimulated

increase of intracellular RONS [32-34] and in part to impairment of some DNA repair components [227-235]. Since RONS readily react with cysteine residues on proteins, many cellular functions are susceptible to disruption from RONS [236]. Indeed, Jaiswal *et al.* demonstrated that inflammatory cytokines were capable of both inducing DNA damage (as measured by the comet assay) and impairing DNA repair activity (as measured by radiolabel incorporation) via a NO-dependent mechanism [227].

More targeted studies have defined particular components of DNA repair that are disrupted by inflammation. Reaction of NO with glutathione (GSH) produces S-nitrosoglutathione (GSNO), which acts as a NO reservoir as well as a vehicle for cysteine nitrosylation on other proteins. S-nitrosylation can have a variety of consequences for protein function, such as altering activity or localization [237], and notable targets include DNA repair enzymes. One of the most thoroughly studied targets of S-nitrosylation is the Direct Reversal protein MGMT, which removes methyl lesions from nucleotides by directly transferring the alkyl group onto a cysteine residue [107]. Nitrosylation of MGMT's active cysteine disables the enzyme [238], causing an accumulation of the genotoxic lesion O^6-methylguanine [232]. While DNA methylation is not a major type of inflammation-derived lesion, all DNA repair pathways are essential for genomic maintenance, so inhibition of MGMT can increase stress on other repair pathways to compensate. It is noteworthy that inflammation can increase sensitivity to types of DNA damage that it does not produce directly.

Ironically, while BER is responsible for repairing many of the inflammation-induced DNA lesions, it is also especially susceptible to disruption by inflammation. For instance, S-nitrosylation of OGG1 decreases its activity [233, 234, 239], and S-nitrosylation of APE1 causes it to be exported from the nucleus [229, 234]. Thus, two key steps in repairing oxidative damage

can be impeded by excess NO. Additionally, some people have a common genetic variant of OGG1 (Ser326Cys), associated with increased lung cancer risk [240], which is susceptible to inactivation by intracellular RONS following pro-inflammatory stimulation [228]. Finally, rejoining broken DNA strands via ligase is the final step of most DNA repair pathways, and evidence suggests that S-nitrosylation reduces ligase activity [235, 239], causing accumulation of unresolved strand breaks that can be lethal or mutagenic.

Interestingly, and underscoring the complexity of the equilibrium between inflammation and DNA repair, S-nitrosylation of AAG slightly increases its activity [234]. However, rather than accelerating BER, increased AAG activity can produce more BER intermediates than the downstream enzymes can efficiently process, leading to increased tissue damage and mutations [131, 133]. Indeed, excess AAG has been shown to contribute to microsatellite instability in the inflamed colon [146], highlighting the importance of balance among DNA repair components in maintaining genomic integrity.

1.6 Inflammation ←→ DNA Damage → Mutations → Cancer

The studies described here all contribute to the paradigm that inflammation and DNA damage contribute to each other and to the development of cancer, but few have explicitly demonstrated their direct connections. In seminal studies, the Samson lab has definitively shown that DNA damage from inflammation drives cancer development [71, 241]. In one such illuminating study, mice lacking the BER glycosylase Aag were treated with a colitis model of DSS in drinking water. The *Aag*$^{-/-}$ animals developed far more severe tissue damage and neoplasia than wild type, which correlated with a dramatic increase in DNA damage. Multiple types of base lesions

accumulated, especially εA, and some genetic deletions were observed, suggesting aberrant repair of broken replication forks. Sequencing tumors revealed point mutations in oncogenes that correspond with the mutational signatures associated with inflammation [71]. Similar results were obtained in stomach tissue when *Aag*$^{-/-}$ and wild type animals were treated with *H. pylori*, a prevalent source of gastric inflammation and cancer [71, 242]. Another Samson lab study demonstrated the importance of BER of deamination products during inflammation, observing more severe pathology in DSS-treated *Mbd4*$^{-/-}$ mice compared to wild type [241]. The Samson lab further established that DNA repair is essential to tolerating inflammation, as mice lacking multiple repair enzymes could not tolerate even a single bout of DSS-induced colitis [72]. With these targeted studies, the Samson lab has uniquely contributed to this field by directly demonstrating the importance of DNA damage and its repair for tolerating inflammation.

Thus, we expand upon Figure 1-1 with the examples described in this paper to arrive at Figure 1-11. Inflammation causes DNA damage primarily via RONS, which can produce DNA base and backbone lesions both by direct reaction or production of reactive LPO intermediates. The detection and response to DNA damage by BER (e.g., PARP, OGG1), HR (e.g., ATM/ATR), or generalized damage recognition can signal for increased inflammation, creating a positive feedback loop. Inflammatory transcription factors such as NRF2 and NFκB can mitigate the damage to DNA by neutralizing reactive chemicals with antioxidants and upregulating DNA repair pathways. However, nitric oxide can impair some repair enzymes, complicating the network and increasing the potential for dysregulation. Failure to repair DNA damage can lead to the mutations that initiate cancer, and many physiological processes involved in inflammation (e.g., proliferation, migration) also promote cancer development. Given the number of

mechanisms by which DNA damage and inflammation stimulate each other, it is no wonder that autoimmune and inflammatory diseases are so prevalent, difficult to control, and carcinogenic.

1.7 Transgenic *In Vivo* Mutation Assays

Measuring mutagenesis *in vivo* is essential to understanding the conditions that promote cancer. Scientists have identified numerous animal models for quantifying different types of mutations. Some *in vivo* mutation assays utilize endogenous gene loci, which are cost-effective because no genetic manipulation is involved, but are generally limited to one or a few tissue types. Several transgenic animal models have been created to detect mutations with reporter genes that are non functional in the animal, enabling measurement of mutations across many tissues.

The first transgenic animals created for detecting mutations *in vivo* incorporated bacterial genes flanked by lambda phage cos sites [243-245]. Since the transgenes do not produce mammalian proteins, and since they were incorporated at genetic loci neutral to the development and health of the animal, the transgenes are non functional in the life of the animal [246, 247]. In these models, the assay is accomplished by treating the animal with the mutagen(s) of interest, extracting genomic DNA, packaging the transgene with lambda phage, and infecting *E. coli* to identify functional mutations in the extracted transgene. To improve assay sensitivity, the bacterial genes are incorporated at high copy numbers [246].

The first two transgenic animal models designed under this strategy employed the *lac* operon. In 1989, Gossen *et al.* described creation of the LacZ mouse (later renamed Muta™Mouse), wherein the reporter contains the complete 3.9 kilobase (kb) bacterial *LacZ* gene. Following treatment, the transgene is recovered from animal tissue and packaged into

phage particles, used to infect *LacZ⁻ E. coli*, and plated on X-Gal plates. Mutants are then scored as colorless plaques, indicating absence of β-galactosidase, and normalized to non-mutant blue plaques [243]. Similarly, the *LacI* mouse (later renamed BigBlue®) was created with the complete 1080 bp *LacI* repressor gene, in which mutants produce blue plaques on X-Gal plates and are normalized to non-mutant clear plaques [244]. Sequencing DNA from mutant samples allows determination of the precise mutation that occurred.

In 1996, Nohmi *et al.* reported the creation of the Gpt-Δ mouse, which employs a similar detection strategy as Muta™Mouse and BigBlue®, but features selection methods for detection of two types of mutations. The gpt delta transgene contains the 456 bp *gpt* gene, which enables detection of point mutations, as well as the *red* and *gam* genes to enable detection of deletions. Point mutations in the *gpt* gene enable infected *E. coli* to grow on 6-thioguanine selection plates, and deletion of both the *red* and *gam* genes causes sensitivity to P2 interference, enabling detection as plaques in P2 lysogens of *E. coli*. While the Muta™Mouse and BigBlue® assays are capable of detecting many types of mutations, sequencing is necessary to determine the type of mutation that occurred. Thus, one significant advantage of the Gpt-Δ model is that two different types of mutations can be assayed separately.

The Muta™Mouse, BigBlue® and Gpt-Δ animal models have been useful for studying point mutations, frameshifts, small insertions, and deletions in many studies. Since the bacterial target genes are generally short and present at high copy numbers, these animals can only detect small-scale mutations [246]. However, many carcinogenic mutations result from large-scale rearrangements during mitotic recombination [119, 124]. To complement the small-scale transgenic *in vivo* mutation assays described above, the Engelward laboratory created the FYDR

Recombomouse, first reported in 2003 [248], as a method to detect large-scale genomic sequence rearrangements.

FYDR transgenic mice contain a direct repeat of truncated copies of the EYFP gene, where the 5' copy lacks the 5' coding region of the gene and the 3' copy likewise lacks the 3' coding region (Fig 1-12). Expression of the truncated EYFP sequences does not produce a fluorescent protein. However, if a DSB occurs within one of the copies, and the Rad51 nucleoprotein filament identifies the homologous sequence in the incorrect copy as the template for repair, HDR will produce a sequence rearrangement that restores the full coding region of the gene, and expression results in a full-length fluorescent EYFP protein [248]. Aberrant recombination events can then be visualized as individual fluorescent foci within intact tissue, or the total proportion of mutated cells can be measured by flow cytometry.

The FYDR transgene was randomly incorporated at a locus on Chromosome 1, and as a result could only be detected in the pancreas and skin [249]. In order to create a more widely usable animal model, the Engelward laboratory created targeting vectors to integrate a similar direct repeat of truncated EGFP sequences at the ubiquitously-expressed Rosa26 locus [250]. This congenic animal model, called the *Rosa26* Direct Repeat (RaDR) mouse, has enabled fluorescent detection of sequence rearrangement mutations in every tissue studied so far [251, 252].

Other transgenic direct repeat animal models for detecting HR-driven mutations have subsequently been created in other labs. The first of these was created in the Jasin laboratory, utilizing a direct repeat of GFP sequences wherein the first is disrupted by an I-SceI restriction site, and the second is truncated at both 5' and 3' ends [253]. Following induction of a DSB by I-SceI, the cell can undergo gene conversion to produce a full length GFP. This model system has

been useful for studying the genetic underpinnings and mechanisms of homologous recombination [253, 254]. However, studies are limited to analysis of a single recombination mechanism following an artificially induced DSB in primary cell cultures.

Recently, the Nakamura lab reported another direct repeat transgenic animal, this one containing a partial duplication in the 3' region of the *HPRT* gene followed by a GFP sequence [255]. The duplication causes inactivation of the *HPRT* gene, but loss of the duplication by intrastrand recombination or sister chromatid exchange produces an HPRT-GFP fusion protein. Similar to RaDR, this model permits *in situ* detection of spontaneous sequence rearrangements. However, this model has not successfully detected gene conversion mutations, which is the predominant mechanism of mitotic HR [256].

1.8 Approaches and Aims of This Thesis

The work described in this thesis was designed to interrogate the contributions of inflammation and DNA damage to the development of mutations and cancer. We utilized RaDR fluorescence as our primary readout of mutagenicity, because this animal model provides the simplest, least laborious, and most cost-effective measurement of mutations *in vivo*. Despite the fact that inflammation produces primarily single base lesions, which are more commonly associated with point mutations, inflammation-induced DNA lesions can lead to strand breaks and replication fork breakdown, initiating repair by HR as described above. Thus, our primary mutation readout derived from large-scale sequence rearrangements can serve as a general indicator of mutagenicity. Our RaDR mice also contain the Gpt-Δ transgene, enabling unprecedented

analysis of sequence rearrangements, point mutations and deletions all within a single tissue sample.

The causative relationship between inflammation and cancer has been thoroughly established in the intestine [4, 7, 11], and so we designed our studies to query intestinal inflammation's contributions to mutagenesis. Further lending itself to studies of mutations and cancer, intestinal architecture is well defined and enables identification of somatic stem cells, which can be difficult or impossible to identify in other tissues. The colon epithelium consists of pore-like divots into the mucosa called crypts, and the small intestine also contains fingerlike projections into the lumen, called villi. At the base of each crypt are one or more somatic stem cells, which give rise to the proliferative transit cells that comprise the length of the crypt (Fig 1-13A) and, in the small intestine, the villi surface [257]. The continual proliferation of stem and transit cells enables continual renewal of crypt (and villus) epithelia. Transit cells are eventually sloughed off into the lumen, and stem cells produce complete epithelial turnover within 3-5 days [258]. In a RaDR animal, mutations in crypt stem cells are visible as large, bright, roughly circular foci that can be distinguished from the smaller, dimmer and/or irregularly shaped foci of mutated transit cells (Fig 1-13B). Colon epithelia can be disaggregated into a suspension of crypts, and both partially and fully fluorescent crypts are visible in suspensions of RaDR crypts (Fig 1-13C). The foci that we believe to be converted crypts are, on average, 10x brighter and 6x larger than foci that appear to be single cells (Fig 1-13D). Since somatic stem cells persist for years, if not the animal's lifetime, whereas transit cells are sloughed off within 5 days, it is of great interest to quantify recombinant stem cell foci rather than all foci.

To distinguish crypt foci from transit cell foci with minimal bias, we collaborated with Dr. Dushan Wadduwage to write MATLAB image analysis programs. This program uses

gradient and intensity features of the image to distinguish RaDR foci from background autofluorescence. The first version of this program identifies all foci within the tissue and is useful for many tissues, such as pancreas and liver, where foci may assume different sizes and shapes due to tissue architecture and morphology. Another version of the program specifically identifies crypt foci based on size, shape and intensity through a training algorithm. The user annotates 3-4 images from the data set for purported crypt foci, which the program interprets to define crypt foci parameters, and then applies those parameters to analyze all images in the data set. Thus, we are able to analyze tissue for all foci as well as crypt foci.

RaDR mutants can also be quantified according to the proportion of the tissue that is fluorescent. The simplest method for quantifying proportion of fluorescent cells is by flow cytometry, but this requires disaggregation of the tissue, so *de novo* mutations cannot be distinguished from clonally expanded mutants and the context of the mutation *in situ* is lost. We can also approximate the overall mutant proportion in RaDR tissue images by comparing the fluorescent area to the total tissue area. Measuring the percent area of fluorescence in the tissue is of particular utility in measuring RaDR mutations in intestinal tumors, where crypt architecture is obliterated and clonal expansion produces patches of fluorescence.

We utilized these methods to quantify mutagenesis from several model systems. The second chapter of this thesis discusses mutagenic consequences of eliminating regulatory elements of the immune system. Next, we explored mutagenesis and clonal expansion resulting from microbially induced inflammation. Finally, we evaluated mutations arising from upregulated base excision repair. Overall, our results indicate that inflammation does not cause a significant increase in de novo sequence rearrangement mutations, but it contributes to cancer in part by increasing the total burden of mutant cells via clonal expansion.

1.9. References

1. Guerra, C., et al., *Chronic pancreatitis is essential for induction of pancreatic ductal adenocarcinoma by K-Ras oncogenes in adult mice.* Cancer Cell, 2007. **11**(3): p. 291-302.
2. Bansal, P. and A. Sonnenberg, *Pancreatitis is a risk factor for pancreatic cancer.* Gastroenterology, 1995. **109**(1): p. 247-51.
3. Guerra, C., et al., *Pancreatitis-induced inflammation contributes to pancreatic cancer by inhibiting oncogene-induced senescence.* Cancer Cell, 2011. **19**(6): p. 728-39.
4. Rutter, M., et al., *Severity of inflammation is a risk factor for colorectal neoplasia in ulcerative colitis.* Gastroenterology, 2004. **126**(2): p. 451-9.
5. Ohata, K., et al., *Hepatic steatosis is a risk factor for hepatocellular carcinoma in patients with chronic hepatitis C virus infection.* Cancer, 2003. **97**(12): p. 3036-43.
6. Beasley, R.P., *Hepatitis B virus. The major etiology of hepatocellular carcinoma.* Cancer, 1988. **61**(10): p. 1942-56.
7. Coussens, L.M. and Z. Werb, *Inflammation and cancer.* Nature, 2002. **420**(6917): p. 860-7.
8. Erdman, S.E., et al., *Nitric oxide and TNF-alpha trigger colonic inflammation and carcinogenesis in Helicobacter hepaticus-infected, Rag2-deficient mice.* Proc Natl Acad Sci U S A, 2009. **106**(4): p. 1027-32.
9. Anuja, K., et al., *Prolonged inflammatory microenvironment is crucial for pro-neoplastic growth and genome instability: a detailed review.* Inflamm Res, 2017. **66**(2): p. 119-128.
10. Allavena, P., et al., *Pathways connecting inflammation and cancer.* Curr Opin Genet Dev, 2008. **18**(1): p. 3-10.
11. Shacter, E. and S.A. Weitzman, *Chronic inflammation and cancer.* Oncology (Williston Park), 2002. **16**(2): p. 217-26, 229; discussion 230-2.
12. Balkwill, F. and A. Mantovani, *Inflammation and cancer: back to Virchow?* Lancet, 2001. **357**(9255): p. 539-45.
13. Erdman, S.E., et al., *CD4+ CD25+ regulatory T lymphocytes inhibit microbially induced colon cancer in Rag2-deficient mice.* Am J Pathol, 2003. **162**(2): p. 691-702.
14. Rayburn, E.R., S.J. Ezell, and R. Zhang, *Anti-Inflammatory Agents for Cancer Therapy.* Mol Cell Pharmacol, 2009. **1**(1): p. 29-43.
15. Mantovani, A., et al., *Cancer-related inflammation.* Nature, 2008. **454**(7203): p. 436-44.
16. Colotta, F., et al., *Cancer-related inflammation, the seventh hallmark of cancer: links to genetic instability.* Carcinogenesis, 2009. **30**(7): p. 1073-81.
17. Pikor, L., et al., *The detection and implication of genome instability in cancer.* Cancer Metastasis Rev, 2013. **32**(3-4): p. 341-52.
18. Negrini, S., V.G. Gorgoulis, and T.D. Halazonetis, *Genomic instability--an evolving hallmark of cancer.* Nat Rev Mol Cell Biol, 2010. **11**(3): p. 220-8.
19. Hanahan, D. and R.A. Weinberg, *Hallmarks of cancer: the next generation.* Cell, 2011. **144**(5): p. 646-74.
20. DeMars, R. and K.R. Held, *The spontaneous azaguanine-resistant mutants of diploid human fibroblasts.* Humangenetik, 1972. **16**(1): p. 87-110.
21. Loeb, L.A., *A mutator phenotype in cancer.* Cancer Res, 2001. **61**(8): p. 3230-9.
22. Drake, J.W., et al., *Rates of spontaneous mutation.* Genetics, 1998. **148**(4): p. 1667-86.
23. Stratton, M.R., P.J. Campbell, and P.A. Futreal, *The cancer genome.* Nature, 2009. **458**(7239): p. 719-24.
24. Vogelstein, B., et al., *Cancer genome landscapes.* Science, 2013. **339**(6127): p. 1546-58.

25. BNID. *BioNumbers*. 2017 [cited 2017 April 16]; Available from: http://www.bionumbers.hms.harvard.edu/.
26. SEER. *Cancer Stat Facts*. 2014 [cited 2017 April 16]; Available from: https://seer.cancer.gov/statfacts/html/all.html.
27. Bredt, D.S. and S.H. Snyder, *Nitric oxide: a physiologic messenger molecule.* Annu Rev Biochem, 1994. **63**: p. 175-95.
28. Moncada, S., R.M. Palmer, and E.A. Higgs, *Nitric oxide: physiology, pathophysiology, and pharmacology.* Pharmacol Rev, 1991. **43**(2): p. 109-42.
29. Thomas, D.D., et al., *The chemical biology of nitric oxide: implications in cellular signaling.* Free Radic Biol Med, 2008. **45**(1): p. 18-31.
30. Lewis, R.S., et al., *Kinetic analysis of the fate of nitric oxide synthesized by macrophages in vitro.* J Biol Chem, 1995. **270**(49): p. 29350-5.
31. Stuehr, D.J. and M.A. Marletta, *Synthesis of nitrite and nitrate in murine macrophage cell lines.* Cancer Res, 1987. **47**(21): p. 5590-4.
32. Colin, I.M., et al., *Differential regulation of the production of reactive oxygen species in Th1 cytokine-treated thyroid cells.* Thyroid, 2014. **24**(3): p. 441-52.
33. Sundaresan, M., et al., *Regulation of reactive-oxygen-species generation in fibroblasts by Rac1.* Biochem J, 1996. **318 (Pt 2)**: p. 379-82.
34. Yang, D., et al., *Pro-inflammatory cytokines increase reactive oxygen species through mitochondria and NADPH oxidase in cultured RPE cells.* Exp Eye Res, 2007. **85**(4): p. 462-72.
35. Dedon, P.C. and S.R. Tannenbaum, *Reactive nitrogen species in the chemical biology of inflammation.* Arch Biochem Biophys, 2004. **423**(1): p. 12-22.
36. Lonkar, P. and P.C. Dedon, *Reactive species and DNA damage in chronic inflammation: reconciling chemical mechanisms and biological fates.* Int J Cancer, 2011. **128**(9): p. 1999-2009.
37. Dizdaroglu, M., *Oxidatively induced DNA damage: mechanisms, repair and disease.* Cancer Lett, 2012. **327**(1-2): p. 26-47.
38. Shibutani, S., M. Takeshita, and A.P. Grollman, *Insertion of specific bases during DNA synthesis past the oxidation-damaged base 8-oxodG.* Nature, 1991. **349**(6308): p. 431-4.
39. Cheng, K.C., et al., *8-Hydroxyguanine, an abundant form of oxidative DNA damage, causes G----T and A----C substitutions.* J Biol Chem, 1992. **267**(1): p. 166-72.
40. Duarte, V., J.G. Muller, and C.J. Burrows, *Insertion of dGMP and dAMP during in vitro DNA synthesis opposite an oxidized form of 7,8-dihydro-8-oxoguanine.* Nucleic Acids Res, 1999. **27**(2): p. 496-502.
41. Hsu, G.W., et al., *Error-prone replication of oxidatively damaged DNA by a high-fidelity DNA polymerase.* Nature, 2004. **431**(7005): p. 217-21.
42. Markkanen, E., et al., *A switch between DNA polymerases delta and lambda promotes error-free bypass of 8-oxo-G lesions.* Proc Natl Acad Sci U S A, 2012. **109**(50): p. 20401-6.
43. Henderson, P.T., et al., *Oxidation of 7,8-dihydro-8-oxoguanine affords lesions that are potent sources of replication errors in vivo.* Biochemistry, 2002. **41**(3): p. 914-21.
44. Henderson, P.T., et al., *The hydantoin lesions formed from oxidation of 7,8-dihydro-8-oxoguanine are potent sources of replication errors in vivo.* Biochemistry, 2003. **42**(31): p. 9257-62.
45. Fenn, D., L.M. Chi, and S.L. Lam, *Effect of hyperoxidized guanine on DNA primer-template structures: spiroiminodihydantoin leads to strand slippage.* FEBS Lett, 2008. **582**(30): p. 4169-75.

46. Zhao, X., et al., *Mutation versus repair: NEIL1 removal of hydantoin lesions in single-stranded, bulge, bubble, and duplex DNA contexts.* Biochemistry, 2010. **49**(8): p. 1658-66.
47. Neeley, W.L. and J.M. Essigmann, *Mechanisms of formation, genotoxicity, and mutation of guanine oxidation products.* Chem Res Toxicol, 2006. **19**(4): p. 491-505.
48. Mangerich, A., et al., *Infection-induced colitis in mice causes dynamic and tissue-specific changes in stress response and DNA damage leading to colon cancer.* Proc Natl Acad Sci U S A, 2012. **109**(27): p. E1820-9.
49. Hailer, M.K., et al., *Recognition of the oxidized lesions spiroiminodihydantoin and guanidinohydantoin in DNA by the mammalian base excision repair glycosylases NEIL1 and NEIL2.* DNA Repair (Amst), 2005. **4**(1): p. 41-50.
50. Kalam, M.A., et al., *Genetic effects of oxidative DNA damages: comparative mutagenesis of the imidazole ring-opened formamidopyrimidines (Fapy lesions) and 8-oxo-purines in simian kidney cells.* Nucleic Acids Res, 2006. **34**(8): p. 2305-15.
51. Asagoshi, K., et al., *Effects of a guanine-derived formamidopyrimidine lesion on DNA replication: translesion DNA synthesis, nucleotide insertion, and extension kinetics.* J Biol Chem, 2002. **277**(17): p. 14589-97.
52. Dong, M., et al., *Absence of 2'-deoxyoxanosine and presence of abasic sites in DNA exposed to nitric oxide at controlled physiological concentrations.* Chem Res Toxicol, 2003. **16**(9): p. 1044-55.
53. Caulfield, J.L., J.S. Wishnok, and S.R. Tannenbaum, *Nitric oxide-induced deamination of cytosine and guanine in deoxynucleosides and oligonucleotides.* J Biol Chem, 1998. **273**(21): p. 12689-95.
54. DeVito, S., et al., *Mutagenic potential of hypoxanthine in live human cells.* Mutat Res, 2017. **803-805**: p. 9-16.
55. Dong, M. and P.C. Dedon, *Relatively small increases in the steady-state levels of nucleobase deamination products in DNA from human TK6 cells exposed to toxic levels of nitric oxide.* Chem Res Toxicol, 2006. **19**(1): p. 50-7.
56. van der Veen, B.S., M.P. de Winther, and P. Heeringa, *Myeloperoxidase: molecular mechanisms of action and their relevance to human health and disease.* Antioxid Redox Signal, 2009. **11**(11): p. 2899-937.
57. Winterbourn, C.C., et al., *Modeling the reactions of superoxide and myeloperoxidase in the neutrophil phagosome: implications for microbial killing.* J Biol Chem, 2006. **281**(52): p. 39860-9.
58. Henderson, J.P., J. Byun, and J.W. Heinecke, *Molecular chlorine generated by the myeloperoxidase-hydrogen peroxide-chloride system of phagocytes produces 5-chlorocytosine in bacterial RNA.* J Biol Chem, 1999. **274**(47): p. 33440-8.
59. Henderson, J.P., et al., *Bromination of deoxycytidine by eosinophil peroxidase: a mechanism for mutagenesis by oxidative damage of nucleotide precursors.* Proc Natl Acad Sci U S A, 2001. **98**(4): p. 1631-6.
60. Wu, W., et al., *Eosinophils generate brominating oxidants in allergen-induced asthma.* J Clin Invest, 2000. **105**(10): p. 1455-63.
61. Kawai, Y., et al., *Endogenous formation of novel halogenated 2'-deoxycytidine. Hypohalous acid-mediated DNA modification at the site of inflammation.* J Biol Chem, 2004. **279**(49): p. 51241-9.
62. Kang, J.I., Jr. and L.C. Sowers, *Examination of hypochlorous acid-induced damage to cytosine residues in a CpG dinucleotide in DNA.* Chem Res Toxicol, 2008. **21**(6): p. 1211-8.

63. Knutson, C.G., et al., *Chemical and cytokine features of innate immunity characterize serum and tissue profiles in inflammatory bowel disease.* Proc Natl Acad Sci U S A, 2013. **110**(26): p. E2332-41.
64. Fedeles, B.I., et al., *Intrinsic mutagenic properties of 5-chlorocytosine: A mechanistic connection between chronic inflammation and cancer.* Proc Natl Acad Sci U S A, 2015. **112**(33): p. E4571-80.
65. Lao, V.V., et al., *Incorporation of 5-chlorocytosine into mammalian DNA results in heritable gene silencing and altered cytosine methylation patterns.* Carcinogenesis, 2009. **30**(5): p. 886-93.
66. Sato, Y., et al., *IL-10 deficiency leads to somatic mutations in a model of IBD.* Carcinogenesis, 2006. **27**(5): p. 1068-73.
67. Nair, U., H. Bartsch, and J. Nair, *Lipid peroxidation-induced DNA damage in cancer-prone inflammatory diseases: a review of published adduct types and levels in humans.* Free Radic Biol Med, 2007. **43**(8): p. 1109-20.
68. Zarkovic, N., *4-hydroxynonenal as a bioactive marker of pathophysiological processes.* Mol Aspects Med, 2003. **24**(4-5): p. 281-91.
69. Nair, J., et al., *Increased etheno-DNA adducts in affected tissues of patients suffering from Crohn's disease, ulcerative colitis, and chronic pancreatitis.* Antioxid Redox Signal, 2006. **8**(5-6): p. 1003-10.
70. Moriya, M., et al., *Mutagenic potency of exocyclic DNA adducts: marked differences between Escherichia coli and simian kidney cells.* Proc Natl Acad Sci U S A, 1994. **91**(25): p. 11899-903.
71. Meira, L.B., et al., *DNA damage induced by chronic inflammation contributes to colon carcinogenesis in mice.* J Clin Invest, 2008. **118**(7): p. 2516-25.
72. Calvo, J.A., et al., *DNA repair is indispensable for survival after acute inflammation.* J Clin Invest, 2012. **122**(7): p. 2680-9.
73. Pang, B., et al., *Lipid peroxidation dominates the chemistry of DNA adduct formation in a mouse model of inflammation.* Carcinogenesis, 2007. **28**(8): p. 1807-13.
74. Chang, S.C., et al., *Next-generation sequencing reveals the biological significance of the N(2),3-ethenoguanine lesion in vivo.* Nucleic Acids Res, 2015. **43**(11): p. 5489-500.
75. Swenberg, J.A., et al., *Endogenous versus exogenous DNA adducts: their role in carcinogenesis, epidemiology, and risk assessment.* Toxicol Sci, 2011. **120 Suppl 1**: p. S130-45.
76. Shrivastav, N., D. Li, and J.M. Essigmann, *Chemical biology of mutagenesis and DNA repair: cellular responses to DNA alkylation.* Carcinogenesis, 2010. **31**(1): p. 59-70.
77. Langouet, S., M. Muller, and F.P. Guengerich, *Misincorporation of dNTPs opposite 1,N2-ethenoguanine and 5,6,7,9-tetrahydro-7-hydroxy-9-oxoimidazo[1,2-a]purine in oligonucleotides by Escherichia coli polymerases I exo- and II exo-, T7 polymerase exo-, human immunodeficiency virus-1 reverse transcriptase, and rat polymerase beta.* Biochemistry, 1997. **36**(20): p. 6069-79.
78. Pandya, G.A. and M. Moriya, *1,N6-ethenodeoxyadenosine, a DNA adduct highly mutagenic in mammalian cells.* Biochemistry, 1996. **35**(35): p. 11487-92.
79. Levine, R.L., et al., *Mutagenesis induced by a single 1,N6-ethenodeoxyadenosine adduct in human cells.* Cancer Res, 2000. **60**(15): p. 4098-104.
80. Gros, L., et al., *Hijacking of the human alkyl-N-purine-DNA glycosylase by 3,N4-ethenocytosine, a lipid peroxidation-induced DNA adduct.* J Biol Chem, 2004. **279**(17): p. 17723-30.

81. Ryan, A.J., et al., *Camptothecin cytotoxicity in mammalian cells is associated with the induction of persistent double strand breaks in replicating DNA.* Nucleic Acids Res, 1991. **19**(12): p. 3295-300.
82. Pommier, Y., et al., *Correlations between intercalator-induced DNA strand breaks and sister chromatid exchanges, mutations, and cytotoxicity in Chinese hamster cells.* Cancer Res, 1985. **45**(7): p. 3143-9.
83. Nelson, W.G. and M.B. Kastan, *DNA strand breaks: the DNA template alterations that trigger p53-dependent DNA damage response pathways.* Mol Cell Biol, 1994. **14**(3): p. 1815-23.
84. Szabo, C., et al., *DNA strand breakage, activation of poly (ADP-ribose) synthetase, and cellular energy depletion are involved in the cytotoxicity of macrophages and smooth muscle cells exposed to peroxynitrite.* Proc Natl Acad Sci U S A, 1996. **93**(5): p. 1753-8.
85. Dasika, G.K., et al., *DNA damage-induced cell cycle checkpoints and DNA strand break repair in development and tumorigenesis.* Oncogene, 1999. **18**(55): p. 7883-99.
86. Kiziltepe, T., et al., *Delineation of the chemical pathways underlying nitric oxide-induced homologous recombination in mammalian cells.* Chem Biol, 2005. **12**(3): p. 357-69.
87. Ashour, M.E., R. Atteya, and S.F. El-Khamisy, *Topoisomerase-mediated chromosomal break repair: an emerging player in many games.* Nat Rev Cancer, 2015. **15**(3): p. 137-51.
88. Bryant, P.E. and P.J. Johnston, *Restriction-endonuclease-induced DNA double-strand breaks and chromosomal aberrations in mammalian cells.* Mutat Res, 1993. **299**(3-4): p. 289-96.
89. Yeeles, J.T., et al., *Rescuing stalled or damaged replication forks.* Cold Spring Harb Perspect Biol, 2013. **5**(5): p. a012815.
90. Zeman, M.K. and K.A. Cimprich, *Causes and consequences of replication stress.* Nat Cell Biol, 2014. **16**(1): p. 2-9.
91. van Gent, D.C., J.H. Hoeijmakers, and R. Kanaar, *Chromosomal stability and the DNA double-stranded break connection.* Nat Rev Genet, 2001. **2**(3): p. 196-206.
92. Hoeijmakers, J.H., *DNA damage, aging, and cancer.* N Engl J Med, 2009. **361**(15): p. 1475-85.
93. Bishop, A.J. and R.H. Schiestl, *Homologous recombination as a mechanism for genome rearrangements: environmental and genetic effects.* Hum Mol Genet, 2000. **9**(16): p. 2427-334.
94. Gu, W., F. Zhang, and J.R. Lupski, *Mechanisms for human genomic rearrangements.* Pathogenetics, 2008. **1**(1): p. 4.
95. Costantino, L., et al., *Break-induced replication repair of damaged forks induces genomic duplications in human cells.* Science, 2014. **343**(6166): p. 88-91.
96. Tolentino, J.H., et al., *Inhibition of DNA replication fork progression and mutagenic potential of 1, N6-ethenoadenine and 8-oxoguanine in human cell extracts.* Nucleic Acids Res, 2008. **36**(4): p. 1300-8.
97. Buisson, R., et al., *Breast cancer proteins PALB2 and BRCA2 stimulate polymerase eta in recombination-associated DNA synthesis at blocked replication forks.* Cell Rep, 2014. **6**(3): p. 553-64.
98. McIlwraith, M.J., et al., *Human DNA polymerase eta promotes DNA synthesis from strand invasion intermediates of homologous recombination.* Mol Cell, 2005. **20**(5): p. 783-92.
99. Kunkel, T.A., *DNA replication fidelity.* J Biol Chem, 2004. **279**(17): p. 16895-8.
100. Kiraly, O., et al., *Inflammation-induced cell proliferation potentiates DNA damage-induced mutations in vivo.* PLoS Genet, 2015. **11**(2): p. e1004901.
101. Sobol, R.W., et al., *Base excision repair intermediates induce p53-independent cytotoxic and genotoxic responses.* J Biol Chem, 2003. **278**(41): p. 39951-9.

102. Sejas, D.P., et al., *Inflammatory reactive oxygen species-mediated hemopoietic suppression in Fancc-deficient mice.* J Immunol, 2007. **178**(8): p. 5277-87.
103. Sakamoto, K., et al., *MUTYH-null mice are susceptible to spontaneous and oxidative stress induced intestinal tumorigenesis.* Cancer Res, 2007. **67**(14): p. 6599-604.
104. Russo, M.T., et al., *Accumulation of the oxidative base lesion 8-hydroxyguanine in DNA of tumor-prone mice defective in both the Myh and Ogg1 DNA glycosylases.* Cancer Res, 2004. **64**(13): p. 4411-4.
105. Chakraborty, A., et al., *Neil2-null Mice Accumulate Oxidized DNA Bases in the Transcriptionally Active Sequences of the Genome and Are Susceptible to Innate Inflammation.* J Biol Chem, 2015. **290**(41): p. 24636-48.
106. Liao, J., et al., *Increased susceptibility of chronic ulcerative colitis-induced carcinoma development in DNA repair enzyme Ogg1 deficient mice.* Mol Carcinog, 2008. **47**(8): p. 638-46.
107. Pegg, A.E., *Multifaceted roles of alkyltransferase and related proteins in DNA repair, DNA damage, resistance to chemotherapy, and research tools.* Chem Res Toxicol, 2011. **24**(5): p. 618-39.
108. Duncan, T., et al., *Reversal of DNA alkylation damage by two human dioxygenases.* Proc Natl Acad Sci U S A, 2002. **99**(26): p. 16660-5.
109. Begley, T.J. and L.D. Samson, *AlkB mystery solved: oxidative demethylation of N1-methyladenine and N3-methylcytosine adducts by a direct reversal mechanism.* Trends Biochem Sci, 2003. **28**(1): p. 2-5.
110. Fu, D., J.A. Calvo, and L.D. Samson, *Balancing repair and tolerance of DNA damage caused by alkylating agents.* Nat Rev Cancer, 2012. **12**(2): p. 104-20.
111. Krishnamurthy, N., et al., *Efficient removal of formamidopyrimidines by 8-oxoguanine glycosylases.* Biochemistry, 2008. **47**(3): p. 1043-50.
112. Jacobs, A.L. and P. Schar, *DNA glycosylases: in DNA repair and beyond.* Chromosoma, 2012. **121**(1): p. 1-20.
113. Krishnamurthy, N., et al., *Superior removal of hydantoin lesions relative to other oxidized bases by the human DNA glycosylase hNEIL1.* Biochemistry, 2008. **47**(27): p. 7137-46.
114. Krejci, L., et al., *Homologous recombination and its regulation.* Nucleic Acids Res, 2012. **40**(13): p. 5795-818.
115. Kim, J.S., et al., *Independent and sequential recruitment of NHEJ and HR factors to DNA damage sites in mammalian cells.* J Cell Biol, 2005. **170**(3): p. 341-7.
116. Sonoda, E., et al., *Differential usage of non-homologous end-joining and homologous recombination in double strand break repair.* DNA Repair (Amst), 2006. **5**(9-10): p. 1021-9.
117. Helleday, T., et al., *DNA double-strand break repair: from mechanistic understanding to cancer treatment.* DNA Repair (Amst), 2007. **6**(7): p. 923-35.
118. Gupta, P.K., et al., *High frequency in vivo loss of heterozygosity is primarily a consequence of mitotic recombination.* Cancer Res, 1997. **57**(6): p. 1188-93.
119. Bishop, A.J. and R.H. Schiestl, *Homologous recombination as a mechanism of carcinogenesis.* Biochim Biophys Acta, 2001. **1471**(3): p. M109-21.
120. Kolomietz, E., et al., *The role of Alu repeat clusters as mediators of recurrent chromosomal aberrations in tumors.* Genes Chromosomes Cancer, 2002. **35**(2): p. 97-112.
121. Ohshima, K., et al., *Whole-genome screening indicates a possible burst of formation of processed pseudogenes and Alu repeats by particular L1 subfamilies in ancestral primates.* Genome Biol, 2003. **4**(11): p. R74.

122. de Koning, A.P., et al., *Repetitive elements may comprise over two-thirds of the human genome.* PLoS Genet, 2011. **7**(12): p. e1002384.
123. Furmaga, W.B., et al., *Alu profiling of primary and metastatic nonsmall cell lung cancer.* Exp Mol Pathol, 2003. **74**(3): p. 224-9.
124. Gupta, P.K., et al., *Loss of heterozygosity analysis in a human fibrosarcoma cell line.* Cytogenet Cell Genet, 1997. **76**(3-4): p. 214-8.
125. Pal, J., et al., *Genomic evolution in Barrett's adenocarcinoma cells: critical roles of elevated hsRAD51, homologous recombination and Alu sequences in the genome.* Oncogene, 2011. **30**(33): p. 3585-98.
126. Strout, M.P., et al., *The partial tandem duplication of ALL1 (MLL) is consistently generated by Alu-mediated homologous recombination in acute myeloid leukemia.* Proc Natl Acad Sci U S A, 1998. **95**(5): p. 2390-5.
127. Roy, R., J. Chun, and S.N. Powell, *BRCA1 and BRCA2: different roles in a common pathway of genome protection.* Nat Rev Cancer, 2012. **12**(1): p. 68-78.
128. Sebesta, M., et al., *Role of PCNA and TLS polymerases in D-loop extension during homologous recombination in humans.* DNA Repair (Amst), 2013. **12**(9): p. 691-8.
129. Sharma, S., et al., *REV1 and polymerase zeta facilitate homologous recombination repair.* Nucleic Acids Res, 2012. **40**(2): p. 682-91.
130. McVey, M., et al., *Eukaryotic DNA Polymerases in Homologous Recombination.* Annu Rev Genet, 2016. **50**: p. 393-421.
131. Kiraly, O., et al., *DNA glycosylase activity and cell proliferation are key factors in modulating homologous recombination in vivo.* Carcinogenesis, 2014. **35**(11): p. 2495-502.
132. Calvo, J.A., et al., *Aag DNA glycosylase promotes alkylation-induced tissue damage mediated by Parp1.* PLoS Genet, 2013. **9**(4): p. e1003413.
133. Ebrahimkhani, M.R., et al., *Aag-initiated base excision repair promotes ischemia reperfusion injury in liver, brain, and kidney.* Proc Natl Acad Sci U S A, 2014. **111**(45): p. E4878-86.
134. Coquerelle, T., J. Dosch, and B. Kaina, *Overexpression of N-methylpurine-DNA glycosylase in Chinese hamster ovary cells renders them more sensitive to the production of chromosomal aberrations by methylating agents--a case of imbalanced DNA repair.* Mutat Res, 1995. **336**(1): p. 9-17.
135. Klapacz, J., et al., *Frameshift mutagenesis and microsatellite instability induced by human alkyladenine DNA glycosylase.* Mol Cell, 2010. **37**(6): p. 843-53.
136. Crosbie, P.A., et al., *Elevated N3-methylpurine-DNA glycosylase DNA repair activity is associated with lung cancer.* Mutat Res, 2012. **732**(1-2): p. 43-6.
137. Leitner-Dagan, Y., et al., *N-methylpurine DNA glycosylase and OGG1 DNA repair activities: opposite associations with lung cancer risk.* J Natl Cancer Inst, 2012. **104**(22): p. 1765-9.
138. Liu, C., et al., *Aberrant expression of N-methylpurine-DNA glycosylase influences patient survival in malignant gliomas.* J Biomed Biotechnol, 2012. **2012**: p. 760679.
139. Zdzalik, D., et al., *Differential repair of etheno-DNA adducts by bacterial and human AlkB proteins.* DNA Repair (Amst), 2015. **30**: p. 1-10.
140. Shafirovich, V., et al., *Base and Nucleotide Excision Repair of Oxidatively Generated Guanine Lesions in DNA.* J Biol Chem, 2016. **291**(10): p. 5309-19.
141. McKibbin, P.L., et al., *Repair of hydantoin lesions and their amine adducts in DNA by base and nucleotide excision repair.* J Am Chem Soc, 2013. **135**(37): p. 13851-61.

142. Escribano-Diaz, C., et al., *A cell cycle-dependent regulatory circuit composed of 53BP1-RIF1 and BRCA1-CtIP controls DNA repair pathway choice.* Mol Cell, 2013. **49**(5): p. 872-83.
143. Chapman, J.R., M.R. Taylor, and S.J. Boulton, *Playing the end game: DNA double-strand break repair pathway choice.* Mol Cell, 2012. **47**(4): p. 497-510.
144. Shibata, A., et al., *DNA double-strand break repair pathway choice is directed by distinct MRE11 nuclease activities.* Mol Cell, 2014. **53**(1): p. 7-18.
145. Kondo, N., et al., *DNA damage induced by alkylating agents and repair pathways.* J Nucleic Acids, 2010. **2010**: p. 543531.
146. Hofseth, L.J., et al., *The adaptive imbalance in base excision-repair enzymes generates microsatellite instability in chronic inflammation.* J Clin Invest, 2003. **112**(12): p. 1887-94.
147. Khanna, K.K. and S.P. Jackson, *DNA double-strand breaks: signaling, repair and the cancer connection.* Nat Genet, 2001. **27**(3): p. 247-54.
148. Lin, R., et al., *Chronic inflammation-related DNA damage response: a driving force of gastric cardia carcinogenesis.* Oncotarget, 2015. **6**(5): p. 2856-64.
149. He, H., et al., *DNA damage response in peritumoral regions of oesophageal cancer microenvironment.* Carcinogenesis, 2013. **34**(1): p. 139-45.
150. Jayakumar, S., D. Pal, and S.K. Sandur, *Nrf2 facilitates repair of radiation induced DNA damage through homologous recombination repair pathway in a ROS independent manner in cancer cells.* Mutat Res, 2015. **779**: p. 33-45.
151. Frontini, M., et al., *A ChIP-chip approach reveals a novel role for transcription factor IRF1 in the DNA damage response.* Nucleic Acids Res, 2009. **37**(4): p. 1073-85.
152. Volcic, M., et al., *NF-kappaB regulates DNA double-strand break repair in conjunction with BRCA1-CtIP complexes.* Nucleic Acids Res, 2012. **40**(1): p. 181-95.
153. Li, N., et al., *Influenza infection induces host DNA damage and dynamic DNA damage responses during tissue regeneration.* Cell Mol Life Sci, 2015. **72**(15): p. 2973-88.
154. Mani, R.S., et al., *Inflammation-Induced Oxidative Stress Mediates Gene Fusion Formation in Prostate Cancer.* Cell Rep, 2016. **17**(10): p. 2620-2631.
155. Chan, M.K., et al., *Targeted deletion of the genes encoding NTH1 and NEIL1 DNA N-glycosylases reveals the existence of novel carcinogenic oxidative damage to DNA.* DNA Repair (Amst), 2009. **8**(7): p. 786-94.
156. Klungland, A., et al., *Accumulation of premutagenic DNA lesions in mice defective in removal of oxidative base damage.* Proc Natl Acad Sci U S A, 1999. **96**(23): p. 13300-5.
157. Rushmore, T.H., M.R. Morton, and C.B. Pickett, *The antioxidant responsive element. Activation by oxidative stress and identification of the DNA consensus sequence required for functional activity.* J Biol Chem, 1991. **266**(18): p. 11632-9.
158. Ma, Q., *Role of nrf2 in oxidative stress and toxicity.* Annu Rev Pharmacol Toxicol, 2013. **53**: p. 401-26.
159. Kobayashi, M. and M. Yamamoto, *Nrf2-Keap1 regulation of cellular defense mechanisms against electrophiles and reactive oxygen species.* Adv Enzyme Regul, 2006. **46**: p. 113-40.
160. Nguyen, T., P. Nioi, and C.B. Pickett, *The Nrf2-antioxidant response element signaling pathway and its activation by oxidative stress.* J Biol Chem, 2009. **284**(20): p. 13291-5.
161. Kim, S.B., et al., *Targeting of Nrf2 induces DNA damage signaling and protects colonic epithelial cells from ionizing radiation.* Proc Natl Acad Sci U S A, 2012. **109**(43): p. E2949-55.

162. Singh, B., et al., *Antioxidant-mediated up-regulation of OGG1 via NRF2 induction is associated with inhibition of oxidative DNA damage in estrogen-induced breast cancer.* BMC Cancer, 2013. **13**: p. 253.
163. Aoki, Y., et al., *Enhanced spontaneous and benzo(a)pyrene-induced mutations in the lung of Nrf2-deficient gpt delta mice.* Cancer Res, 2007. **67**(12): p. 5643-8.
164. Kwak, M.K., et al., *Role of phase 2 enzyme induction in chemoprotection by dithiolethiones.* Mutat Res, 2001. **480-481**: p. 305-15.
165. Ramos-Gomez, M., et al., *Interactive effects of nrf2 genotype and oltipraz on benzo[a]pyrene-DNA adducts and tumor yield in mice.* Carcinogenesis, 2003. **24**(3): p. 461-7.
166. Ba, X., et al., *Trypanosoma cruzi induces the reactive oxygen species-PARP-1-RelA pathway for up-regulation of cytokine expression in cardiomyocytes.* J Biol Chem, 2010. **285**(15): p. 11596-606.
167. Stilmann, M., et al., *A nuclear poly(ADP-ribose)-dependent signalosome confers DNA damage-induced IkappaB kinase activation.* Mol Cell, 2009. **36**(3): p. 365-78.
168. Kameoka, M., et al., *Evidence for regulation of NF-kappaB by poly(ADP-ribose) polymerase.* Biochem J, 2000. **346 Pt 3**: p. 641-9.
169. Pamment, J., et al., *Regulation of the IRF-1 tumour modifier during the response to genotoxic stress involves an ATM-dependent signalling pathway.* Oncogene, 2002. **21**(51): p. 7776-85.
170. Kim, T.K., et al., *Chemotherapeutic DNA-damaging drugs activate interferon regulatory factor-7 by the mitogen-activated protein kinase kinase-4-cJun NH2-terminal kinase pathway.* Cancer Res, 2000. **60**(5): p. 1153-6.
171. Lee, R.B., et al., *Interactions of Campylobacter jejuni cytolethal distending toxin subunits CdtA and CdtC with HeLa cells.* Infect Immun, 2003. **71**(9): p. 4883-90.
172. Cuevas-Ramos, G., et al., *Escherichia coli induces DNA damage in vivo and triggers genomic instability in mammalian cells.* Proc Natl Acad Sci U S A, 2010. **107**(25): p. 11537-42.
173. Ge, Z., D.B. Schauer, and J.G. Fox, *In vivo virulence properties of bacterial cytolethal-distending toxin.* Cell Microbiol, 2008. **10**(8): p. 1599-607.
174. Chan, T.K., et al., *House dust mite-induced asthma causes oxidative damage and DNA double-strand breaks in the lungs.* J Allergy Clin Immunol, 2016. **138**(1): p. 84-96 e1.
175. Rai, P., et al., *Pneumococcal Pneumolysin Induces DNA Damage and Cell Cycle Arrest.* Sci Rep, 2016. **6**: p. 22972.
176. Xue, W., et al., *Senescence and tumour clearance is triggered by p53 restoration in murine liver carcinomas.* Nature, 2007. **445**(7128): p. 656-60.
177. Rodier, F., et al., *Persistent DNA damage signalling triggers senescence-associated inflammatory cytokine secretion.* Nat Cell Biol, 2009. **11**(8): p. 973-9.
178. Biton, S. and A. Ashkenazi, *NEMO and RIP1 control cell fate in response to extensive DNA damage via TNF-alpha feedforward signaling.* Cell, 2011. **145**(1): p. 92-103.
179. Brzostek-Racine, S., et al., *The DNA damage response induces IFN.* J Immunol, 2011. **187**(10): p. 5336-45.
180. Yang, X., et al., *HMGB1: a novel protein that induced platelets active and aggregation via Toll-like receptor-4, NF-kappaB and cGMP dependent mechanisms.* Diagn Pathol, 2015. **10**: p. 134.
181. Aggen, J.B., A.C. Nairn, and R. Chamberlin, *Regulation of protein phosphatase-1.* Chem Biol, 2000. **7**(1): p. R13-23.

182. Kim, S.B., et al., *Radiation promotes colorectal cancer initiation and progression by inducing senescence-associated inflammatory responses.* Oncogene, 2016. **35**(26): p. 3365-75.
183. Chaudhry, M.A., *Bystander effect: biological endpoints and microarray analysis.* Mutat Res, 2006. **597**(1-2): p. 98-112.
184. Nagasawa, H. and J.B. Little, *Unexpected sensitivity to the induction of mutations by very low doses of alpha-particle radiation: evidence for a bystander effect.* Radiat Res, 1999. **152**(5): p. 552-7.
185. Rugo, R.E., et al., *Methyltransferases mediate cell memory of a genotoxic insult.* Oncogene, 2011. **30**(6): p. 751-6.
186. Rugo, R.E., et al., *A single acute exposure to a chemotherapeutic agent induces hyper-recombination in distantly descendant cells and in their neighbors.* Oncogene, 2005. **24**(32): p. 5016-25.
187. Rao, V.P., et al., *Innate immune inflammatory response against enteric bacteria Helicobacter hepaticus induces mammary adenocarcinoma in mice.* Cancer Res, 2006. **66**(15): p. 7395-400.
188. Westbrook, A.M., et al., *Intestinal mucosal inflammation leads to systemic genotoxicity in mice.* Cancer Res, 2009. **69**(11): p. 4827-34.
189. Westbrook, A.M., et al., *Intestinal inflammation induces genotoxicity to extraintestinal tissues and cell types in mice.* Int J Cancer, 2011. **129**(8): p. 1815-25.
190. Poutahidis, T., et al., *Pathogenic intestinal bacteria enhance prostate cancer development via systemic activation of immune cells in mice.* PLoS One, 2013. **8**(8): p. e73933.
191. Satoh, M.S., G.G. Poirier, and T. Lindahl, *Dual function for poly(ADP-ribose) synthesis in response to DNA strand breakage.* Biochemistry, 1994. **33**(23): p. 7099-106.
192. Langelier, M.F., et al., *Structural basis for DNA damage-dependent poly(ADP-ribosyl)ation by human PARP-1.* Science, 2012. **336**(6082): p. 728-32.
193. Bryant, H.E., et al., *PARP is activated at stalled forks to mediate Mre11-dependent replication restart and recombination.* EMBO J, 2009. **28**(17): p. 2601-15.
194. Hegde, M.L., T.K. Hazra, and S. Mitra, *Early steps in the DNA base excision/single-strand interruption repair pathway in mammalian cells.* Cell Res, 2008. **18**(1): p. 27-47.
195. Haince, J.F., et al., *Ataxia telangiectasia mutated (ATM) signaling network is modulated by a novel poly(ADP-ribose)-dependent pathway in the early response to DNA-damaging agents.* J Biol Chem, 2007. **282**(22): p. 16441-53.
196. Oliver, F.J., et al., *Resistance to endotoxic shock as a consequence of defective NF-kappaB activation in poly (ADP-ribose) polymerase-1 deficient mice.* EMBO J, 1999. **18**(16): p. 4446-54.
197. Altmeyer, M., et al., *Absence of poly(ADP-ribose) polymerase 1 delays the onset of Salmonella enterica serovar Typhimurium-induced gut inflammation.* Infect Immun, 2010. **78**(8): p. 3420-31.
198. Mazzon, E., et al., *Effects of 3-aminobenzamide, an inhibitor of poly (ADP-ribose) polymerase, in a mouse model of acute pancreatitis induced by cerulein.* Eur J Pharmacol, 2006. **549**(1-3): p. 149-56.
199. Chopra, M. and A.C. Sharma, *Distinct cardiodynamic and molecular characteristics during early and late stages of sepsis-induced myocardial dysfunction.* Life Sci, 2007. **81**(4): p. 306-16.
200. Czapski, G.A., et al., *Poly(ADP-ribose) polymerase-1 inhibition protects the brain against systemic inflammation.* Neurochem Int, 2006. **49**(8): p. 751-5.

201. Mota, R.A., et al., *Poly(ADP-ribose) polymerase-1 inhibition increases expression of heat shock proteins and attenuates heat stroke-induced liver injury.* Crit Care Med, 2008. **36**(2): p. 526-34.
202. Garcia, S., et al., *Partial protection against collagen antibody-induced arthritis in PARP-1 deficient mice.* Arthritis Res Ther, 2006. **8**(1): p. R14.
203. von Lukowicz, T., et al., *PARP1 is required for adhesion molecule expression in atherogenesis.* Cardiovasc Res, 2008. **78**(1): p. 158-66.
204. Boulares, A.H., et al., *Gene knockout or pharmacological inhibition of poly(ADP-ribose) polymerase-1 prevents lung inflammation in a murine model of asthma.* Am J Respir Cell Mol Biol, 2003. **28**(3): p. 322-9.
205. Veres, B., et al., *Decrease of the inflammatory response and induction of the Akt/protein kinase B pathway by poly-(ADP-ribose) polymerase 1 inhibitor in endotoxin-induced septic shock.* Biochem Pharmacol, 2003. **65**(8): p. 1373-82.
206. Mabley, J.G., et al., *Anti-inflammatory effects of a novel, potent inhibitor of poly (ADP-ribose) polymerase.* Inflamm Res, 2001. **50**(11): p. 561-9.
207. Haddad, M., et al., *Anti-inflammatory effects of PJ34, a poly(ADP-ribose) polymerase inhibitor, in transient focal cerebral ischemia in mice.* Br J Pharmacol, 2006. **149**(1): p. 23-30.
208. Hasko, G., et al., *Poly(ADP-ribose) polymerase is a regulator of chemokine production: relevance for the pathogenesis of shock and inflammation.* Mol Med, 2002. **8**(5): p. 283-9.
209. Ba, X. and N.J. Garg, *Signaling mechanism of poly(ADP-ribose) polymerase-1 (PARP-1) in inflammatory diseases.* Am J Pathol, 2011. **178**(3): p. 946-55.
210. Szabo, C., et al., *Inhibition of poly (ADP-ribose) synthetase attenuates neutrophil recruitment and exerts antiinflammatory effects.* J Exp Med, 1997. **186**(7): p. 1041-9.
211. Jagtap, P. and C. Szabo, *Poly(ADP-ribose) polymerase and the therapeutic effects of its inhibitors.* Nat Rev Drug Discov, 2005. **4**(5): p. 421-40.
212. Davar, D., et al., *Role of PARP inhibitors in cancer biology and therapy.* Curr Med Chem, 2012. **19**(23): p. 3907-21.
213. Meehan, R.S. and A.P. Chen, *New treatment option for ovarian cancer: PARP inhibitors.* Gynecol Oncol Res Pract, 2016. **3**: p. 3.
214. Pan, L., et al., *OGG1-DNA interactions facilitate NF-kappaB binding to DNA targets.* Sci Rep, 2017. **7**: p. 43297.
215. Pan, L., et al., *Oxidized Guanine Base Lesions Function in 8-Oxoguanine DNA Glycosylase-1-mediated Epigenetic Regulation of Nuclear Factor kappaB-driven Gene Expression.* J Biol Chem, 2016. **291**(49): p. 25553-25566.
216. Ba, X., et al., *8-oxoguanine DNA glycosylase-1 augments proinflammatory gene expression by facilitating the recruitment of site-specific transcription factors.* J Immunol, 2014. **192**(5): p. 2384-94.
217. Bacsi, A., et al., *Down-regulation of 8-oxoguanine DNA glycosylase 1 expression in the airway epithelium ameliorates allergic lung inflammation.* DNA Repair (Amst), 2013. **12**(1): p. 18-26.
218. Mabley, J.G., et al., *Potential role for 8-oxoguanine DNA glycosylase in regulating inflammation.* FASEB J, 2005. **19**(2): p. 290-2.
219. Aguilera-Aguirre, L., et al., *Innate inflammation induced by the 8-oxoguanine DNA glycosylase-1-KRAS-NF-kappaB pathway.* J Immunol, 2014. **193**(9): p. 4643-53.
220. Boldogh, I., et al., *Activation of ras signaling pathway by 8-oxoguanine DNA glycosylase bound to its excision product, 8-oxoguanine.* J Biol Chem, 2012. **287**(25): p. 20769-73.

221. Gasser, S., et al., *The DNA damage pathway regulates innate immune system ligands of the NKG2D receptor.* Nature, 2005. **436**(7054): p. 1186-90.
222. Tanaka, Y., et al., *Effects of growth arrest and DNA damage-inducible protein 34 (GADD34) on inflammation-induced colon cancer in mice.* Br J Cancer, 2015. **113**(4): p. 669-79.
223. Chen, N., et al., *Growth arrest and DNA damage-inducible protein (GADD34) enhanced liver inflammation and tumorigenesis in a diethylnitrosamine (DEN)-treated murine model.* Cancer Immunol Immunother, 2015. **64**(6): p. 777-89.
224. Dombrowski, Y., et al., *Cytosolic DNA triggers inflammasome activation in keratinocytes in psoriatic lesions.* Sci Transl Med, 2011. **3**(82): p. 82ra38.
225. Ferguson, B.J., et al., *DNA-PK is a DNA sensor for IRF-3-dependent innate immunity.* Elife, 2012. **1**: p. e00047.
226. Kondo, T., et al., *DNA damage sensor MRE11 recognizes cytosolic double-stranded DNA and induces type I interferon by regulating STING trafficking.* Proc Natl Acad Sci U S A, 2013. **110**(8): p. 2969-74.
227. Jaiswal, M., et al., *Inflammatory cytokines induce DNA damage and inhibit DNA repair in cholangiocarcinoma cells by a nitric oxide-dependent mechanism.* Cancer Res, 2000. **60**(1): p. 184-90.
228. Morreall, J., et al., *Inactivation of a common OGG1 variant by TNF-alpha in mammalian cells.* DNA Repair (Amst), 2015. **26**: p. 15-22.
229. Qu, J., et al., *Nitric oxide controls nuclear export of APE1/Ref-1 through S-nitrosation of cysteines 93 and 310.* Nucleic Acids Res, 2007. **35**(8): p. 2522-32.
230. Laval, F. and D.A. Wink, *Inhibition by nitric oxide of the repair protein, O6-methylguanine-DNA-methyltransferase.* Carcinogenesis, 1994. **15**(3): p. 443-7.
231. Wink, D.A. and J. Laval, *The Fpg protein, a DNA repair enzyme, is inhibited by the biomediator nitric oxide in vitro and in vivo.* Carcinogenesis, 1994. **15**(10): p. 2125-9.
232. Wei, W., et al., *S-nitrosylation from GSNOR deficiency impairs DNA repair and promotes hepatocarcinogenesis.* Sci Transl Med, 2010. **2**(19): p. 19ra13.
233. Jaiswal, M., et al., *Human Ogg1, a protein involved in the repair of 8-oxoguanine, is inhibited by nitric oxide.* Cancer Res, 2001. **61**(17): p. 6388-93.
234. Jones, L.E., Jr., et al., *Differential effects of reactive nitrogen species on DNA base excision repair initiated by the alkyladenine DNA glycosylase.* Carcinogenesis, 2009. **30**(12): p. 2123-9.
235. Graziewicz, M., D.A. Wink, and F. Laval, *Nitric oxide inhibits DNA ligase activity: potential mechanisms for NO-mediated DNA damage.* Carcinogenesis, 1996. **17**(11): p. 2501-5.
236. Wink, D.A., et al., *Reaction kinetics for nitrosation of cysteine and glutathione in aerobic nitric oxide solutions at neutral pH. Insights into the fate and physiological effects of intermediates generated in the NO/O2 reaction.* Chem Res Toxicol, 1994. **7**(4): p. 519-25.
237. Foster, M.W., D.T. Hess, and J.S. Stamler, *Protein S-nitrosylation in health and disease: a current perspective.* Trends Mol Med, 2009. **15**(9): p. 391-404.
238. Liu, L., et al., *Inactivation and degradation of O(6)-alkylguanine-DNA alkyltransferase after reaction with nitric oxide.* Cancer Res, 2002. **62**(11): p. 3037-43.
239. Tang, C.H., W. Wei, and L. Liu, *Regulation of DNA repair by S-nitrosylation.* Biochim Biophys Acta, 2012. **1820**(6): p. 730-5.
240. Sugimura, H., et al., *hOGG1 Ser326Cys polymorphism and lung cancer susceptibility.* Cancer Epidemiol Biomarkers Prev, 1999. **8**(8): p. 669-74.

241. Yu, A.M., et al., *The Mbd4 DNA glycosylase protects mice from inflammation-driven colon cancer and tissue injury.* Oncotarget, 2016. **7**(19): p. 28624-36.
242. Parkin, D.M., *The global health burden of infection-associated cancers in the year 2002.* Int J Cancer, 2006. **118**(12): p. 3030-44.
243. Gossen, J.A., et al., *Efficient rescue of integrated shuttle vectors from transgenic mice: a model for studying mutations in vivo.* Proc Natl Acad Sci U S A, 1989. **86**(20): p. 7971-5.
244. Kohler, S.W., et al., *Spectra of spontaneous and mutagen-induced mutations in the lacI gene in transgenic mice.* Proc Natl Acad Sci U S A, 1991. **88**(18): p. 7958-62.
245. Nohmi, T., et al., *A new transgenic mouse mutagenesis test system using Spi- and 6-thioguanine selections.* Environ Mol Mutagen, 1996. **28**(4): p. 465-70.
246. Swiger, R.R., et al., *Further characterization and validation of gpt delta transgenic mice for quantifying somatic mutations in vivo.* Environ Mol Mutagen, 2001. **37**(4): p. 297-303.
247. Cosentino, L. and J.A. Heddle, *A test for neutrality of mutations of the lacZ transgene.* Environ Mol Mutagen, 1996. **28**(4): p. 313-6.
248. Hendricks, C.A., et al., *Spontaneous mitotic homologous recombination at an enhanced yellow fluorescent protein (EYFP) cDNA direct repeat in transgenic mice.* Proc Natl Acad Sci U S A, 2003. **100**(11): p. 6325-30.
249. Wiktor-Brown, D.M., et al., *Tissue-specific differences in the accumulation of sequence rearrangements with age.* DNA Repair (Amst), 2008. **7**(5): p. 694-703.
250. Soriano, P., *Generalized lacZ expression with the ROSA26 Cre reporter strain.* Nat Genet, 1999. **21**(1): p. 70-1.
251. Sukup-Jackson, M.R., et al., *Rosa26-GFP direct repeat (RaDR-GFP) mice reveal tissue- and age-dependence of homologous recombination in mammals in vivo.* PLoS Genet, 2014. **10**(6): p. e1004299.
252. Kimoto, T., et al., *Recombinant cells in the lung increase with age via de novo recombination events and clonal expansion.* Environ Mol Mutagen, 2017. **58**(3): p. 135-145.
253. Kass, E.M., et al., *Double-strand break repair by homologous recombination in primary mouse somatic cells requires BRCA1 but not the ATM kinase.* Proc Natl Acad Sci U S A, 2013. **110**(14): p. 5564-9.
254. Moynahan, M.E. and M. Jasin, *Mitotic homologous recombination maintains genomic stability and suppresses tumorigenesis.* Nat Rev Mol Cell Biol, 2010. **11**(3): p. 196-207.
255. Noda, A., et al., *Creation of Mice Bearing a Partial Duplication of HPRT Gene Marked with a GFP Gene and Detection of Revertant Cells In Situ as GFP-Positive Somatic Cells.* PLoS One, 2015. **10**(8): p. e0136041.
256. Andersen, S.L. and J. Sekelsky, *Meiotic versus mitotic recombination: two different routes for double-strand break repair: the different functions of meiotic versus mitotic DSB repair are reflected in different pathway usage and different outcomes.* Bioessays, 2010. **32**(12): p. 1058-66.
257. Simons, B.D. and H. Clevers, *Stem cell self-renewal in intestinal crypt.* Exp Cell Res, 2011. **317**(19): p. 2719-24.
258. Barker, N., *Adult intestinal stem cells: critical drivers of epithelial homeostasis and regeneration.* Nat Rev Mol Cell Biol, 2014. **15**(1): p. 19-33.

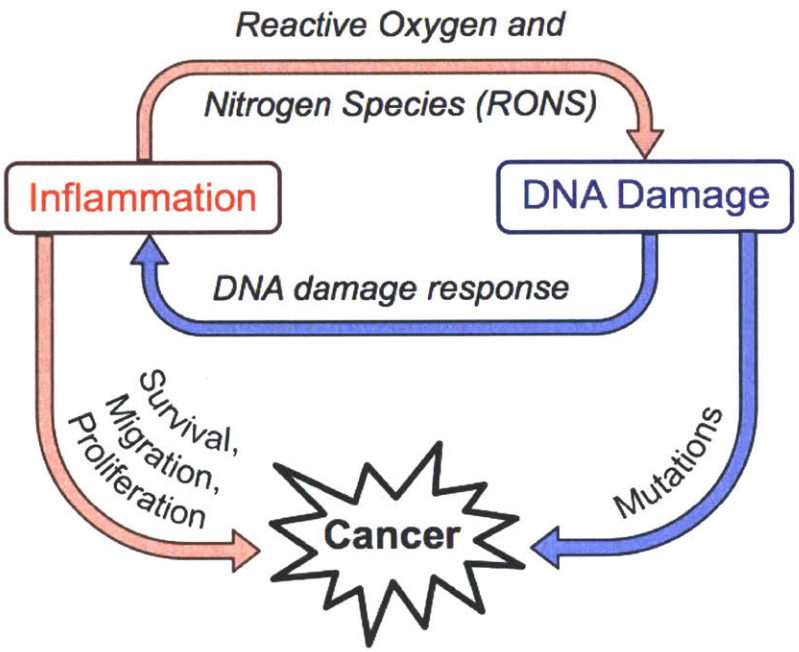

Figure 1-1. Diagram describing the relationship between inflammation and DNA damage and how they contribute to cancer.

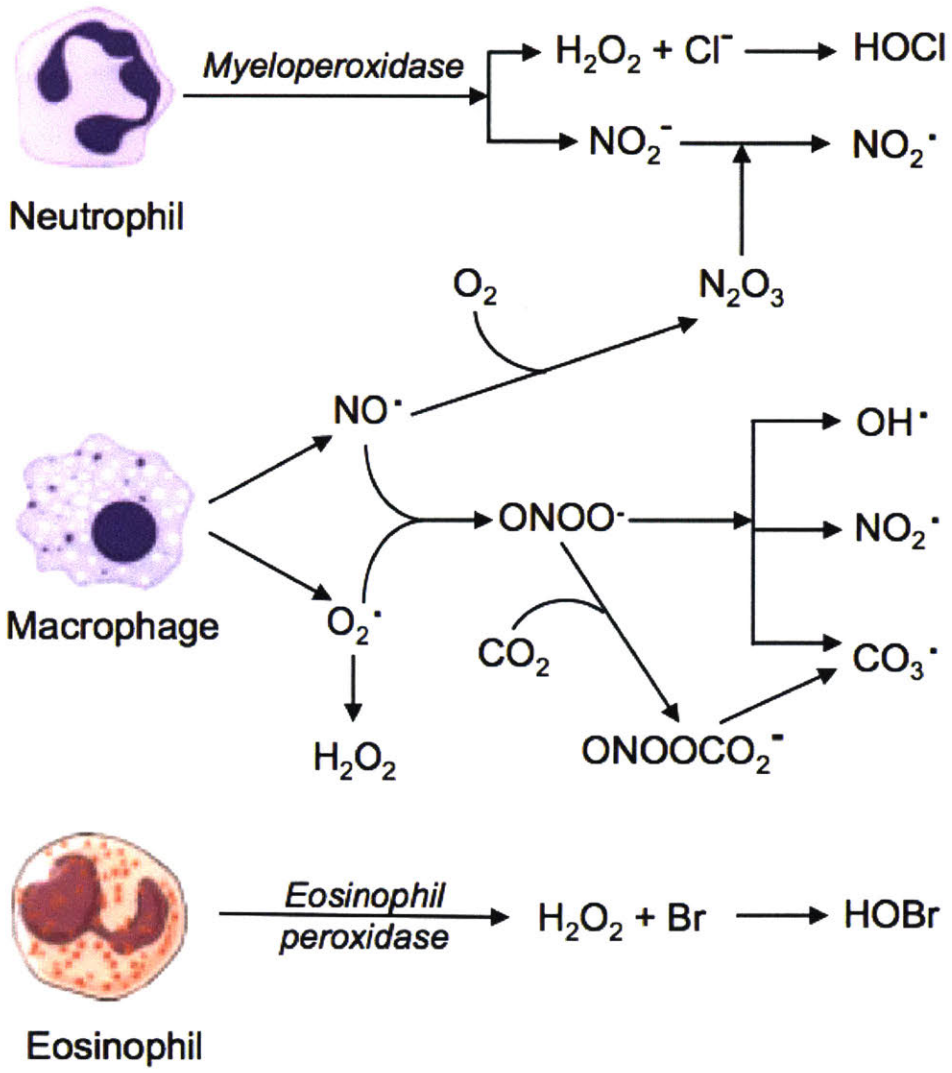

Figure 1-2. Reactive oxygen and nitrogen species produced from innate immune cells. Adapted from Dedon and Tannenbaum, *Arch Biochem Biophys*, 2004.

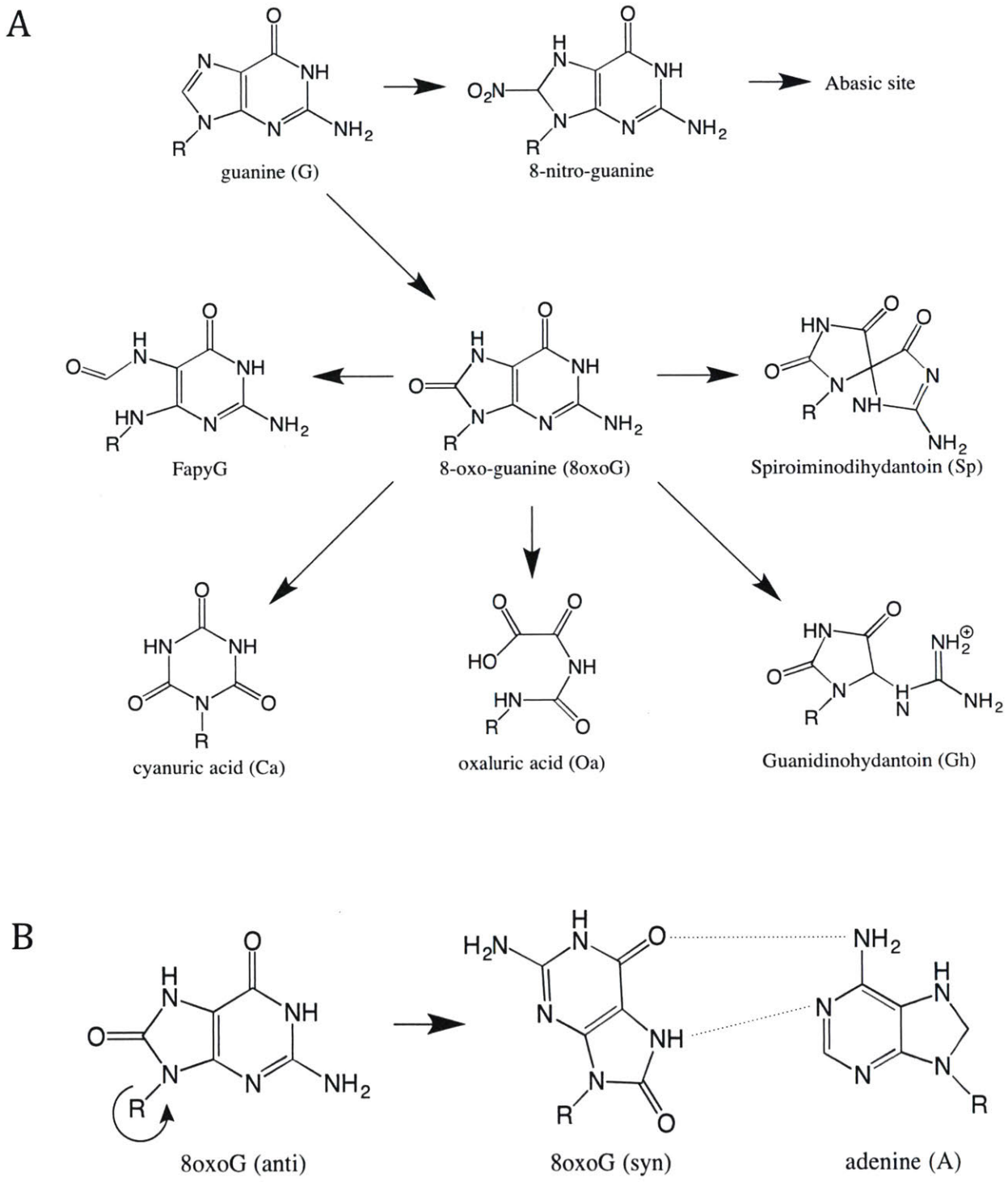

Figure 1-3. (A) Products of guanine oxidation. (B) Rotation of 8oxoG around its glycosydic bond causes mispairing with A.

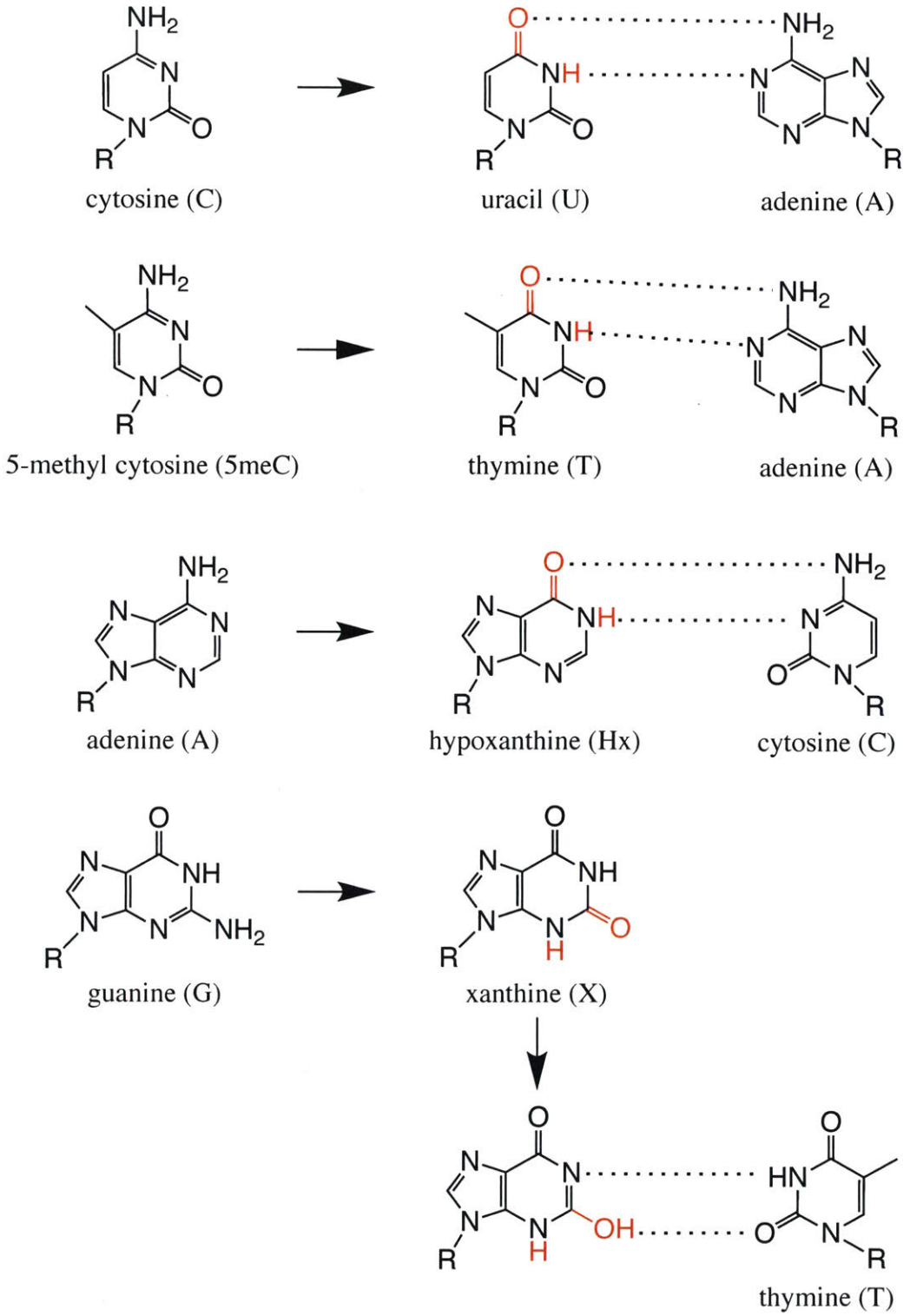

Figure 1-4. Products of DNA deamination and subsequent base mispairing.

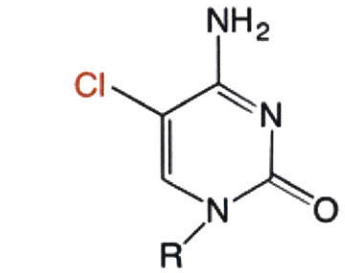

5-chloro-cytosine

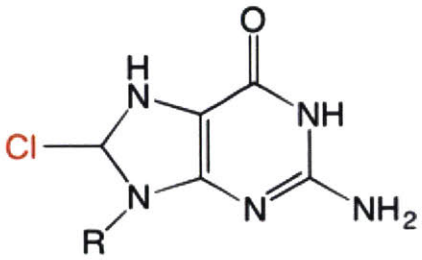

8-chloro-guanine

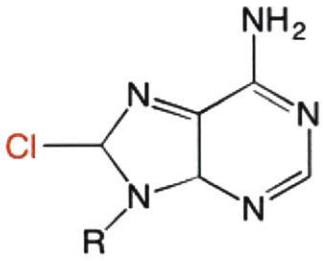

8-chloro-adenine

Figure 1-5. Products of DNA halogenation.

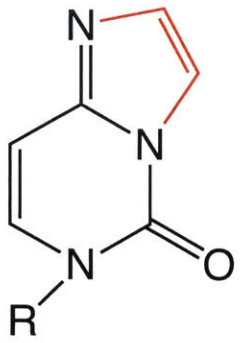

3, N^4-etheno-cytosine

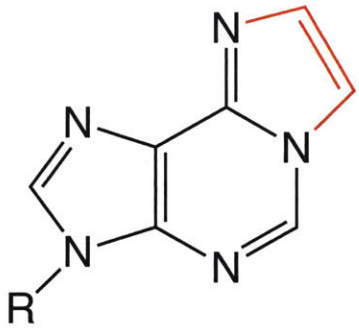

1, N^6-etheno-adenine

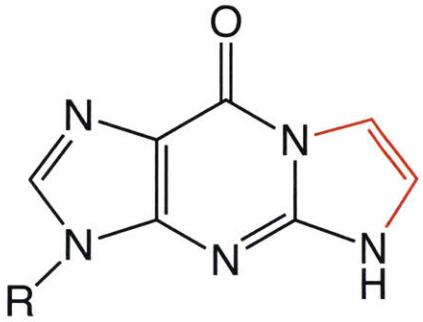

1, N^2-etheno-guanine

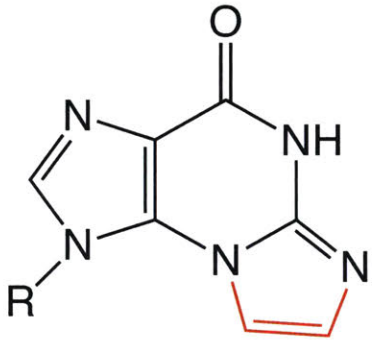

N^2, 3-etheno-guanine

Figure 1-6. Products of DNA alkylation following electrophilic attack by lipid peroxidation products.

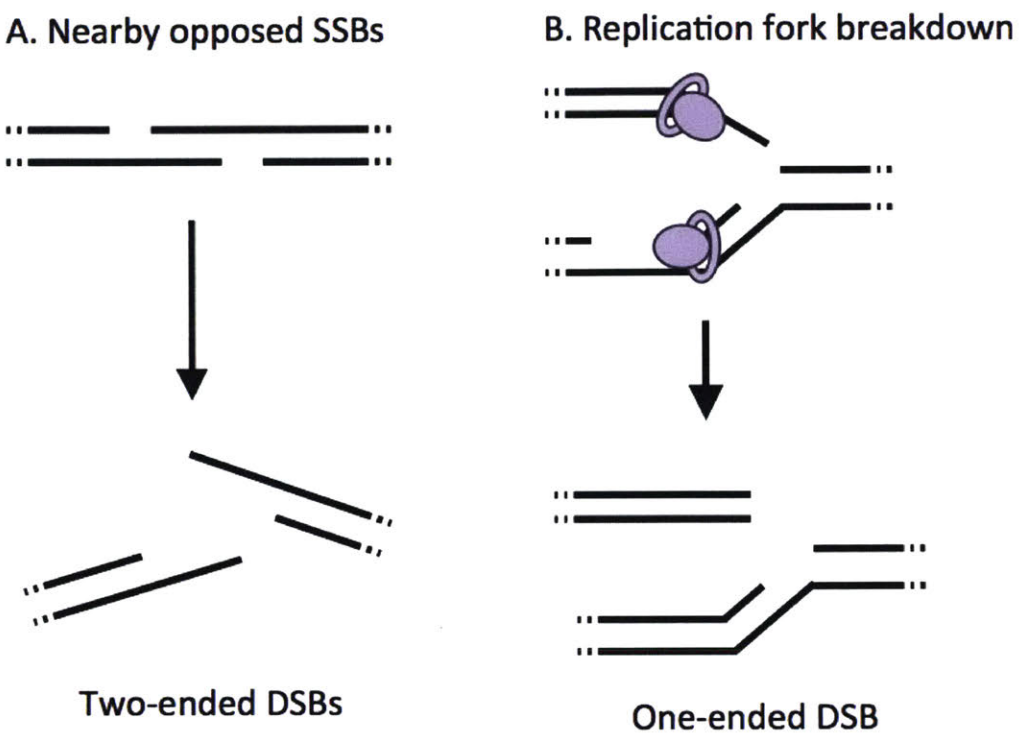

Figure 1-7. Modes by which single strand breaks may become double strand breaks.

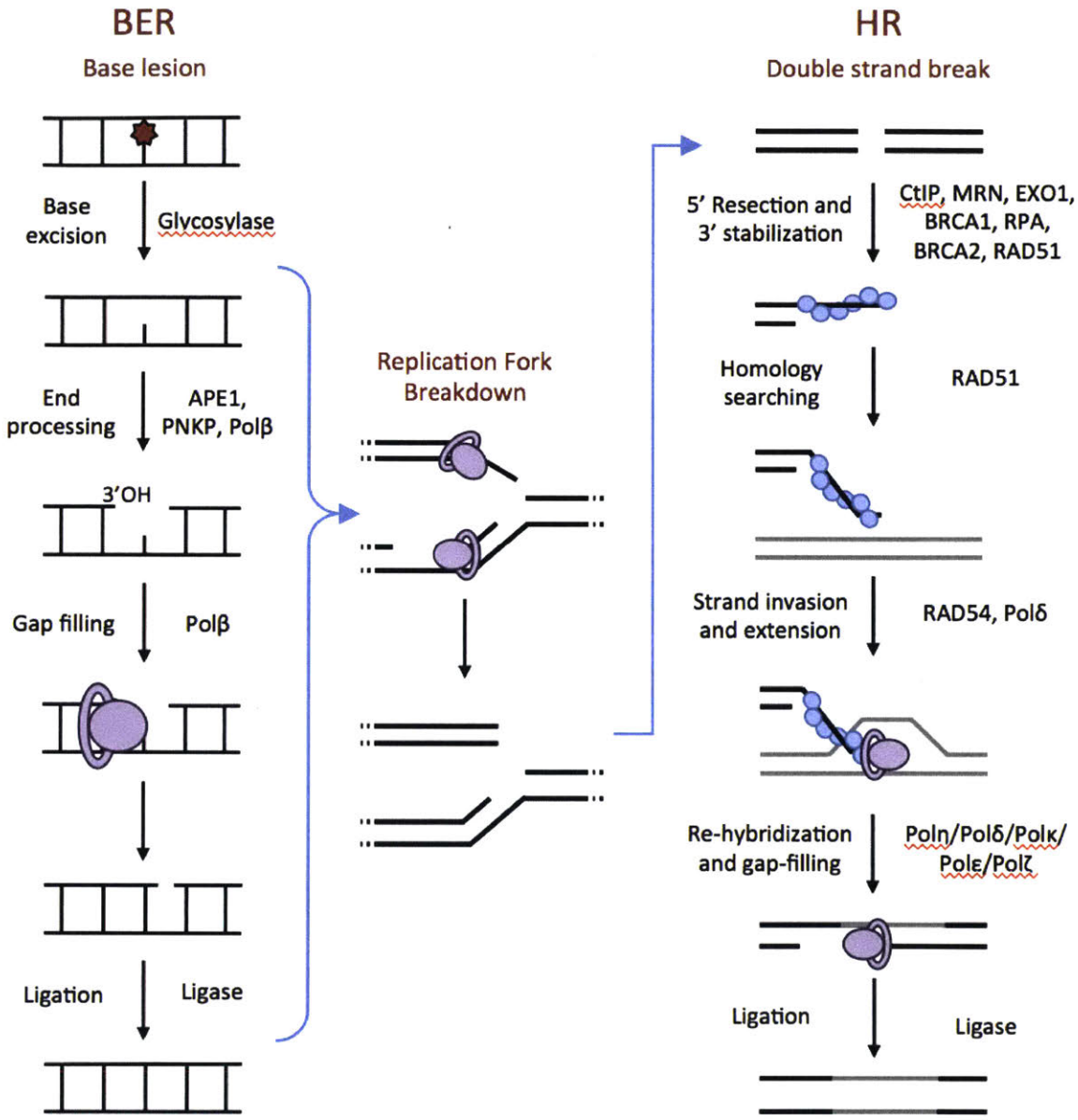

Figure 1-8. Base excision repair pathway, homologous recombination pathway, and how BER intermediates may lead to HR.

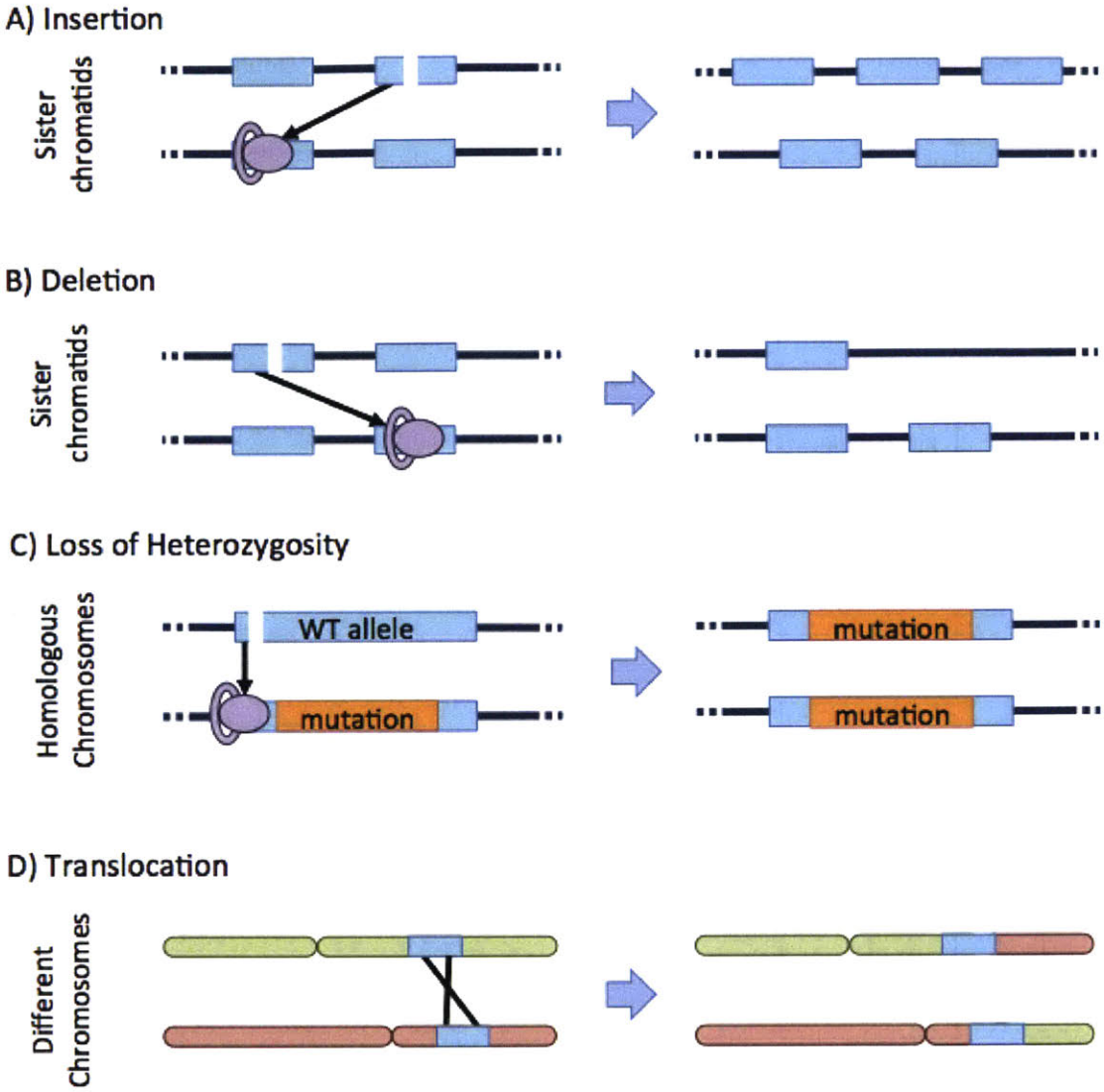

Figure 1-9. Potential mechanisms for HR-derived mutations

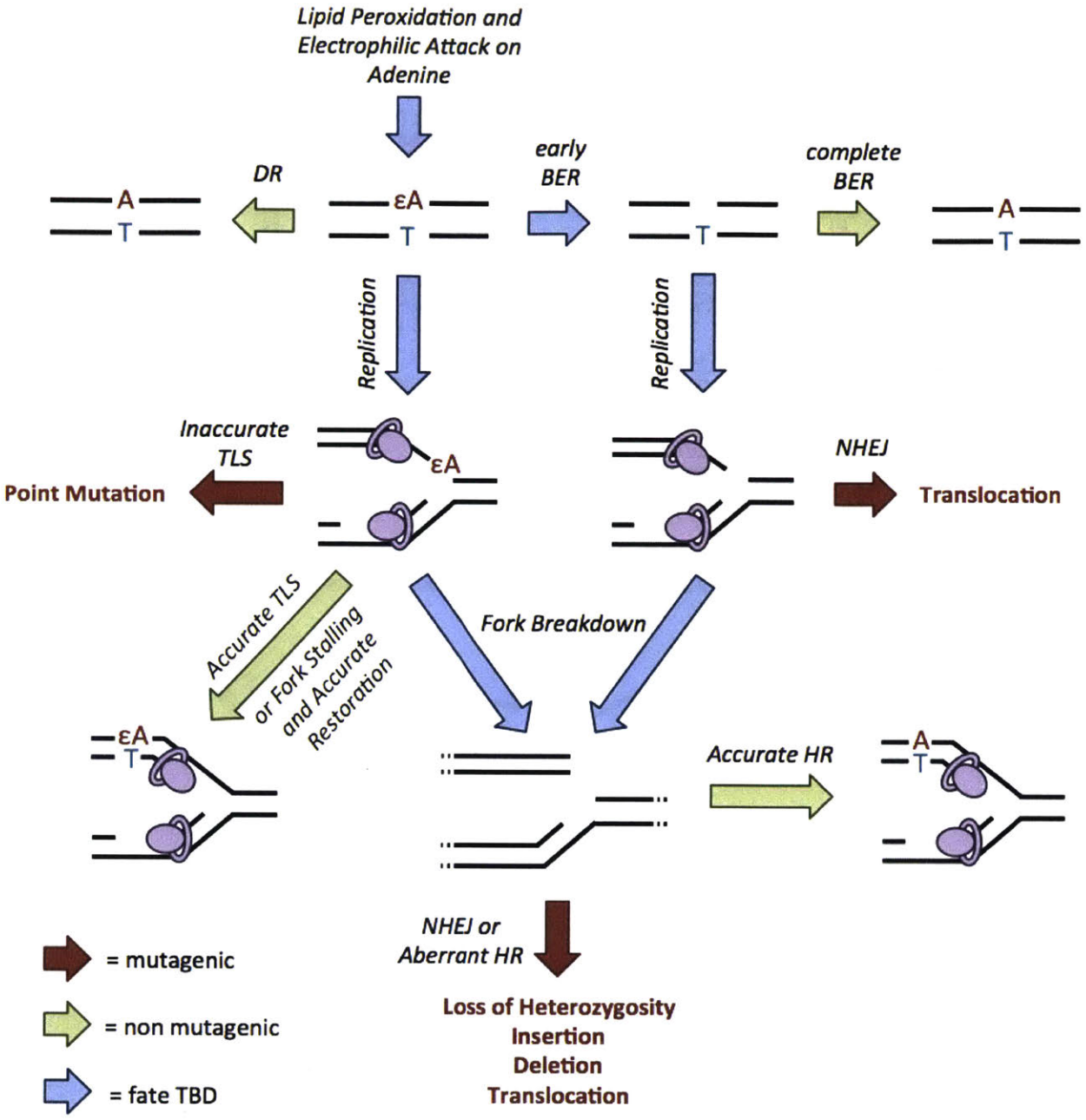

Figure 1-10. Pathways leading from a single base lesion to multiple types of mutations.

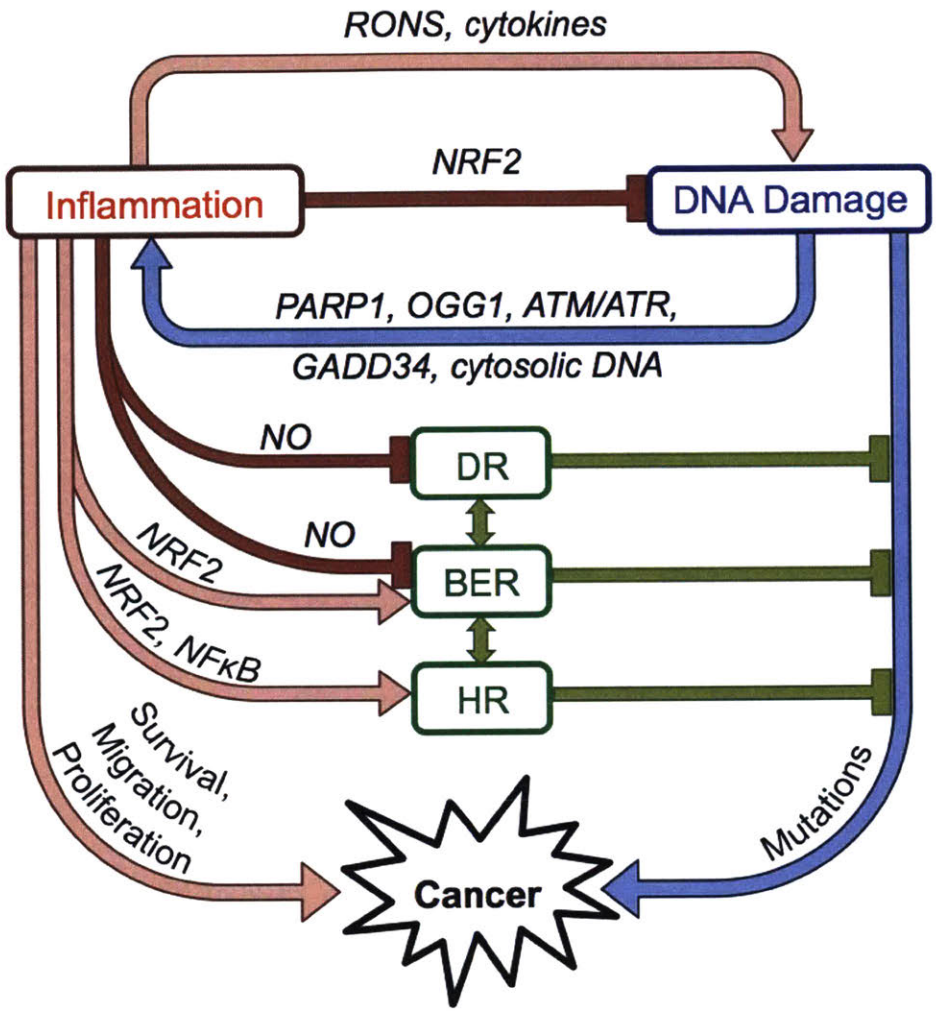

Figure 1-11. Expanded paradigm describing relationships between inflammation, DNA damage and cancer.

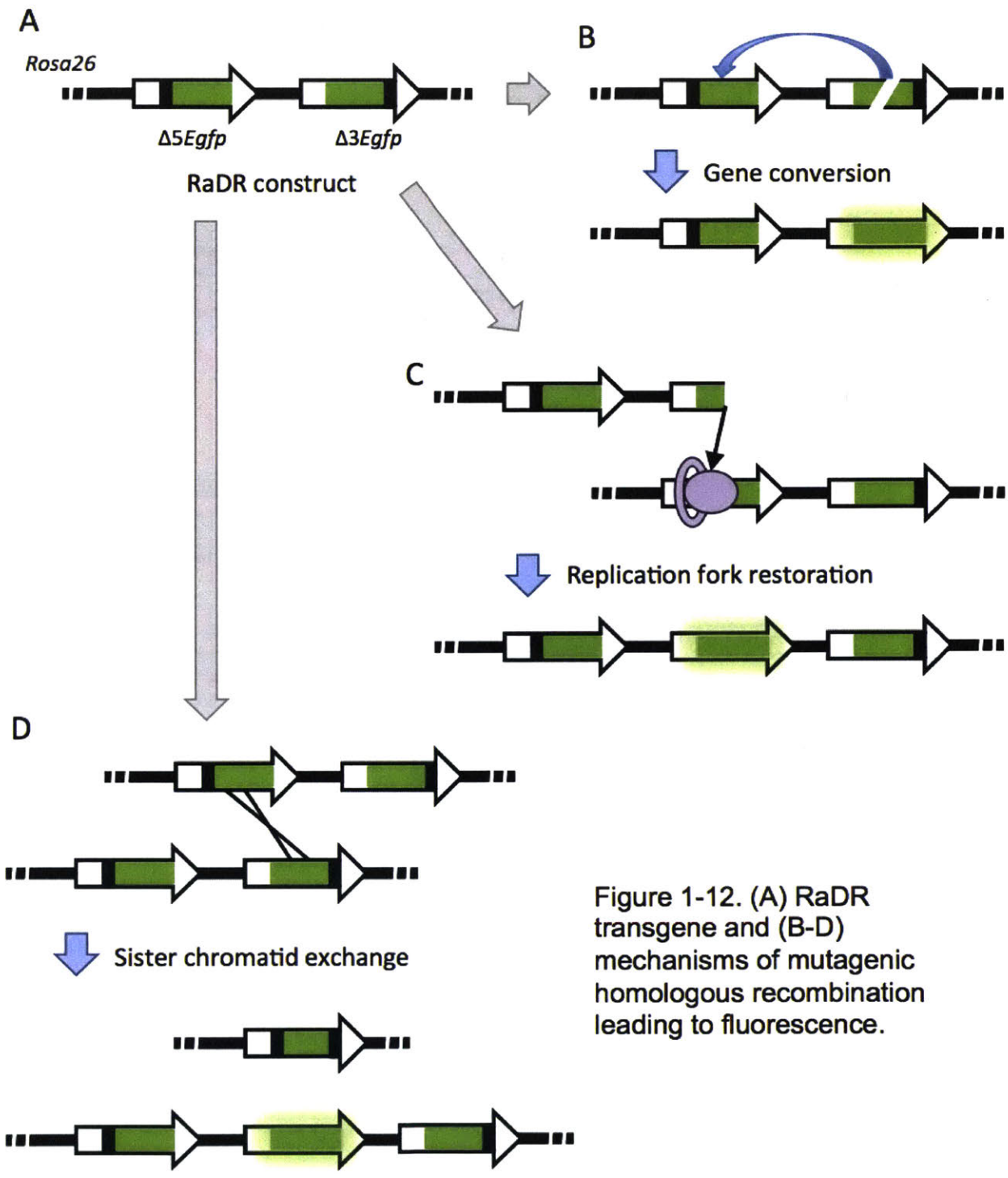

Figure 1-12. (A) RaDR transgene and (B-D) mechanisms of mutagenic homologous recombination leading to fluorescence.

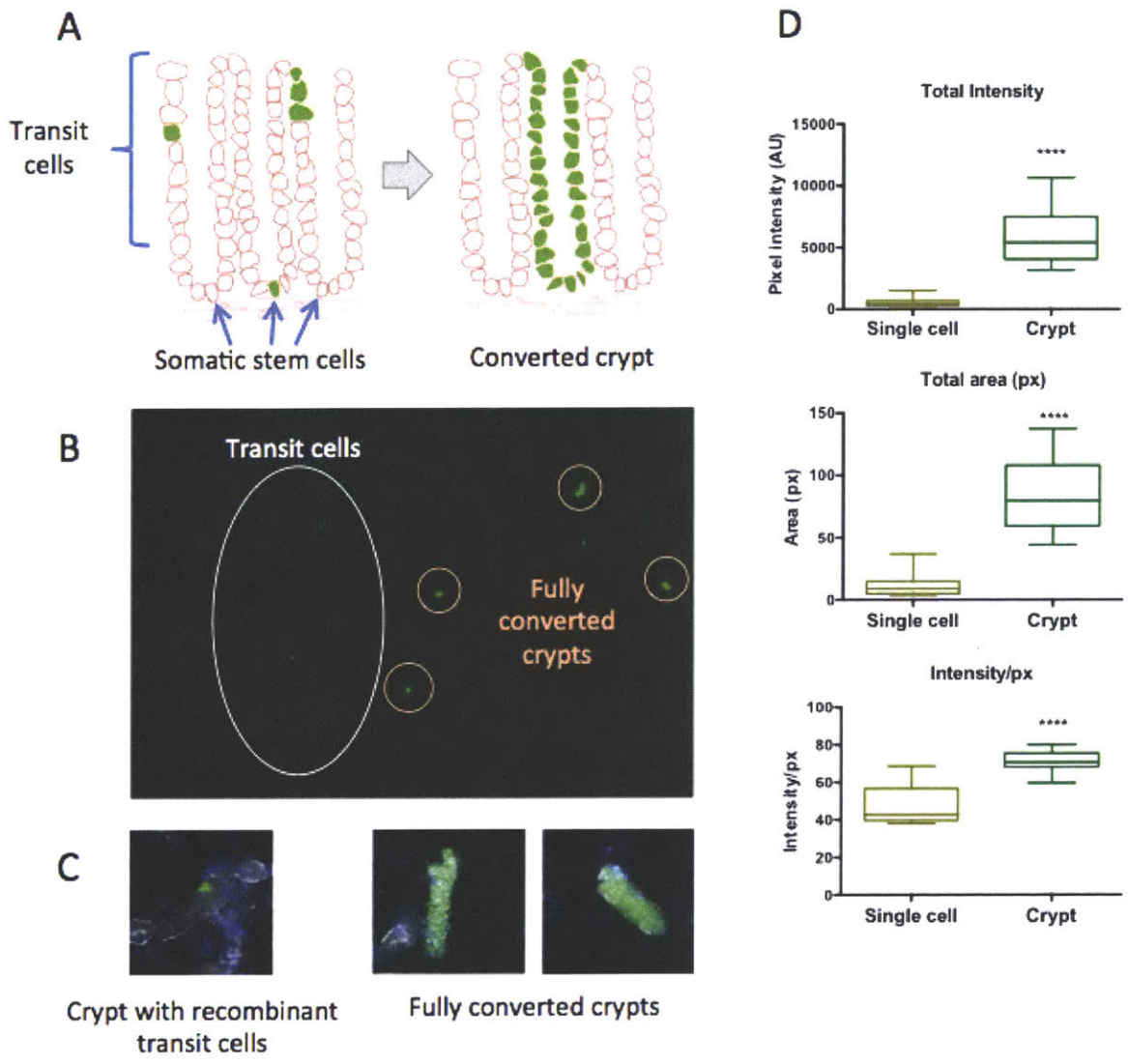

Figure 1-13. (A) Cross-sectional diagram of crypt epithelium. (B) Appearance of transit cell and crypt foci in RaDR colon tissue. (C) Disaggregated RaDR crypts in suspension. Left, crypt with mutant transit cells left. Right, fully fluorescent crypts. (D) Intensity and size comparisons of single cell and crypt foci.

Chapter 2

Roles of Immune Regulation in Initiation of Sequence Rearrangement Mutations

2.1 Abstract

Chronic inflammation is a major risk factor for cancer, but its roles in cancer initiation and promotion have yet to be fully delineated. Cancer arises from the accumulation of genetic alterations (i.e., mutations and epigenetics), and inflammation is known to promote mutations, but it remains unclear whether the mutations caused by inflammation drive cancer or simply accelerate it. Furthermore, it is unclear whether inflammation must be severe, chronic, and/or dysregulated to be carcinogenic. In this study, we utilized the RaDR transgenic mouse, which allows *in situ* detection of sequence rearrangement mutations, to query how different aspects of inflammation regulation impact mutagenesis. First, we examined the accumulation of RaDR mutations in unchallenged immunocompromised mice to determine whether regulation of the innate immune system has a role in preventing or promoting mutagenesis. Second, we evaluated RaDR mutations in $Apc^{Min/+}$ mice, which contain a driver mutation for intestinal cancer, and were given an anti-inflammatory treatment. The first of these studies revealed that impairment of the adaptive immune system may promote mutagenesis, suggesting a role for dysregulated inflammation in cancer initiation. Attenuation of endogenous inflammation reduced tumor multiplicity as well as overall burden of recombinant cells in the tissue, but we did not observe a significant reduction in recombination frequency indicating that inflammation promotes cancer

through mechanisms aside from *de novo* mutagenesis. Together, these studies indicate that while adaptive immunity may protect against mutations, the promotion of cancer by inflammation does not rely on increased mutagenesis.

2.2 Introduction

Chronic inflammatory diseases, such as Crohn's disease, ulcerative colitis, pancreatitis, and hepatitis, are major risk factors for cancer. Inflammation contributes to cancer development in a variety of ways, and one of the most important is that inflammation causes DNA damage, which leads to mutations. During inflammation, innate immune cells produce large amounts of reactive oxygen and nitrogen species (RONS) evolved to destroy pathogens, but those chemicals can also damage the body's own DNA. Dysregulation of the innate immune system can lead to autoinflammatory diseases, a form of autoimmunity, wherein RONS are produced excessively and often not in response to an insult, causing a great deal of host tissue damage [1].

Chronic inflammatory diseases are difficult to characterize because they generally act in bouts or cycles of severe inflammation with periods of relatively normal physiology in between [2-4]. The timing and kinetics of these bouts can be unpredictable, making controlled studies of dysregulated inflammation difficult to define [5, 6]. Since inflammatory diseases strongly predispose patients to cancer, it is of great interest to determine what aspects of inflammation contribute to mutagenesis during cancer initiation and promotion.

It is broadly hypothesized that cancer undergoes a multistage developmental process: initiation, promotion, and progression. Initiation refers to the stage where a cell or cells develop one or more oncogenic driver mutations, and promotion describes the clonal expansion of

initiated cells and accumulation of further mutations within the lineage. Importantly, genomic instability and progressive mutagenesis are hallmarks of cancer, enabling tumor cells to evolve increased malignancy and drug resistance over time (Fig 2-1). Thus, mutations accumulate through all stages of cancer development, contributing not just to initiation, but all stages of cancer progression. Inflammation displays features of both initiation, in that it can induce mutations, as well as promotion, because the inflammatory microenvironment facilitates growth and cellular migration. Indeed, it is likely that inflammation can impact both stages of carcinogenesis. In this work, we utilized animals that contain a fluorescent reporter transgene to detect sequence rearrangement mutations [7] to query how different aspects of inflammation impact mutagenesis.

To study mutagenesis, we utilized the RaDR mouse model, which allows detection of sequence rearrangement mutations *in situ*. The RaDR mouse was created with a tandem repeat of truncated EGFP coding sequences inserted at the Rosa26 locus for ubiquitous expression [8]. The 5' copy of the EGFP gene contains a deletion in the 5' region of the sequence, and likewise the 3' copy has a deletion of the 3' end of the gene. Cells that contain the un-mutated transgene express the truncated sequences, which do not produce a fluorescent product. However, if there is a double strand break (DSB) in one of the EGFP genes during S or G2 phase, homologous recombination (HR) may errantly produce a sequence rearrangement mutation as it repairs the breakage. For example, if the DSB occurs in the 3' copy, then during homology searching of HR, the cell may identify the homologous region of the 5' copy on the sister chromatid, producing a full-length EGFP gene. The resulting mutated cell and all of its progeny then express EGFP and can be identified by fluorescent microscopy or flow cytometry. For more detailed descriptions and validation of the RaDR mouse, please see [7]. Importantly, although HR is widely

considered an "error-free" DNA repair mechanism, the presence of many repetitive elements throughout the genome [9] presents many opportunities for HR to cause insertions, deletions and loss of heterozygosity [10-14]. Numerous studies have identified HR as a mechanism by which cancer cells may acquire these mutations [15-20]. Therefore, the RaDR animal provides a relevant proxy for quantifying mutagenesis within a tissue.

To study whether inflammation contributes to possible initiating mutations, we aged animals that lack key regulatory elements of inflammation with no additional manipulation. Therefore, any differences in mutation accumulation would be derived from the animal's deficiencies in regulating its innate immune system. This model system allowed us to assess aspects of innate immune regulation for mutagenicity without inducing inflammation, which could potentially obscure results.

We also studied the potential for inflammation to promote cancer and mutations using animals that contain a cancer driver mutation ($Apc^{Min/+}$) and thus spontaneously develop intestinal tumors. By inhibiting the prominent pro-inflammatory cytokine TNF in these animals, we reduced inflammation's contribution to cancer promotion, allowing us to determine whether inflammation promotes mutagenesis as well as tumorigenesis in this model.

2.2.1 *Rag2*$^{-/-}$ and *Rag2*$^{-/-}$;*IL10*$^{-/-}$ animals lack key factors involved in regulation of inflammation

The immune system comprises a network of cells and signals that co-regulate to optimize responses to pathogens. Whereas the innate immune system's macrophages and neutrophils produce non-targeted reactive chemicals that damage any biomolecule they contact (in addition to phagocytic and antigen-presenting functions), the adaptive immune system identifies and

attacks specific pathogens with minimal collateral damage. The adaptive immune system helps regulate and redirect the innate immune system to prevent self-injury when possible [21-23]. For example, effector T cells have been shown to block macrophage activity, neutrophil recruitment and pro-inflammatory cytokine secretion [24, 25], and regulatory T cells (Tregs) suppress the innate immune system to reduce inflammation [22, 23, 26]. However, it is unclear if the adaptive immune system has any impact on the development of mutations, either on its own or through moderation of the innate immune system.

In order to query whether the adaptive immune system plays a role in preventing or promoting mutagenesis, we crossed the RaDR transgene into *Rag2*$^{-/-}$ mice, which lack a functional adaptive immune system [27]. In order for B and T cells to mature and function, they must undergo a series of genetic rearrangements to produce unique antibodies and T cell receptors. The *Rag2* gene is essential for an early step of this process, called V(D)J recombination. When *Rag2* is absent, B and T cells never reach maturity and the adaptive immune system is unable to function. Therefore, with a non-functional adaptive immune system, a layer of innate immune regulation is lost.

Another important regulatory element of the immune system is the anti-inflammatory cytokine IL10. This pleiotropic cytokine downregulates macrophage stimulation [28-30] and blocks NFκB [31, 32], and it is thus heavily involved in regulating inflammation. Indeed, production of IL-10 is one mode by which Tregs suppress innate immune inflammation [22]. Since IL10 plays key roles in moderating the innate immune system, we also bred RaDR mice with *Rag2*$^{-/-}$;*IL10*$^{-/-}$ animals in order to see whether the absence of this cytokine promotes mutagenesis.

2.2.2 *Apc*$^{Min/+}$ animals spontaneously develop inflammation and cancer

In an effort to focus on inflammation's contributions to the promotion stage of cancer, we attenuated inflammation in animals that contain an oncogenic driver mutation by treating with an antibody against the pro-inflammatory cytokine TNF.

Apc$^{Min/+}$ (Min) animals have been used to study intestinal carcinogenesis for decades. They contain an inactivating point mutation in the tumor suppressor Apc, which results in spontaneous intestinal tumorigenesis within the first two months of life. The Min model can be considered as all cells already having an initiating mutation, which is why tumors develop so quickly, and also why this model lends itself to studying cancer promotion (Fig 2-1). The Min phenotype also includes elevated metrics of systemic inflammation, splenomegaly, thymic involution, and lymphodepletion [33, 34].

TNF is a multifunctional cytokine that is secreted primarily by macrophages to promote inflammation [35]. The far-reaching effects of TNF are perhaps best illustrated with the range of diseases that can be effectively treated by blocking the cytokine, including rheumatoid arthritis, inflammatory bowel disease and psoriasis [35]. Previous studies have shown that mitigating Min animals' endogenous inflammation with anti-TNF significantly reduced tumor burden, and possibly even induced regression [36]. We aimed to recapitulate this treatment paradigm with RaDR Min mice to determine whether suppression of inflammation by anti-TNF affects mutagenesis as well as tumorigenesis.

2.3 Materials and Methods

2.3.1 *RaDR* vs. *Rag2$^{-/-}$;RaDR* vs. *Rag2$^{-/-}$;IL10$^{-/-}$;RaDR*

RaDR$^{R/R}$, *Rag2$^{-/-}$;RaDR$^{R/R}$*, and *Rag2$^{-/-}$;IL10$^{-/-}$;RaDR$^{R/R}$* mice were housed in an AAALAC-accredited barrier facility free of known murine *Helicobacter* species, viruses, *Salmonella* species, *Citrobacter rodentium*, ecto- and endoparasites. *Rag2$^{-/-}$;IL10$^{-/-}$* mice were maintained in SCID housing, while WT and *Rag2$^{-/-}$* mice were housed in normal clean cages. Animals were aged with no manipulation for 6 months, at which time they were euthanized by CO_2 according to AVMA guidelines and necropsied with standard procedures. Samples collected and analyzed immediately included: body weight, spleen weight, thymus weight, pancreas RaDR imaging, liver RaDR imaging, colon RaDR imaging, mammary RaDR imaging.

2.3.2 Anti-TNF treatment in *RaDR;Apc$^{Min/+}$* mice

C57Bl/6 *RaDR$^{R/R}$* and C57Bl/6 *Apc$^{Min/+}$* animals were bred to produce *RaDR$^{R/+}$;Apc$^{Min/+}$* and *RaDR$^{R/+}$* offspring. The animals were separated by sex and housed in large cages containing up to 10 mice per cage. Each cage contained both Min and wild type mice, and mice of each genotype were split evenly into anti-TNF and sham treatment groups. Mice began receiving i.p. injections of anti-TNF antibody (XT3.11, BioXCell, West Lebanon NH) or anti-IgG sham antibody (HRPN, BioXCell, West Lebanon NH) at 3.5-4 months of age. The initial loading dose was 0.4 mL of 1 mg/mL antibody diluted in sterile PBS, and subsequent injections were 0.2 mL of 1 mg/mL antibody given three times a week for a total of 6 weeks. At the end of the 6-week treatment period, mice were euthanized by CO_2 according to AVMA guidelines and necropsied with standard procedures. Samples collected and analyzed immediately included: body weight,

complete blood count, spleen weight and RaDR flow, thymus weight and RaDR flow, pancreas RaDR imaging, liver RaDR imaging, mammary RaDR imaging, and intestine segment RaDR imaging. Samples collected and stored included: serum (-80°C), feces (RNA-later, -80°C), spleen portions (RNA-later, -80°C and formalin, room temperature) thymus portions (RNA-later, -80°C and formalin, room temperature), pancreas portion (formalin, room temperature), intestine segment portions (RNA-later, -80°C), whole intestine segments (on bibulous paper in formalin, room temperature), and lymph tissue from the mammary, mesentery, Peyer's patch and ceco-colonic lymph nodes (RNA-later, -80°C). Animal carcasses were saved in formalin.

2.3.3 RaDR Necropsy and Tissue Imaging

Animals were euthanized with CO_2 according to AVMA guidelines. Tissues were excised and held on ice in tubes containing PBS (mammary, spleen) or PBS with 0.01% trypsin inhibitor (T9008 Sigma-Aldrich or P-1540 Westnet Inc) (pancreas, liver, intestines) until use. Intestines were cut open on one side and the lumen was rinsed of fecal matter before placing in PBS + trypsin inhibitor. Mammary, pancreas, liver and intestine tissues were compressed to 0.5 mm between coverslips and imaged for EGFP under the 1x objective with the FITC filter of a Nikon 80i fluorescent microscope.

2.3.4 RaDR Image Analysis

RaDR images can be analyzed for the number of *de novo* recombination events by quantifying individual fluorescent foci, or for total burden of recombinant cells by measuring the fluorescent area of the tissue. Both metrics are normalized to tissue area, measured in ImageJ. To quantify fluorescent foci, Dushan Wadduwage of Peter So's laboratory designed MATLAB-based

programs that use gradient and intensity features of the image to distinguish individual foci (manuscript under review). The program "FociCounter_3.1" was used to enumerate all foci in pancreas, liver, and mammary tissues, and the program "17.03.27_Crypt counter with GUI" was utilized to enumerate converted colonic crypts. The crypt counting program is trained to recognize crypt foci based on 3-4 researcher-annotated images from the data set, then the program is able to apply those parameters to identify crypt foci in other images. To quantify the fluorescent area within the tissue, conservative intensity thresholds were set in ImageJ such that background and artifactual fluorescence was excluded, and only brightly fluorescent pixels would be measured. After marking the outline of the tissue, the area of pixels above the threshold intensity were measured as well as the total tissue area.

2.3.5 RaDR Flow Cytometry

Tissues analyzed by flow cytometry were processed after imaging was completed. Briefly, tissues were placed in 5 mL of 2 mg/ml collagenase type V (C9263, Sigma) in HBSS (Life Technologies) in a GentleMACS C tube and mechanically dissociated with the GentleMACS tissue grinder (Miltenyi Biotec). After mechanical disaggregation, the tissues were placed in a 37C incubator for 40 minutes to allow collagenase to degrade connective tissue. Cell suspensions were then triterated 10-15 times and passed through a 70 micron cell strainer into 10 mL of cold media (DMEM + 10% FBS + pen/strep) to halt collagenase digestion. The samples were then centrifuged at 180 x *g* for 10 minutes and supernatant was discarded. The cell pellet was resuspended in 350-500 uL of Opti-MEM reduced serum media (ThermoFisher Scientific) and held on ice until analyzed. The samples were analyzed by a FACScan or FACS Calibur flow cytometer for green fluorescence (530 nm) and red (585 nm) to account for autofluorescence.

2.3.6 Tumor Quantitation

Following RaDR imaging, intestine segments were laid flat on bibulous paper and fixed in 10% formalin. After several days, the formalin was discarded and replaced with 100% ethanol for 24 hours. The ethanol was then discarded and replaced with 70% ethanol. To count tumors, intestine segments were carefully removed from the bibulous paper cassettes and placed on a stereoscopic 10x microscope. The approximate sizes and locations of tumors within each segment were recorded on paper.

2.3.7 Histopathology

Formalin-fixed tissues were embedded in paraffin, cut in 5 μm sections, and stained with hematoxylin and eosin. Sections were scored by a pathologist blinded to sample identity. For intestines, after tumors had been counted, intestine segments were rolled into swiss rolls and placed in cassettes for paraffin embedding.

2.3.8 Immunofluorescence

Formalin-fixed tissue sections were embedded in paraffin and cut in 5 μm sections. Slides stained for immunofluorescence were first deparaffinized with three five-minute washes in xylenes, two five-minute washes in 100% ethanol, and 10-minute washes each in 95% ethanol, 90% ethanol, and 70% ethanol. Slides were washed twice in PBS, then boiled in Dako citric acid antigen retrieval buffer (S1700, Agilent Technologies, Santa Clara, CA) for 30 min. After cooling, slides were washed twice in diH_2O and tissue sections were circled with hydrophobic marker. Sections were blocked for one hour with 5% BSA + 0.3% Triton in PBST at room temp.

All antibodies were diluted in 1% BSA + 0.3% Triton in PBST, and sections were stained overnight at 4C. Slides were then washed three times for five minutes each in PBST and incubated with the appropriate secondary antibody for one hour at room temperature. Slides were then washed five times in PBST for five minutes each. Finally, a drop of DAPI with ProLong AntiFade reagent was placed on the section, and a cover slip was laid overtop and sealed with clear nail polish.

Primary antibodies used were: anti-Ki67 (Abcam ab15580, rabbit), anti-phospho-H2A.X Ser-139 (Millipore 05-636, mouse), anti-nitrotyrosine (Millipore AB5411, rabbit), and anti-F4/80 (Abcam ab6640, rat). Secondary antibodies used were: Alexa Fluor 647 (goat anti-rabbit) (used for both Ki67 and nitrotyrosine, but not simultaneously), Alexa Fluor 488 (goat anti-mouse), Alexa Fluor 568 (goat anti-rat).

2.3.9 Statistical Analyses

RaDR foci were quantified as the number of foci per square centimeter of area (foci/cm^2), and RaDR flow cytometry measurements were given as % fluorescent*10^6. Due to the fact that the distribution of EGFP-positive cells in RaDR mice is non-normal across tissues and among individuals, RaDR data sets were compared by Mann-Whitney *U*-test. It was not clear that tumor multiplicity was normally distributed between individuals, and therefore tumor counts were also compared by Mann-Whitney *U*-test. Body and tissue weights were compared by unpaired Student's *t*-test. All statistical comparisons were calculated using GraphPad Prism 5.

2.4 Results

2.4.1 *Rag2*$^{-/-}$ and *Rag2*$^{-/-}$;*IL10*$^{-/-}$ develop more sequence rearrangement mutations than wild type in the pancreas

The primary endpoint of interest in these studies is mutagenicity, which we evaluated with the RaDR transgenic mouse for detecting sequence rearrangement mutations. When cells acquire the RaDR mutation, fluorescent foci are visible *in situ* by fluorescence microscopy. As mutated cells divide, the fluorescent progeny remain in close spatial proximity, creating larger foci. Therefore, *de novo* mutations are quantified by enumeration of distinct foci. In intestine tissue, where well-defined tissue architecture includes somatic stem cells that give rise to crypts, somatic stem cell mutations can be identified and quantified by characteristic large, round foci.

During necropsy, the pancreas, colon, and left lobe of the liver were excised and imaged for RaDR mutations. The number of foci and area of the tissue were initially quantified manually, and later analyzed with MATLAB foci counting software (manuscript under review). Colon images were analyzed for all foci as well as converted crypts. Surprisingly, there was a significant increase in the number of mutations that occurred in *Rag2*$^{-/-}$ animals' pancreata (Fig 2-2A), indicating that either the adaptive immune system or Rag2 itself impacts the development of pancreatic mutations. There were no significant differences between strains in the density of mutant foci in the liver and colon tissue (Fig 2-2B and C).

In order to study why *Rag2*$^{-/-}$ pancreata develop more mutations, we examined histology sections from 5-6 animals for each strain of mice. A trained pathologist blinded to sample identity scored pancreas sections for pathology and noted observations (Table 2-1). Consistent with the fact that these mice were not exposed to any inflammatory stimuli, the pancreata of each

strain did not show signs of inflammation nor other pathology (Fig 2-3). We also stained pancreas sections for molecular markers that could indicate causes for increased mutagenesis. First, we stained for nitrotyrosine (3-NT) as a marker for nitrosative protein damage, a feature of inflammation (Fig 2-4A). We also stained for the presence of F4/80-positive macrophages to determine if the innate immune system was upregulated in mice that lacked adaptive immunity. For both markers of inflammatory stress, there were no differences between genotypes (Fig 2-4B).

Since RaDR mutations arise from HR, and HR generally occurs at double strand breaks (DSBs) during S or G2, we also stained sections of pancreas tissue for proliferation with Ki67 antibody and DNA DSBs with γH2AX antibody. While HR-derived mutations should correlate with proliferation and DSBs, we did not observe differences in Ki67 nor γH2AX staining among mouse strains (Fig 2-4C).

These results show that, at the time of necropsy, there were no significant differences in inflammation, proliferation, nor DSBs that could explain the increase in RaDR foci in *Rag2*$^{-/-}$ pancreata.

2.4.2 *Rag2*$^{-/-}$ and *Rag2*$^{-/-}$;*IL10*$^{-/-}$ have smaller lymphoid organs than wild type

As a surrogate measure of overall health, body weights were measured at the time of necropsy. As hypothesized, since all animals are 129 background and unchallenged, the animals developed normally and had similar body weights at necropsy (Fig 2-5A). Weights of the thymus and spleen were also measured for each mouse at necropsy. Consistent with previous reports, the spleen and thymus of Rag2-/- animals are smaller than that of WT mice [37, 38] (Fig 2-5B). Since the spleen and thymus are the organs in which B and T lymphocytes complete maturation,

and the *Rag2* gene is essential for B and T cell maturation, it is unsurprising that both knockout strains have smaller lymphoid organs than wild type animals.

2.4.3 Anti-TNF treatment decreases intestinal inflammation, tumor multiplicity, and mutant burden in $Apc^{Min/+}$ mice, but does not affect mutation frequency.

To complement our studies of mice lacking regulatory components of the immune system, we utilized the $Apc^{Min/+}$ mouse model of intestinal cancer. *Apc* is a tumor suppressor gene that regulates the Wnt signaling pathway, and over 80% of human colon cancers contain *Apc* mutations [39, 40]. Min mice are heterozygous for an inactivating point mutation in *Apc* and were named for their spontaneous development of multiple intestinal neoplasia [41, 42]. These animals accumulate intestinal adenomatous polyps starting within two months of life, with the majority arising in the distal third of the small intestine (ileum). Whether inflammation promotes cancer in these mice or is merely a symptom of cancer development has not been determined, but studies have shown that mitigation of inflammation reduces Min tumor development [43-46]. In this experiment, we aimed to recapitulate findings of Rao *et al.* showing that anti-TNF treatment decreases tumorigenesis [36], and to contribute information regarding whether reducing inflammation affects mutagenicity as well.

Min and WT littermates were divided evenly between anti-TNF and sham antibody treatments as described above. Animals were separated by sex, but both genotypes and treatment groups were cohoused in large cages to limit the potential for confounding variables such as microbiota. Our treatment regimen closely paralleled that of the Rao *et al.* study, and indeed we also observed fewer polyps in the Min ileum (Fig 2-6) and an overall reduction in intestinal inflammation (Fig 2-7).

Although intestinal tumorigenesis decreased with anti-TNF treatment, the frequency of mutant crypts did not vary significantly between genotypes nor treatments (Fig 2-8A). However, quantifying the overall burden of mutant cells revealed that although mutation frequency did not increase, Min ilea and colons had a greater burden of mutant cells compared to WT, and anti-TNF treatment decreased the overall mutant burden in Min ilea (Fig 2-8B). The fact that ileal polyps and overall mutant burden both decreased with anti-TNF treatment while *de novo* recombination mutations were unchanged indicates that reducing inflammation also reduces tumorigenesis, but it does not significantly impact the production of sequence rearrangement mutations. Thus, the decreased overall mutant burden in anti-TNF treated animals probably results from decreased proliferation corresponding to decreased tumorigenesis.

Although our target tissues for this experiment were intestines, we also analyzed pancreas, liver, mammary, and spleen tissues for RaDR mutations. Pancreas, liver and mammary mutation frequencies were quantified as foci in fluorescent images, and there was no difference in the number of *de novo* sequence rearrangements in any of these tissues (Fig 2-9A). The total proportion of fluorescent cells in the tissue was also measured by flow cytometry. By this metric, Min mice were found to have significantly higher proportions of mutant cells than WT in anti-TNF treated pancreata and sham-treated livers (Fig 2-9B). This increase in total recombinant cells in the Min pancreas and liver can likely be attributed to dysregulated Wnt signaling causing increased proliferation.

2.4.4 *Apc*$^{Min/+}$ mice suffer from low body weight, thymic involution, and splenomegaly, and anti-TNF treatment minimally improves those metrics

Min mice exhibit a number of pathologies that worsen with age, including: elevated intestinal inflammation, cachexia, splenomegaly, lymphodepletion, and premature thymic involution [33, 34, 47, 48]. We compared these pathologies between genotypes and treatment groups as measurements of overall health.

Min mice were smaller than WT and had much larger spleens (Fig 2-10A, B), as expected for this strain [34]. Also consistent with Min physiology, thymi of sham-treated Min mice were smaller than WT (Fig 2-10C) [33, 34]. Anti-TNF treatment appeared to result in larger thymi for both Min and WT animals, but this effect was only statistically significant in Min mice (Fig2.10C). Given the trends of increased lymphoid organ size, it is possible that anti-TNF treatment attenuates lymphodepletion in Min mice, but this has not been quantified.

Interestingly, Min animals had a significantly lower proportion of mutated spleen cells compared to WT (Fig 2-9B). Min mice are known to suffer depletion of lymphocytes, which compose the splenic white pulp, and a greatly increased mass and proportion of red pulp, which contains hematopoietic cells [34]. Identification of which spleen cell types acquire the RaDR mutation could reveal the physiological explanation for the decreased proportion of mutated cells in the Min spleen.

2.5 Discussion

In the studies described here, we aimed to ascertain whether modulating regulatory elements of innate immunity could contribute to or protect against mutations. We compared wild type

animals to those that lack a functional adaptive immune system (*Rag2*$^{-/-}$) as well as animals lacking both adaptive immunity and an important anti-inflammatory cytokine (*Rag2*$^{-/-}$;*IL10*$^{-/-}$), because both the adaptive immune system and IL10 play major roles in regulating the innate immune system and inflammation. We aged animals for six months with no manipulation so that all animals were healthy and exposed only to their commensal microbiota; thus, mutations were not induced but would arise from normal physiology. We hypothesized that animals lacking key regulatory elements of inflammation may experience increased levels of RONS throughout their lives, contributing to an increase in mutagenesis.

Previous studies using a plasmid assay analogous to the RaDR transgene have shown that inflammatory RONS are indeed capable of inducing mutations through homologous recombination [49, 50]. During inflammation, replication blocking lesions and single strand breaks can arise from direct reaction with RONS or as intermediates during Base Excision Repair, and these lesions can be recombinogenic, particularly during cell division [49-51]. Subsequent *in vivo* studies demonstrated that inflammation during cellular proliferation synergistically increases mutagenesis in the pancreas [52], but the contributions of inflammation to mutagenesis had not yet been quantified in other tissues.

Interestingly, we did observe an increase in mutations in both *Rag2*$^{-/-}$ and *Rag2*$^{-/-}$;*IL10*$^{-/-}$ pancreata as compared to wild type, though there was no significant difference between *Rag2*$^{-/-}$ and *Rag2*$^{-/-}$;*IL10*$^{-/-}$ pancreas mutations. This supports our hypothesis that knockout of functional adaptive immune cells leads to increased mutagenesis, possibly through innate immune dysregulation. We therefore sought to explore how the adaptive immune system protects the pancreas from sequence rearrangements. To determine whether inflammation was present, we evaluated pancreas sections for histopathology scores, nitrosative tissue damage, and

macrophage infiltration, but observed no quantifiable differences between strains. Since HR-derived sequence rearrangement mutations generally arise from mis-repaired DSBs during cellular proliferation, we also assayed pancreas sections for γH2AX (DSBs) and Ki67 (proliferation). Again, we did not observe quantifiable differences between strains.

It is important to note that immunofluorescent staining only captures the physiology of the tissue at a single point in time, whereas RaDR-mutated cells have accumulated throughout the 6 months of the animal's life. Thus, while staining does not indicate measurable differences in inflammation, proliferation, nor DSBs at the 6 month timepoint, there may have been differences in any of these metrics earlier in the animal's life that contributed to the increased formation of sequence rearrangement mutations. It is also possible that a very low degree of inflammation is present in *Rag2*$^{-/-}$ animals, but to such a small extent that it cannot be distinguished in tissue sections.

Our hypothesis as to why *Rag2*$^{-/-}$ mice develop more HR-driven mutations is that RAG2 may play a role in DSB repair pathway choice. Gigi *et al.* demonstrated that the C-terminus of the RAG2 protein promotes canonical non-homologous end joining (c-NHEJ), and that truncation of the RAG2 protein at the C-terminus promotes alternative NHEJ (alt-NHEJ) in V(D)J recombination during lymphocyte development [53]. Other studies have shown that Rag2 restricts DSB repair to c-NHEJ in embryonic stem cells [54]. We hypothesize that deletion of the *Rag2* gene diminishes the choice for c-NHEJ during DSB repair, and HR compensates. We also hypothesize that this effect is only observable in the pancreas because the pancreas accumulates up to an order of magnitude more mutations than the other tissue types studied, and thus the differences in other tissues is not as pronounced. However, Rag2 is thought to be a lymphoid

cell-specific gene [55], and data repositories report no detectable expression of Rag2 in the pancreas [56]. Thus, more studies are necessary to test these hypotheses.

We also studied the effects of inflammation on the promotion phase of carcinogenesis. We treated Min mice, which contain a cancer driver mutation and spontaneously develop intestinal tumors and inflammation, with anti-TNF to mitigate systemic inflammation. Previous studies have shown that inflammation strongly promotes cancer development [36, 43, 57, 58], but whether that includes increased mutagenesis has not been elucidated. Our studies reproduced previous findings that anti-TNF reduced tumorigenesis in Min mice [36][other refs], and contributed the endpoint of accumulated sequence rearrangement mutations. Our results indicate that reducing inflammation in mice that already contain a cancer driver mutation helps to decrease tumor multiplicity but has little effect on sequence rearrangement mutagenesis, at least at the RaDR locus. This suggests that while inflammation helps promote tumor development, this promotion does not depend on increased mutagenesis.

Together, these studies suggest that while regulation of inflammation may protect against mutagenesis, the mechanism by which inflammation promotes cancer is not dependent on increased mutagenesis.

2.6 Acknowledgements

The work described in this chapter was performed in collaboration with members of several laboratories. The foci counting programs used to quantify *de novo* recombination events were written by Dr. Dushan Wadduwage of Prof. Peter So's laboratory. Histology sections were analyzed and scored by Dr. Theofilis Poutahidis of Aristotle University of Thessaloniki. Sheyla

Mirabal of Dr. Susan Erdman's laboratory assisted with necropsies for the anti-TNF treatment experiment. We also thank Glenn Paradis for training and use of the Koch Institute Flow Cytometry Core. This work was supported by the NIH/NIGMS Interdepartmental Biotechnology Training Program (5 T32 GM008334).

2.7 References

1. Ciccarelli, F., M. De Martinis, and L. Ginaldi, *An update on autoinflammatory diseases.* Curr Med Chem, 2014. **21**(3): p. 261-9.
2. Franklin, W.A., et al., *Immunohistologic demonstration of abnormal colonic crypt cell kinetics in ulcerative colitis.* Hum Pathol, 1985. **16**(11): p. 1129-32.
3. Mikami, T., et al., *Apoptosis regulation differs between ulcerative colitis-associated and sporadic colonic tumors. Association with survivin and bcl-2.* Am J Clin Pathol, 2003. **119**(5): p. 723-30.
4. Langhorst, J., et al., *Distinct kinetics in the frequency of peripheral CD4+ T cells in patients with ulcerative colitis experiencing a flare during treatment with mesalazine or with a herbal preparation of myrrh, chamomile, and coffee charcoal.* PLoS One, 2014. **9**(8): p. e104257.
5. Zelante, A., et al., *Adherence to medical treatment in inflammatory bowel disease patients.* Minerva Gastroenterol Dietol, 2014. **60**(4): p. 269-74.
6. Bannaga, A.S. and C.P. Selinger, *Inflammatory bowel disease and anxiety: links, risks, and challenges faced.* Clin Exp Gastroenterol, 2015. **8**: p. 111-7.
7. Sukup-Jackson, M.R., et al., *Rosa26-GFP direct repeat (RaDR-GFP) mice reveal tissue- and age-dependence of homologous recombination in mammals in vivo.* PLoS Genet, 2014. **10**(6): p. e1004299.
8. Soriano, P., *Generalized lacZ expression with the ROSA26 Cre reporter strain.* Nat Genet, 1999. **21**(1): p. 70-1.
9. de Koning, A.P., et al., *Repetitive elements may comprise over two-thirds of the human genome.* PLoS Genet, 2011. **7**(12): p. e1002384.
10. Bishop, A.J. and R.H. Schiestl, *Homologous recombination as a mechanism for genome rearrangements: environmental and genetic effects.* Hum Mol Genet, 2000. **9**(16): p. 2427-334.
11. Bishop, A.J. and R.H. Schiestl, *Homologous recombination as a mechanism of carcinogenesis.* Biochim Biophys Acta, 2001. **1471**(3): p. M109-21.
12. Jonnalagadda, V.S., T. Matsuguchi, and B.P. Engelward, *Interstrand crosslink-induced homologous recombination carries an increased risk of deletions and insertions.* DNA Repair (Amst), 2005. **4**(5): p. 594-605.
13. Gu, W., F. Zhang, and J.R. Lupski, *Mechanisms for human genomic rearrangements.* Pathogenetics, 2008. **1**(1): p. 4.
14. Costantino, L., et al., *Break-induced replication repair of damaged forks induces genomic duplications in human cells.* Science, 2014. **343**(6166): p. 88-91.
15. Loeb, L.A., C.F. Springgate, and N. Battula, *Errors in DNA replication as a basis of malignant changes.* Cancer Res, 1974. **34**(9): p. 2311-21.
16. Gupta, P.K., et al., *High frequency in vivo loss of heterozygosity is primarily a consequence of mitotic recombination.* Cancer Res, 1997. **57**(6): p. 1188-93.
17. Strout, M.P., et al., *The partial tandem duplication of ALL1 (MLL) is consistently generated by Alu-mediated homologous recombination in acute myeloid leukemia.* Proc Natl Acad Sci U S A, 1998. **95**(5): p. 2390-5.
18. Shao, C., et al., *Mitotic recombination produces the majority of recessive fibroblast variants in heterozygous mice.* Proc Natl Acad Sci U S A, 1999. **96**(16): p. 9230-5.

19. Pal, J., et al., *Genomic evolution in Barrett's adenocarcinoma cells: critical roles of elevated hsRAD51, homologous recombination and Alu sequences in the genome.* Oncogene, 2011. **30**(33): p. 3585-98.
20. Roy, R., J. Chun, and S.N. Powell, *BRCA1 and BRCA2: different roles in a common pathway of genome protection.* Nat Rev Cancer, 2012. **12**(1): p. 68-78.
21. Shanker, A., *Adaptive control of innate immunity.* Immunol Lett, 2010. **131**(2): p. 107-12.
22. Maloy, K.J., et al., *CD4+CD25+ T(R) cells suppress innate immune pathology through cytokine-dependent mechanisms.* J Exp Med, 2003. **197**(1): p. 111-9.
23. Erdman, S.E., et al., *CD4+ CD25+ regulatory T lymphocytes inhibit microbially induced colon cancer in Rag2-deficient mice.* Am J Pathol, 2003. **162**(2): p. 691-702.
24. Guarda, G., et al., *T cells dampen innate immune responses through inhibition of NLRP1 and NLRP3 inflammasomes.* Nature, 2009. **460**(7252): p. 269-73.
25. Sun, K. and D.W. Metzger, *Inhibition of pulmonary antibacterial defense by interferon-gamma during recovery from influenza infection.* Nat Med, 2008. **14**(5): p. 558-64.
26. Maloy, K.J., et al., *Cure of innate intestinal immune pathology by CD4+CD25+ regulatory T cells.* Immunol Lett, 2005. **97**(2): p. 189-92.
27. Shinkai, Y., et al., *RAG-2-deficient mice lack mature lymphocytes owing to inability to initiate V(D)J rearrangement.* Cell, 1992. **68**(5): p. 855-67.
28. Minton, K., *Immune regulation: IL-10 targets macrophage metabolism.* Nat Rev Immunol, 2017. **17**(6): p. 345.
29. Inoue, M., et al., *T cells down-regulate macrophage TNF production by IRAK1-mediated IL-10 expression and control innate hyperinflammation.* Proc Natl Acad Sci U S A, 2014. **111**(14): p. 5295-300.
30. Ip, W.K.E., et al., *Anti-inflammatory effect of IL-10 mediated by metabolic reprogramming of macrophages.* Science, 2017. **356**(6337): p. 513-519.
31. Wang, P., et al., *Interleukin (IL)-10 inhibits nuclear factor kappa B (NF kappa B) activation in human monocytes. IL-10 and IL-4 suppress cytokine synthesis by different mechanisms.* J Biol Chem, 1995. **270**(16): p. 9558-63.
32. Driessler, F., et al., *Molecular mechanisms of interleukin-10-mediated inhibition of NF-kappaB activity: a role for p50.* Clin Exp Immunol, 2004. **135**(1): p. 64-73.
33. Coletta, P.L., et al., *Lymphodepletion in the ApcMin/+ mouse model of intestinal tumorigenesis.* Blood, 2004. **103**(3): p. 1050-8.
34. You, S., et al., *Developmental abnormalities in multiple proliferative tissues of Apc(Min/+) mice.* Int J Exp Pathol, 2006. **87**(3): p. 227-36.
35. Bradley, J.R., *TNF-mediated inflammatory disease.* J Pathol, 2008. **214**(2): p. 149-60.
36. Rao, V.P., et al., *Proinflammatory CD4+ CD45RB(hi) lymphocytes promote mammary and intestinal carcinogenesis in Apc(Min/+) mice.* Cancer Res, 2006. **66**(1): p. 57-61.
37. Mombaerts, P., et al., *RAG-1-deficient mice have no mature B and T lymphocytes.* Cell, 1992. **68**(5): p. 869-77.
38. Prockop, S.E. and H.T. Petrie, *Regulation of thymus size by competition for stromal niches among early T cell progenitors.* J Immunol, 2004. **173**(3): p. 1604-11.
39. Rowan, A.J., et al., *APC mutations in sporadic colorectal tumors: A mutational "hotspot" and interdependence of the "two hits".* Proc Natl Acad Sci U S A, 2000. **97**(7): p. 3352-7.
40. Kinzler, K.W. and B. Vogelstein, *Lessons from hereditary colorectal cancer.* Cell, 1996. **87**(2): p. 159-70.

41. Moser, A.R., H.C. Pitot, and W.F. Dove, *A dominant mutation that predisposes to multiple intestinal neoplasia in the mouse.* Science, 1990. **247**(4940): p. 322-4.
42. Su, L.K., et al., *Multiple intestinal neoplasia caused by a mutation in the murine homolog of the APC gene.* Science, 1992. **256**(5057): p. 668-70.
43. Erdman, S.E., et al., *CD4+CD25+ regulatory lymphocytes induce regression of intestinal tumors in ApcMin/+ mice.* Cancer Res, 2005. **65**(10): p. 3998-4004.
44. Liu, H.P., et al., *Chemoprevention of intestinal adenomatous polyposis by acetyl-11-keto-beta-boswellic acid in APC(Min/+) mice.* Int J Cancer, 2013. **132**(11): p. 2667-81.
45. Orner, G.A., et al., *Suppression of tumorigenesis in the Apc(min) mouse: down-regulation of beta-catenin signaling by a combination of tea plus sulindac.* Carcinogenesis, 2003. **24**(2): p. 263-7.
46. Sanchez-Tena, S., et al., *Grape antioxidant dietary fiber inhibits intestinal polyposis in ApcMin/+ mice: relation to cell cycle and immune response.* Carcinogenesis, 2013. **34**(8): p. 1881-8.
47. McClellan, J.L., et al., *Intestinal inflammatory cytokine response in relation to tumorigenesis in the Apc(Min/+) mouse.* Cytokine, 2012. **57**(1): p. 113-9.
48. Narsale, A.A., et al., *Liver inflammation and metabolic signaling in ApcMin/+ mice: the role of cachexia progression.* PLoS One, 2015. **10**(3): p. e0119888.
49. Kiziltepe, T., et al., *Delineation of the chemical pathways underlying nitric oxide-induced homologous recombination in mammalian cells.* Chem Biol, 2005. **12**(3): p. 357-69.
50. Spek, E.J., et al., *Nitric oxide-induced homologous recombination in Escherichia coli is promoted by DNA glycosylases.* J Bacteriol, 2002. **184**(13): p. 3501-7.
51. Kiraly, O., et al., *DNA glycosylase activity and cell proliferation are key factors in modulating homologous recombination in vivo.* Carcinogenesis, 2014. **35**(11): p. 2495-502.
52. Kiraly, O., et al., *Inflammation-induced cell proliferation potentiates DNA damage-induced mutations in vivo.* PLoS Genet, 2015. **11**(2): p. e1004901.
53. Gigi, V., et al., *RAG2 mutants alter DSB repair pathway choice in vivo and illuminate the nature of 'alternative NHEJ'.* Nucleic Acids Res, 2014. **42**(10): p. 6352-64.
54. Corneo, B., et al., *Rag mutations reveal robust alternative end joining.* Nature, 2007. **449**(7161): p. 483-6.
55. Alt, F.W., et al., *Mechanisms of programmed DNA lesions and genomic instability in the immune system.* Cell, 2013. **152**(3): p. 417-29.
56. Atlas, H.P. *Rag2.* September 1, 2017]; Available from: https://www.proteinatlas.org/ENSG00000175097-RAG2/tissue.
57. Li, Y., et al., *Gut microbiota accelerate tumor growth via c-jun and STAT3 phosphorylation in APCMin/+ mice.* Carcinogenesis, 2012. **33**(6): p. 1231-8.
58. Niku, M., et al., *Western diet enhances intestinal tumorigenesis in Min/+ mice, associating with mucosal metabolic and inflammatory stress and loss of Apc heterozygosity.* J Nutr Biochem, 2017. **39**: p. 126-133.

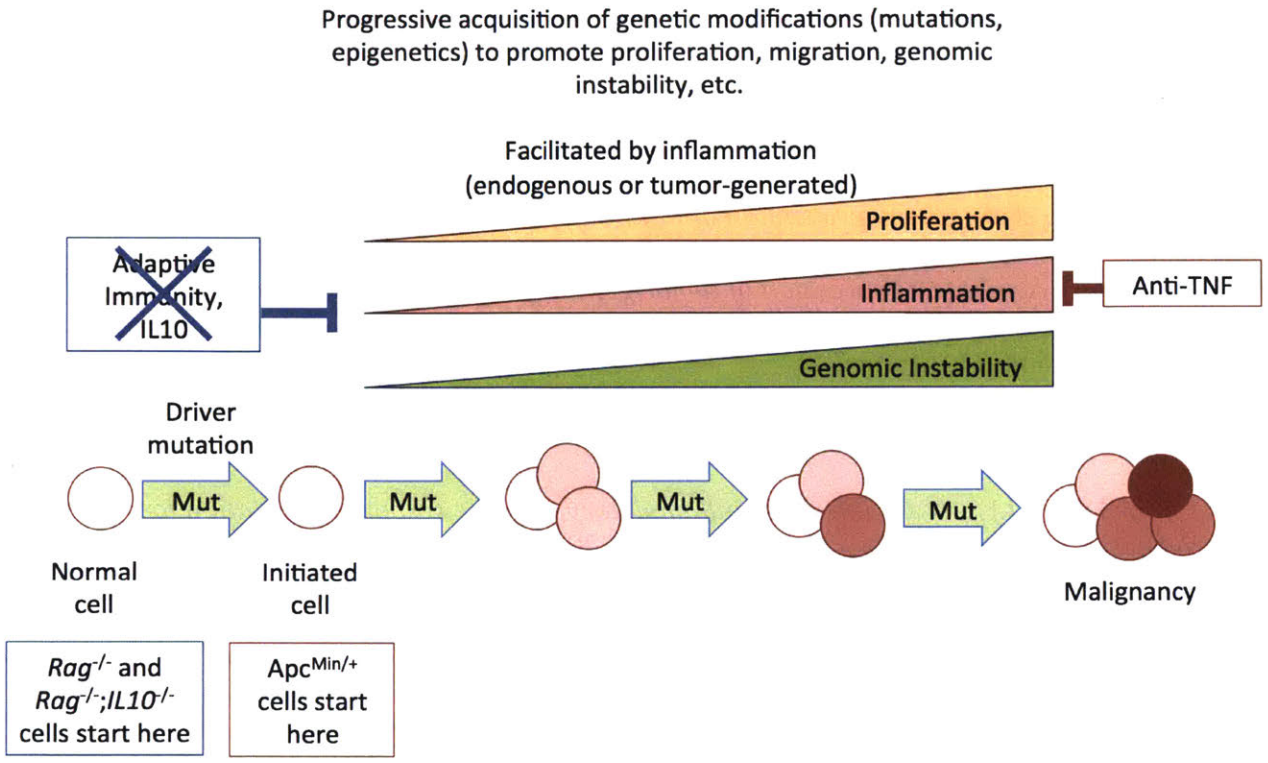

Figure 2-1. Stepwise model of cancer progression and context of experimental setups

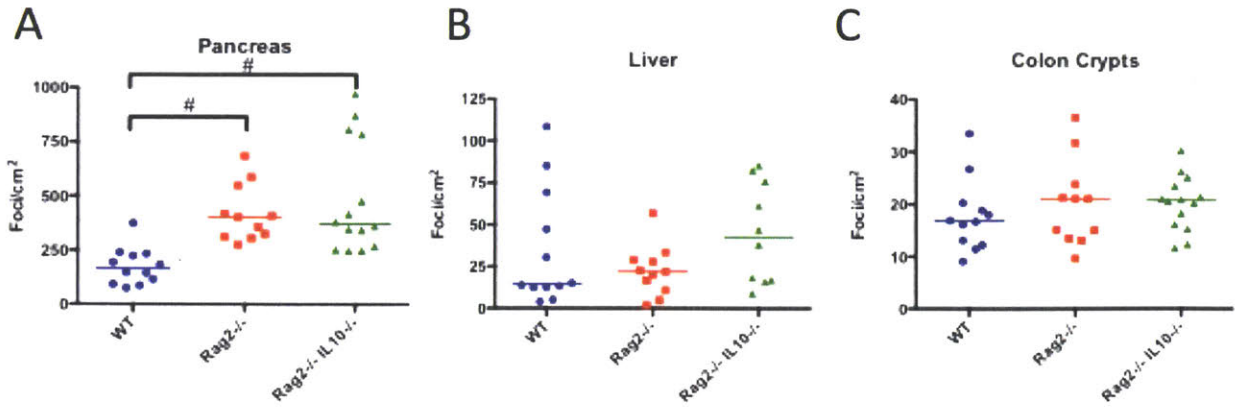

Figure 2-2. RaDR mutation frequency. At necropsy, pancreas, liver and colon tissues were excised and imaged for fluorescent foci. Foci were quantified by MATLAB automated image analysis and normalized to tissue area. (A) Pancreata of *Rag2*$^{-/-}$ animals developed significantly more *de novo* recombination events compared to WT. *Rag2*$^{-/-}$;*IL10*$^{-/-}$ pancreas foci were not statistically different from *Rag2*$^{-/-}$. (B, C) RaDR foci in the liver (B) and colonic crypts (C) were not statistically significant between genotypes. Bar indicates median. Mann-Whitney *U*-test, $^{\#}p < 0.0001$.

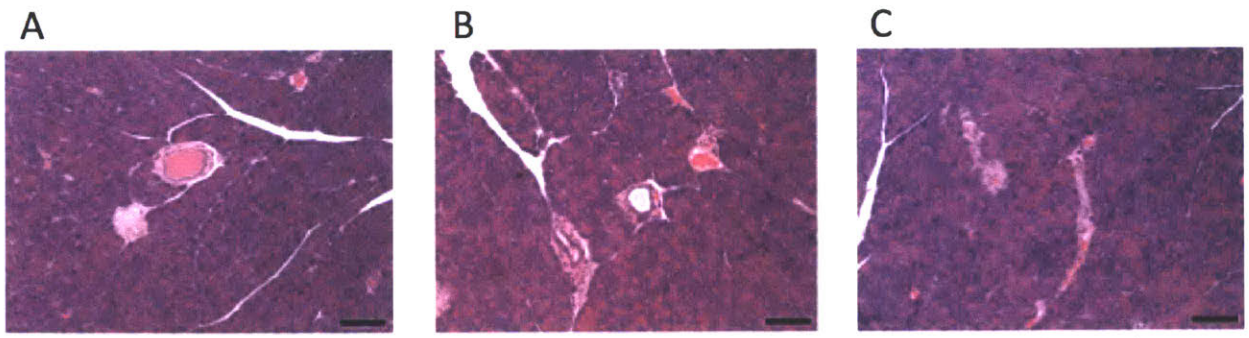

Figure 2-3. Pancreas histology sections. A pathologist blinded to sample identity scored pancreata for signs of inflammation and other pathology. No differences were found between genotypes.

Table 2-1 Pathologist Observations of Pancreas Histology Sections

Sample ID	PANCREAS pathology	Notes (random, rather insignificant findings)	Genotype	pancreas mutant frequency (foci/cm²)
14_2801	Without pathological findings		*Rag2*$^{-/-}$;*IL10*$^{-/-}$	253
14_2802	Without pathological findings	Small-sized single area of cytological alteration (eosinophilic focus)	*Rag2*$^{-/-}$	324
14_2803	Without pathological findings	Small-sized areas (3) of cytological alteration (eosinophilic foci)	WT	93
14_2804	Without pathological findings	Small-sized areas (3) of cytological alteration (eosinophilic foci)	*Rag2*$^{-/-}$;*IL10*$^{-/-}$	417
14_2805	Without pathological findings	Small-sized single area of cytological alteration (eosinophilic focus) Ocassional pancreatic acinar cell vacuolation, minimal Peripancreatic fat, focal granulomatous inflammation	WT	194
14_2806	Without pathological findings	Focal pancreatic acinar cell vacuolation, minimal interlobular edema which is probably an artifact (very small piece)	*Rag2*$^{-/-}$	357
14_2807	Without pathological findings	Small-sized areas (2) of cytological alteration (eosinophilic foci)	*Rag2*$^{-/-}$	409
14_2808	Without pathological findings	Small-sized areas (3) of cytological alteration (eosinophilic foci) Focal acinar cell degeneration (small, unremarkable)	*Rag2*$^{-/-}$	402
14_2809	Without pathological findings	Focal pancreatic acinar cell vacuolation, minimal Focal acinar cell degeneration (small, unremarkable)	WT	233
14_2810	Without pathological findings	Several small-sized areas of cytological alteration (eosinophilic foci)	WT	115
14-2122	Without pathological findings	Focal pancreatic acinar cell vacuolation, minimal Peripancreatic fat, single small focal granulomatous inflammation	*Rag2*$^{-/-}$;*IL10*$^{-/-}$	381
14-2121	Without pathological findings	Small-sized single area of cytological alteration (eosinophilic focus)	*Rag2*$^{-/-}$;*IL10*$^{-/-}$	349
14_2120	Without pathological findings	Small-sized areas (3) of cytological alteration (eosinophilic foci) Peripancreatic fat, single small focal granulomatous inflammation	WT	239
14_2119	Without pathological findings	Several small-sized areas of cytological alteration (eosinophilic foci)	WT	182
14_2118	Without pathological findings		*Rag2*$^{-/-}$;*IL10*$^{-/-}$	363
14_2812	Without pathological findings		*Rag2*$^{-/-}$;*IL10*$^{-/-}$	250
14_2811	Without pathological findings	Small-sized single area of cytological alteration (eosinophilic focus) Focal pancreatic acinar cell vacuolation, minimal	*Rag2*$^{-/-}$	311

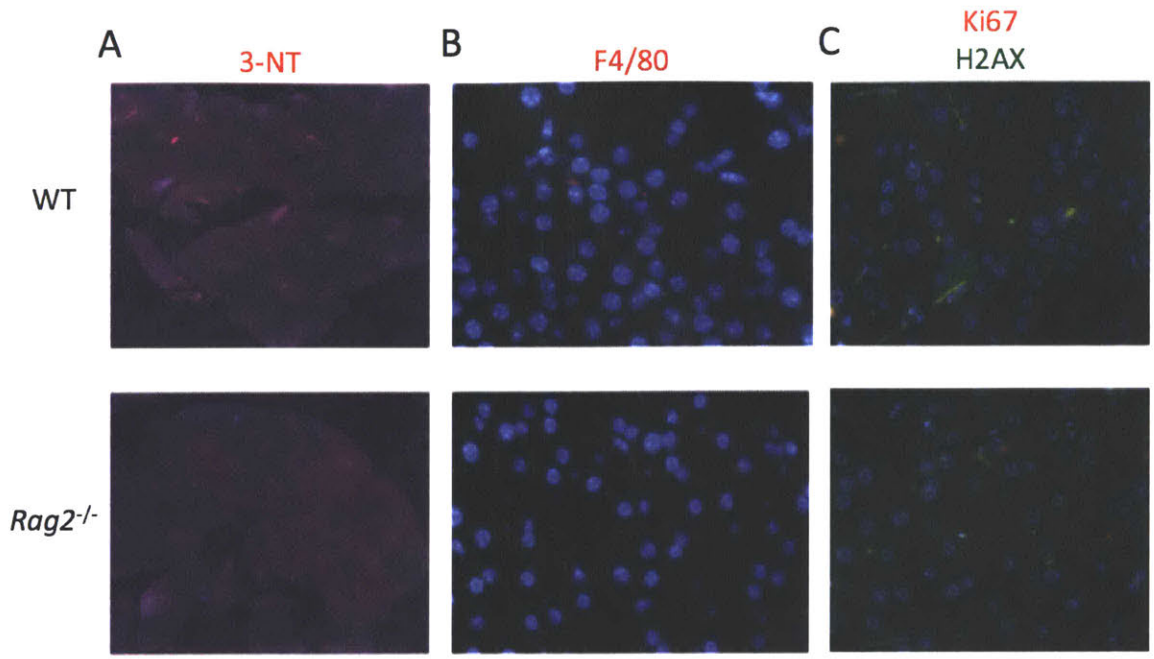

Figure 2-4. Immunofluorescence staining for markers of inflammation do not indicate differences between WT and *Rag2*$^{-/-}$ pancreata. Sections of pancreas tissue from three WT and five *Rag2*$^{-/-}$ animals were used to stain for nitrosative tissue damage (3-nitrotyrosine, A), macrophage presence (F4/80, B), DNA double strand breaks (γH2AX), and proliferation (Ki67) (C). F4/80 and 3-Nitrotyrosine staining were scored by the researcher blinded to sample identity according to intensity of staining. γH2AX-positive cells were defined as having five or more foci within the nucleus. Representative images for each genotype are shown. Scoring of all markers indicated no differences between genotypes (data not shown).

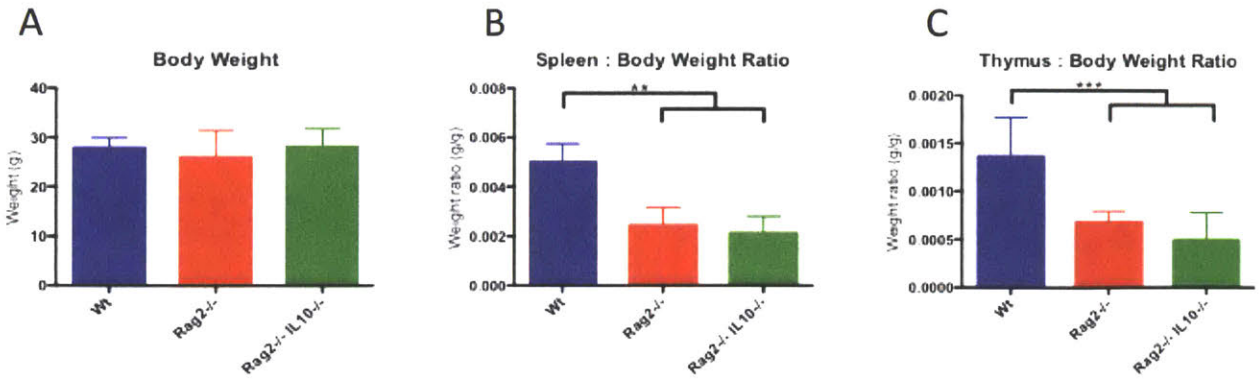

Figure 2-5. Gross pathology metrics. Animals were aged for 6 months with no manipulation. Body, spleen and thymus weights were measured at necropsy. (A) Body weights do not differ among genotypes studied. (B, C) Spleen (B) and thymus (C) weights relative to body weight are significantly decreased in *Rag2*$^{-/-}$ animals. Bar height indicates median, error bars indicate interquartile range. Student's *t*-test, *$p < 0.05$, **$p < 0.01$, ***$p < 0.001$.

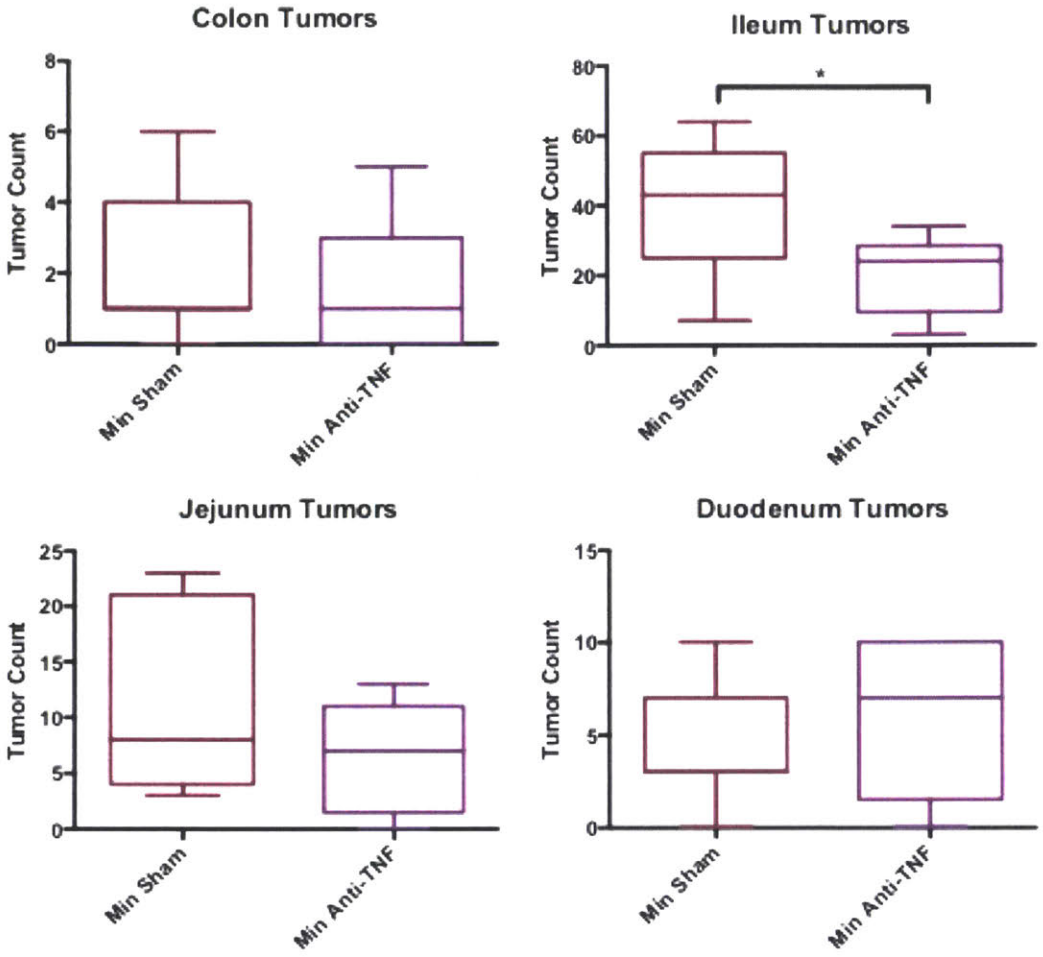

Figure 2-6. Anti-TNF treatment reduces tumor multiplicity in the *Apc*$^{Min/+}$ ileum. Tukey boxplot. Mann-Whitney *U*-test, *$p < 0.05$.

Figure 2-7. Histology sections demonstrate that anti-TNF treatment diminishes degree of intestinal inflammation.

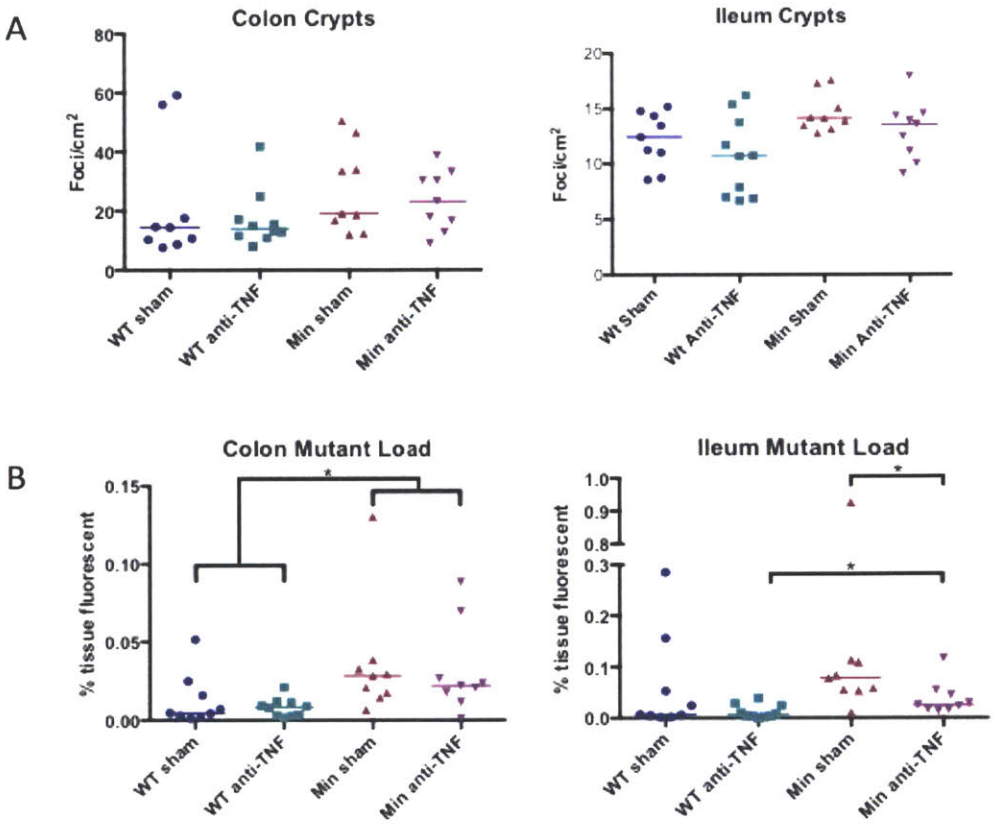

Figure 2-8. RaDR mutation data for intestines. (A) Crypt foci were enumerated by MATLAB foci counting software. (B) Area of tissue fluorescence was approximated by ImageJ analysis (see Materials and Methods). Mann-Whitney *U*-test, $*p < 0.05$.

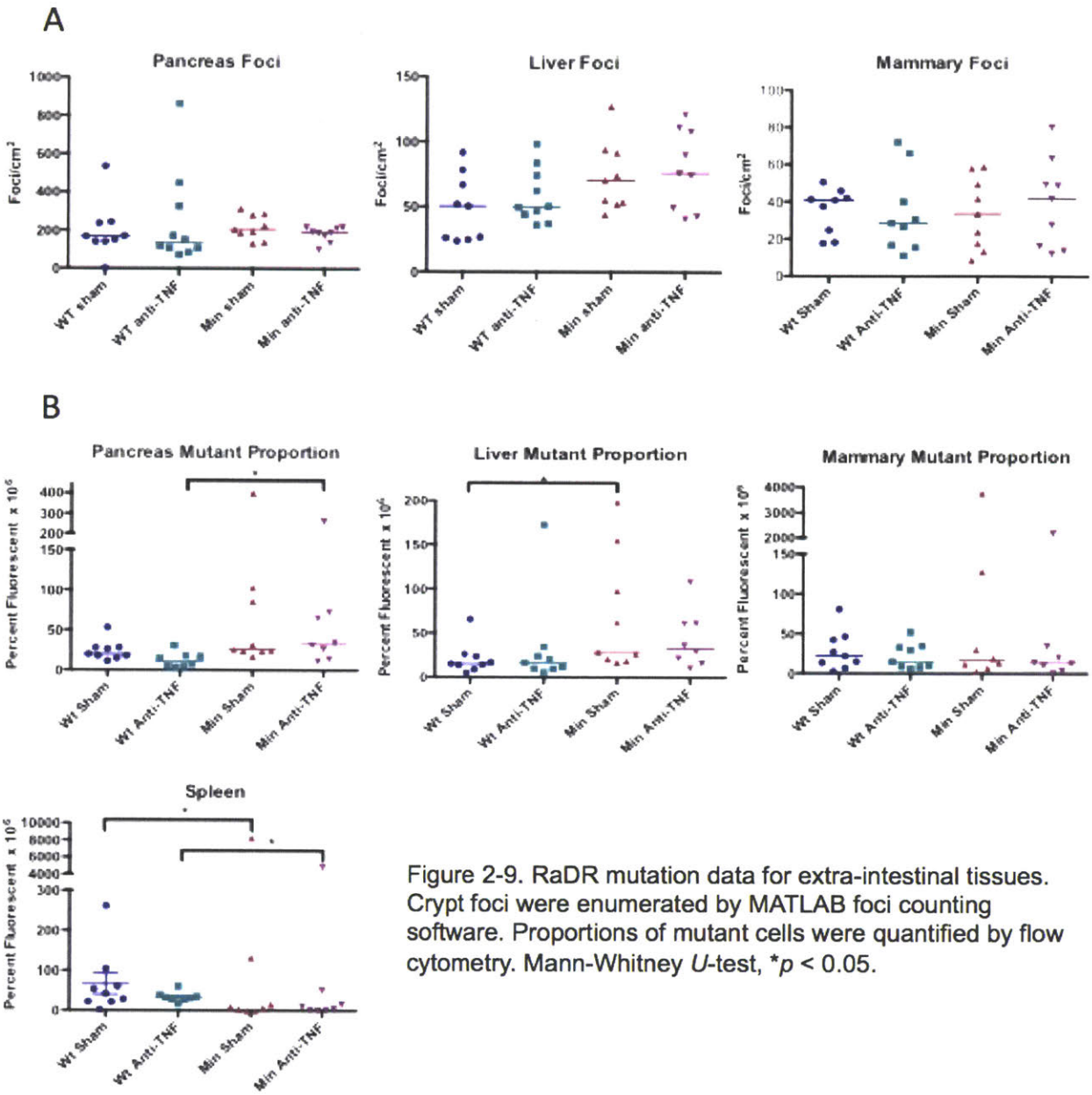

Figure 2-9. RaDR mutation data for extra-intestinal tissues. Crypt foci were enumerated by MATLAB foci counting software. Proportions of mutant cells were quantified by flow cytometry. Mann-Whitney *U*-test, $*p < 0.05$.

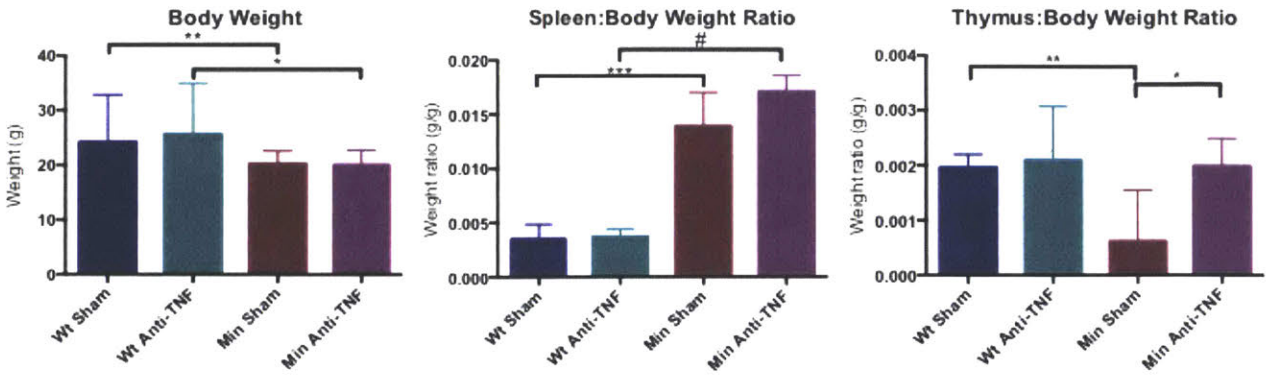

Figure 2-10. Body, spleen and thymus weights at necropsy. (A) *Apc*$^{Min/+}$ mice are smaller than WT. (B) *Apc*$^{Min/+}$ mice suffer from splenomegaly, which is not reduced by anti-TNF treatment. (C) *Apc*$^{Min/+}$ mice suffer from thymic involution, which is partially rescued by anti-TNF treatment. Bar height indicates median, error bar indicates interquartile range. Unpaired Student's *t*-test, $^{*}p < 0.05$, $^{**}p < 0.01$, $^{***}p < 0.001$, $^{\#}p < 0.0001$.

Chapter 3

Exploring the Mutagenic Consequences of Intestinal Inflammation and DNA Damage

3.1 Abstract

Inflammation is a major risk factor for many types of cancers, particularly colorectal. Intestinal inflammation can arise from pathogenic infection or in the form of inflammatory diseases, such as Crohn's disease or ulcerative colitis (UC). To expand upon our understanding of how inflammation promotes mutations and cancer, we analyzed two model systems. First, we treated *Rag2*$^{-/-}$ mice with *Helicobacter hepaticus*, a pathogenic strain of bacteria that causes colonic inflammation and cancer. Second, we utilized the *Apc*$^{Min/+}$ mouse model of colon cancer and treated animals with dextran sodium sulfate (DSS) in drinking water to induce colitis and/or with azoxymethane (AOM) to induce DNA damage. The results of these experiments suggest that inflammation does not strongly induce *de novo* mutagenesis, but increases the total mutation burden, likely due to heightened proliferation. Together, these studies indicate that inflammation does not produce a significant amount of *de novo* sequence rearrangements, but it is a potent promoter of cancer. However, inflammation does promote the overall burden of mutant cells by increased proliferation, which increases the potential for mutant cells to acquire progressively more mutations leading to cancer. Our experiments further suggest that DNA damage in colon stem cells causes preferential apoptosis rather than mutation resulting in a decrease in recombinant crypt foci, though this mechanism has not yet been verified. Thus, we conclude that

inflammation promotes cancer, at least in part, through elevated proliferation, which enables cells to accumulate and propagate mutations.

3.2 Introduction

Chronic intestinal inflammation is the single greatest risk factor for non-hereditary colorectal cancer [1, 2], making the intestine a prime model tissue for studying inflammation-associated carcinogenesis. Intestinal inflammation can arise from a variety of sources, such as pathogenic infection, weak mucosal barrier function, or autoimmunity.

As a model of pathogen-induced inflammation, we selected *Helicobacter hepaticus*. *H. hepaticus* bacteria release cytolethal distending toxin (CDT), a holotoxin comprised of the subunits CdtA, CdtB, and CdtC [3]. CdtA and CdtC form a heterodimer that enable translocation of the catalytically active CdtB into the host cytoplasm [4]. CdtB is a DNase-I-family nuclease that causes double strand breaks [5] and subsequent cell cycle arrest and apoptosis [6]. The DNA damage response induced by CDT is similar to that of ionizing radiation, mediated by ATM and causing cell cycle arrest at the G2/M and G1/S checkpoints [7, 8]. Since CDT is the only known virulence factor for *H. hepaticus* [9], and since the host cellular responses closely mirror those of DSB-induced cell cycle arrest and apoptosis [8], the production of DNA double strand breaks by CDT is likely a major source of its pathogenicity.

While *H. hepaticus* is known to induce inflammation, DNA damage and apoptosis, the potential for *H. hepaticus* to induce mutations has not been studied. To determine whether *H. hepaticus* infection can contribute to mutagenesis, we utilized *RaDR;Rag2*$^{-/-}$ mice, which lack a functional adaptive immune system and sustain a stable inflammatory infection from *H.*

hepaticus [10]. Since many human pathogens also produce CDT [7, 8, 11], humans likely also experience inflammation- and toxin-induced DNA damage simultaneously. Thus, this model system allowed us to interrogate mutagenicity from two important and physiologically relevant sources with a single agent. Surprisingly, however, while *H. hepaticus* produced evident inflammation for several months, we did not observe a difference in sequence rearrangement mutations.

We also evaluated mutagenicity arising from several widely used and well-characterized models of colon cancer. We exposed $Apc^{Min/+}$ (Min) mice with two chemical treatments, dextran sodium sulfate in drinking water and azoxymethane injection, which are used to model colitis-associated and sporadic colon cancer, respectively.

Min mice have been used to study intestinal carcinogenesis for decades [12]. They contain an inactivating point mutation in the tumor suppressor Apc, which results in spontaneous intestinal tumorigenesis within the first two months of life. The Min phenotype also includes elevated metrics of systemic inflammation, splenomegaly, thymic involution, and lymphodepletion [13, 14]. Germline mutations in the human APC gene result in familial adenomatous polyposis (FAP) [15], an inherited disorder resulting in spontaneous development of adenomatous polyps in the colon. Like Min mice, FAP polyps start out benign but can progress to malignancy. Mutations in APC are also a rate-limiting step in the progression of sporadic cancer [16], and indeed APC has been found to be mutated in over 80% of all human colon cancers [17]. Since inflammation is known to play an important role in the progression of Min mouse tumors [18-20], we utilized this model as the basis of our second set of experiments.

Another widely used model of carcinogenic intestinal inflammation is dextran sodium sulfate (DSS) dissolved in drinking water. DSS in drinking water has been used as a model of

acute and chronic colitis for decades [21]. DSS is a detergent that produces nanovesicles with medium chain fatty acids, which disrupt the mucosal surface of the colon epithelium and increase permeability, causing inflammation [22]. Many DSS treatment regimens have been designed for use in murine models to simulate varying degrees and kinetics of human colitis [23]. Generally, 2-5% DSS w/v is dissolved in drinking water and provided to animals for 5-7 days. Multiple bouts of colitis can be simulated by providing DSS water for several days followed by intervals of normal drinking water. Min mice treated with DSS water were found to develop more numerous and severe intestinal polyps than those receiving normal water [24], further supporting the supposition that inflammation contributes to progression of Min tumors.

DSS is frequently used in combination with the chemical mutagen azoxymethane (AOM). AOM is delivered via intraperitoneal injection and gets metabolized in the liver and colon by CYP2E1[25] to produce the reactive methyldiazonium ion, which can then alkylate DNA bases [26]. Typically, when AOM is used in combination with DSS, the AOM is delivered first to induce purported initiating mutations, and then the colitis induced by DSS promotes accelerated proliferation and progressive accumulation of further mutations to produce cancer. Importantly, while AOM is primarily considered a mutation-initiating agent, it may also contribute to tumor promotion [27]. Further, there is evidence that tumorigenesis from AOM can be mitigated by blocking inflammation [28], indicating that inflammation is important to the progression from AOM-initiation to neoplastic growth.

A key finding from the Engelward lab shows that when DNA damage occurs during heightened proliferation, mutagenesis synergistically increases [29, 30]. We incorporated this observation into our experimental design, electing to inject Min mice with AOM during the regenerative proliferation following DSS treatment. Since every cell in the Min mouse is

heterozygous for an inactivating mutation in the *Apc* gene, all Min cells can be thought of as "initiated" in the multistep model of cancer progression, so in this experiment we are investigating how inflammation (DSS) and DNA damage (AOM) contribute to cancer promotion.

The results of our experiments treating Min mice with DSS and AOM show several surprising features. First, we found that DSS-induced inflammation potently increases colon tumorigenesis as well as a corresponding increase in the overall burden of recombinant cells. We also discovered that, counterintuitively, AOM treatment reduced the density of recombinant colon crypt foci. AOM treatment increased tumor multiplicity in the small intestine but not the colon. Finally, analyzing mutations in extra-intestinal tissues revealed that AOM and/or DSS treatment may promote sequence rearrangement mutations in off-target tissues.

3.3 Materials and Methods

3.3.1 *Rag2*$^{-/-}$ animals for *H. hepaticus* treatment

Experimental *RADR*$^{R/R}$;*gpt-Δ;Rag2*$^{-/-}$ (RGR) animals were created by crossing *Rag2*$^{-/-}$ (129S6/SvEvTac-*Rag2*^{tm1Fwa}) [10] with *RADR*$^{R/R}$;*gpt-Δ* animals also on the 129 background. Litters were split into infection and control cohorts with equal numbers of males and females in each group. Uninfected mice were housed in a barrier facility free of known murine *Helicobacter* species, viruses, *Salmonella* species, *Citrobacter rodentuim*, ecto- and endoparasites.

3.3.2. *H. hepaticus* treatment

H. hepaticus (strain 3B1, no. 51449; ATCC, Rockville, MD) was grown as described under microaerobic conditions on blood agar plates and collected into sterile freeze media [10]. A total of 41 experimental animals 6-8 weeks of age received 0.2 ml freezing medium (n=19) or freshly prepared *H. hepaticus* inoculum (total organism dose of 10^8 CFU, n=22) via gastric gavage every other day for 3 doses. Two weeks later, the mice received a second round of 3 doses every other day for a total of 6 doses. Prior to dosing, all *H. hepaticus* samples were examined via gram stain to ensure >85% of the bacteria were in the spirochete form (virulent form). Tissues were harvested at 10 weeks post infection utilizing standard necropsy procedures.

3.3.3 *H. hepaticus* PCR

Feces were collected from each animal during necropsy to confirm presence of *H. hepaticus*. DNA was extracted from feces using the QIAamp DNA Stool Mini Kit. PCR was run using primers specific to the *H. hepaticus* strain [31].

3.3.4 Histopathology

Formalin-fixed tissues were embedded in paraffin, cut in 5 μm sections, and stained with hematoxylin and eosin. Sections were scored by a pathologist blinded to sample identity.

3.3.5 *Apc*$^{Min/+}$ animals and AOM and DSS treatments

Experimental C57 *RADR*$^{R/R}$;*gpt-Δ*;*Apc*$^{Min/+}$ (RMin) animals were created by crossing *RADR*$^{R/R}$;*gpt-Δ* animals with C57Bl/6J *Apc*$^{Min/+}$ mice donated by Dr. Susan Erdman. Animals were bred and maintained in an AAALAC-accredited barrier facility free of known murine

Helicobacter species, viruses, *Salmonella* species, *Citrobacter rodentium*, ecto- and endoparasites. At six weeks of age, experimental animals were transferred to a hazardous materials containment facility at least two days prior to the beginning of treatment.

DSS (MP Biomedicals, 35,000-50,000 kDa) was dissolved in water obtained from the mouse colony at 1% w/v. DSS-treated animals were supplied with this water for seven days, at which point they resumed normal drinking water.

AOM (Sigma-Aldrich) was diluted to 10 mg/mL in sterile PBS and stored in aliquots at -20°C. On the day of treatment, AOM was diluted to 1 mg/mL in sterile PBS and sterile filtered with a 0.2 μm filter just prior to dosing. Each animal was weighed and the appropriate volume of AOM was calculated such that the animal would receive a single i.p. injection of 4 mg AOM per kg body weight. Sham-treated animals were weighed and injected with an equivalent volume of sterile PBS.

Following pilot studies to determine appropriate dosing, three treatment regimens were performed. The first, main experiment entailed mice at 6 weeks of age to be split evenly between control, DSS, AOM, and DSS+AOM treatment regimens. All animals were housed in a hazardous material containment facility for the duration of the experiment regardless of treatment. Animals received either 1% DSS or normal drinking water for seven days, then all animals were given normal water. On day 10 (three days after return to normal water), animals were dosed with an i.p. injection of either 4 mg/kg AOM or sterile PBS. Animals were necropsied on days 21-23. The second experiment was set up identically, but with no control group, and animals were necropsied on day 12 (two days after AOM). The final experimental cohort received 4 mg/kg AOM i.p. injection on the first day, then 1% DSS water from days 5-12, and were necropsied on day 21.

Animals were monitored daily for signs of distress and morbidity and weighed at least every other day. Animals that dropped below 80% of their initial body weight were humanely euthanized. At the end of the experiment, mice were euthanized by CO_2 according to AVMA guidelines and necropsied with standard procedures.

3.3.6 DSS Pilot Ki67 Immunofluorescence

Formalin-fixed tissue sections were embedded in paraffin and cut in 5 μm sections. Slides stained for immunofluorescence were first deparaffinized with three five-minute washes in xylenes, two five-minute washes in 100% ethanol, and 10-minute washes each in 95% ethanol, 90% ethanol, and 70% ethanol. Slides were washed twice in PBS, then boiled in Dako citric acid antigen retrieval buffer (S1700, Agilent Technologies, Santa Clara, CA) for 30 min. After cooling, slides were washed twice in diH_2O and tissue sections were circled with hydrophobic marker. Sections were blocked for one hour with 5% BSA + 0.3% Triton in PBST at room temp. All antibodies were diluted in 1% BSA + 0.3% Triton in PBST, and sections were stained overnight at 4°C. Slides were then washed three times for five minutes each in PBST and incubated with the appropriate secondary antibody for one hour at room temperature. Slides were then washed five times in PBST for five minutes each. Finally, a drop of DAPI with ProLong™ AntiFade reagent (Invitrogen) was placed on the section, and a cover slip was laid overtop and sealed with clear nail polish. Anti-Ki67 antibody was Abcam ab15580, rabbit origin, and the secondary antibody was Alexa Fluor 647 (goat anti-rabbit).

Slides from each intestine segment were stained in parallel and imaged on the same day under identical conditions. The researcher was blinded to sample identity for scoring. Images

were evaluated in Photoshop CS6, and the number of Ki67+ cells in complete crypt cross sections were counted and recorded. Each crypt served as a single data point.

3.3.7 RaDR Necropsy and Tissue Imaging

Animals were euthanized with CO_2 according to AVMA guidelines. Tissues were excised and held on ice in tubes containing PBS (mammary) or PBS with 0.01% trypsin inhibitor (T9008 Sigma-Aldrich or P-1540 Westnet Inc) (pancreas, liver, intestines) until use. The entire colon was excised (cecum to anus), and the small intestine was divided roughly into thirds, such that the duodenum (proximal, attached to stomach), jejunum (middle section), and ileum (distal, attached to cecum) were approximately equal lengths. Intestines were cut open on one side and the lumen was rinsed of fecal matter before placing in PBS + trypsin inhibitor. Mammary, pancreas, liver and intestine tissues were compressed to 0.5 mm between coverslips and imaged for EGFP under the 1x objective with the FITC filter of a Nikon 80i fluorescent microscope.

3.3.8 Quantifying RaDR Mutagenesis

RaDR transgenic mice develop fluorescent (EGFP+) cells following a sequence rearrangement mutation at the transgenic construct. Mutagenesis can be quantified in a variety of ways with varying biological significance. This data is collected either by imaging the whole tissue on a fluorescence microscope or cell sorting by flow cytometry.

Foci counting

Imaging of a RaDR tissue allows enumeration of individual foci, which correspond to single mutation events. Cells that have acquired the RaDR mutation may clonally expand, leading to

various sizes of foci, and so it is often of interest how many mutation events occurred in the tissue instead of, or in addition to, the total proportion of mutated cells. In collaboration with Dr. Dushan Wadduwage of Peter So's laboratory, we have developed a MATLAB program that enumerates the total number of foci in the tissue and measures the area of the tissue, providing results as foci/cm^2. This is the preferred method for quantifying *de novo* recombination events in pancreas and liver tissues.

Crypt foci counting

Intestines have regular, distinct architecture that enables identification of mutations in somatic stem cells. Intestine epithelium consists of pore-like divots into the mucosa called crypts, and the small intestine also contains fingerlike projections into the lumen, called villi. At the base of each crypt are one or more somatic stem cells, which give rise to the proliferative transit cells that comprise the length of the crypt and, in the small intestine, the villi surface. The continual proliferation of stem and transit cells enables continual renewal of crypt (and villus) epithelia. Transit cells are eventually sloughed off into the lumen, and stem cells produce complete epithelial turnover within 3-5 days [32]. In a RaDR animal, mutations in crypt stem cells are visible as large, bright, roughly circular foci that can be distinguished from the smaller, dimmer and/or irregularly shaped foci of mutated transit cells. The foci that we believe to be converted crypts are, on average, 10x brighter and 6x larger than foci that appear to be single cells. Since somatic stem cells persist for years, if not the animal's lifetime, whereas transit cells are sloughed off within 5 days, it is of great interest to quantify recombinant stem cell foci rather than all foci. To this end, we have collaborated with Dr. Wadduwage to develop a modified version of the MATLAB foci counting program that allows the user to "train" the program which

foci to count based on size, shape and intensity, enabling quantification of mutated stem cells in the tissue normalized to tissue area in tumor-free tissue (see Fig 3-1B for example).

Percent area mutated

When intestinal tumors develop, the regular architecture of the intestine becomes disrupted, and somatic stem cells are no longer distinguishable and cannot be quantified. For this reason, we have developed a method to approximate the area of the tissue that can be classified as EGFP+. By defining conservative thresholds for pixel intensity in ImageJ, we quantify the area of tissue that is brightly fluorescent and thus have a rough measure for the total mutation burden in the tissue (see Fig 3-1C for example). These results are given as the percent area of tissue that is fluorescent.

Flow cytometry

Flow cytometric sorting allows quantification of the overall proportion of mutated cells in the tissue. This method is most useful for tissues that are too thick for imaging (e.g., spleen) or have very small cells with irregular internal structures that make focus counting intractable (e.g., thymus, lung). Since flow cytometry requires disaggregation of the tissue, it is not possible to distinguish between mutation events and clonal expansion of mutated cells, nor is it possible to perform additional assays, making this method appropriate only for tissues that cannot be analyzed with the methods described below.

3.3.9 Tumor Quantitation

Following RaDR imaging, intestine segments were laid flat on bibulous paper and cut in half longitudinally. Half the tissue was fixed in 10% formalin for tumor counting, and half was snap-frozen in liquid nitrogen for Gpt assay (see below). After several days, the formalin was discarded and replaced with 100% ethanol for 24 hours. The ethanol was then discarded and replaced with 70% ethanol. To count tumors, intestine segments were carefully removed from the bibulous paper cassettes and placed on a stereoscopic 10x microscope. The approximate sizes and locations of tumors within each segment were recorded on paper. Tumors counts are represented by Tukey boxplots, wherein the boxes represent quartiles of data and whiskers represent the data lying within 1.5*IQR (interquartile range). Data points lying outside 1.5*IQR are represented as dots.

3.3.10 Gpt point mutation assay

The Gpt assay was performed as described previously [33, 34]. DNA was extracted from snap-frozen colon and ileum samples using the RecoverEase DNA Isolation Kit (Agilent Technologies, Santa Clara, CA). In order to ensure a sufficiently large volume of high molecular weight DNA with each preparation, two samples of colon (or ileum) tissue were combined in the mortar before grinding the tissues, so each data point represents the DNA of two animals. The same individuals were paired for both colon and ileum sample sets.

DNA was packaged with λ-EG10 phage extracts, which were prepared in-house. Empty phage head extracts were prepared by culturing NM759 *E. coli* in NZY broth at 32°C, heat-shocking the culture at 45°C for 15 min, then re-expanding at 38°C. Bacteria were then pelleted at 1,800 *x g* and resuspended in a buffer containing 20 mM TrisCl, 10 mM EDTA, and 0.035%

β-mercaptoethanol. The suspension was sonicated 12x in three-second bursts on a Misonix Sonicator 3000 at power level 4, between which the suspension was held on ice for 25-30 seconds. The suspension was then pelleted at 6,000 *x g*, supernatants collected and combined with a packaging buffer containing 6 mM TrisCl, 50 mM Spermidine-HCl, 50 mM Putrescine-HCl, 20 mM MgCl2, 30 mM ATP, and 0.021% β-mercaptoethanol. Aliquots were then snap frozen in liquid nitrogen.

Phage "pre-head" complexes were prepared by culturing BHB2866 *E. coli* in NZY broth at 32°C, heat-shocking the culture at 45°C for 15 min, then re-expanding at 38°C. Bacteria were then pelleted at 1,800 *x g*, resuspended in a 10% sucrose solution containing 50mM TrisCl, snap frozen in 0.5 mL aliquots, and stored at -80°C. Frozen bacteria were later thawed on ice and ultracentrifuged at 163,000 *x g* for three hours at 4°C. The supernatant was combined with packaging buffer containing 6 mM TrisCl, 50 mM Spermidine-HCl, 50 mM Putrescine-HCl, 20 mM MgCl2, 30 mM ATP, and 0.021% β-mercaptoethanol, then snap-frozen in aliquots.

Each time DNA was packaged and the Gpt assay was performed, five samples were processed: one from each treatment group, and one internal control. DNA was packaged by combining thawed aliquots of both phage extracts with high molecular weight intestine DNA, incubating at 32°C for 90 minutes, adding an additional set of thawed phage extracts for 90 minutes at 32°C, and finally halting the reaction by addition of a buffer and setting on ice.

Phage packaging efficiency was evaluated by infecting lysogenic MRA *E. coli* with packaged phage and quantifying plaques. The titer of packaged Gpt DNA was quantified by infecting YG6020 *E. coli* with packaged phage and selecting for chloramphenicol resistant colonies, and the mutant fraction was determined by plating infected YG6020 *E. coli* on chloramphenicol and 6-thioguanine selection plates.

3.3.11 Statistical Analyses

RaDR foci were quantified as the number of foci per square centimeter of area (foci/cm^2), and RaDR flow cytometry measurements were given as % fluorescent*10^6. Due to the fact that the distribution of EGFP-positive cells in RaDR mice is non-normal across tissues and among individuals, RaDR data sets were compared by Mann-Whitney *U*-test. It was not clear that tumor multiplicity was normally distributed between individuals, and therefore tumor counts were also compared by Mann-Whitney *U*-test. Body and tissue weights were compared by unpaired Student's *t*-test. All statistical comparisons were calculated using GraphPad Prism 5.

3.4 Results

3.4.1 *H. hepaticus* infection causes inflammation but does not significantly alter mutagenesis

We confirmed that *H. hepaticus*-infected animals had retained the bacteria through the duration of the experiment by collecting feces at necropsy, extracting DNA, and performing PCR (data not shown). Histopathological evaluation confirmed that infected animals were experiencing colonic inflammation (Fig 3-2). This experiment predated the development of the MATLAB foci counting programs, and so initial quantification of RaDR foci was accomplished by manual counting of blinded images. Despite being blind to sample identity, this method of quantifying foci still risks user bias, so we subsequently re-analyzed images with the unbiased MATLAB program. While manual enumeration of RaDR foci in the colon, liver and pancreas indicated a slight but significant decrease in mutation frequency in infected animals (Fig 3-3, left panels), re-

analysis by the MATLAB program showed no significant differences in mutagenicity due to *H. hepaticus* infection (Fig 3-3, right panels).

Unfortunately, the RaDR image data was collected in under inconsistent exposure conditions, and a single intensity threshold for estimating percent tissue fluorescence with ImageJ could not be applied to all images in the data set. Therefore, we were unable to compare the overall mutant burden in *H. hepaticus* colons.

3.4.2 DSS recovery pilot to determine dosing schedule

A key observation from other recombination studies in the pancreas is that if DNA damage occurs during a period of increased proliferation, sequence rearrangement mutations synergistically increase compared to DNA damage or proliferation alone. Thus, we hypothesized that if DNA damage from AOM occurs during the regenerative proliferation following DSS-induced inflammation, we would similarly see a large increase in recombination.

Six 6-week old males were given 1% DSS in drinking water for 7 days, and then two mice each were sacrificed on days 8, 10 and 12 (one, three and five days after return to normal drinking water). Intestines were saved as swiss rolls in formalin, embedded in paraffin, and sectioned for Ki67 immunofluorescence. Slides from D8, D10 and D12 were grouped by intestine segment, stained in parallel for Ki67, and imaged on the same day. Three images per slide were taken and filenames were blinded. Ki67+ nuclei were counted for each full crypt cross-section in the field and recorded. Quantification indicated that colon crypts had a peak in the number of proliferating cells on D10 (Fig 3-4A), and so this day was selected for AOM treatment.

Subsequently, six 6-week old animals (three of each sex, see Table 3-1) were sacrificed as a day zero untreated control and intestines were again saved for immunostaining. Slides from D0, D8, D10 and D12 were grouped by intestine segment, stained in parallel for Ki67, and imaged on the same day. Four images per slide were taken and filenames were blinded. This second quantification indicated that peak proliferation in colon crypts was on D12, but the median on D12 (14 Ki67+ cells) was only two more than the median on D0 (12 Ki67+ cells). Thus, while the difference between D0 and D12 is statistically significant, it is by only a small amount.

We also stained and imaged one slide from each intestine segment for H&E (representative images shown in Fig 3-4C). Colon polyps are visible in all DSS-treated samples (Fig 3-4C, circles), but in all samples there also appear to be regions of relatively normal physiology. Note that since we only counted Ki67+ cells in complete crypt cross-sections, we necessarily excluded proliferating cells in tumors (which no longer have intact crypts).

3.4.3 Experimental treatments cause some morbidity

Based on pilot experiments, we treated animals according to the timeline shown in Figure 3-5A. As *RADR*$^{R/R}$;*gpt-Δ*;*Apc*$^{Min/+}$ (RMin) mice reached six weeks of age, they were divided between Control, AOM, DSS and DSS+AOM treatment groups such that all treatments would be performed in parallel. Each of the treatments produced some morbidity (Fig 3-5B), so as the experiment progressed, animals were divided between groups to aim for similar numbers of males and females with necropsy data (see Table 3-1). Data is not presented for animals sacrificed before the end of the experiment because the primary objective was to analyze accumulation of mutant cells, which requires that all animals are analyzed at the same timepoint.

Animals that were able to tolerate treatments had fully recovered their body weight by the end of the experiment (Fig 3-5C). DSS treatment caused significant loss of body weight after returning to normal water (Fig 3-5C) and exacerbated Min splenomegaly (Fig 3-5D), both of which are consistent with DSS causing severe inflammation [23]. AOM treatment produced a significant drop in body weight the day after dosing (D11), but mice quickly recovered (Fig 3-5C).

3.4.4 DSS induces distal colon tumors and AOM induces ileum and duodenum tumors

DSS treatment produced a significant increase in tumors in animals' colons (Fig 3-6A). Notably, DSS consistently caused densely packed tumors in the distal two-thirds of the colon, but the proximal third of the colon rarely had any polyps. In contrast, AOM-treated animals developed more polyps in the ileum and duodenum (Fig 3-6B, D). Neither treatment altered tumorigenesis in the middle portion of the small intestine, the jejunum (Fig 3-6C).

3.4.5 DSS increases the total burden of recombinant cells

We analyzed intestinal mutations by several different methods for different perspectives of mutagenicity. First, we quantified the total area of the tissue above a defined threshold pixel intensity as an approximation of the total burden of recombinant cells in the tissue (see Materials and Methods, Quantifying RaDR mutagenesis, Percent area mutated). By this metric, we observed a significant increase in the overall burden of mutant cells in colons that had received DSS treatment (Fig 3-7A). We also observed a larger overall mutant burden in colons and ilea of animals that received both DSS and AOM compared to animals that received AOM alone (Fig 3-7A, B).

Importantly, the increase in DSS-treated colons' overall mutant burden was driven in large part by tumors. Tumors can acquire the RaDR rearrangement mutation at any point during development, and thus tumors may be partially or fully fluorescent. For example, the colon shown in Figure 3-1A received DSS treatment and thus has densely packed tumors in the distal two-thirds of the tissue (white box). Analyzing this tissue for total mutant burden indicates that 4.3% of the tissue fluoresces above the pixel intensity threshold, the vast majority of which results from the large fluorescent tumors near the middle of the tissue (Fig 3-1C). More commonly, tumors have patches of fluorescence, and the total area that exceeds the threshold intensity is less than 1% of the tissue.

Interestingly, despite the fact that AOM induced tumors in animals' ilea and jejuna, AOM did not increase the total burden of recombinant cells in any intestine segment.

3.4.6 AOM reduces frequency of somatic stem cell recombination

Since tumors were almost exclusively present in the distal two-thirds of the colon, macroscopic folds of tissue characterize the proximal third of the colon, and large tumors are often visible in RaDR tissue images, we were able to identify a consistently tumor-free region in all colon samples to analyze for recombinant crypt foci (Fig 3-1B). We analyzed the same region in every sample by the crypt foci counting program (see Materials and Methods, Quantifying RaDR mutagenesis, Crypt foci counting). Surprisingly, we found that animals treated with AOM alone had a significantly lower frequency of recombinant crypt foci (Fig 3-8A).

We also quantified mutant crypts in ileum tissue by excluding any tumors that were visible in the RaDR image in the counting program. These results suggest that AOM-treated ilea contained a lower frequency of converted crypts compared to animals that received both AOM

and DSS (Fig 3-8B). However, the crypt-counting program performs less reliably in distinguishing small intestine crypts compared to colon because the small intestine villi create more variability in the appearance of foci.

3.4.7 DSS+AOM combination treatment may increase point mutations

To provide a more comprehensive analysis of mutations from DSS and AOM treatments, we performed the Gpt assay for point mutations. Animals treated with the combination of DSS and AOM were found to have a larger mutant fraction in the colon compared to other groups (Fig 3-9A), but there were no significant differences in point mutations in animals' ilea (Fig 3-9B). Due to great variability in the data from this assay, we do not draw firm conclusions from the data collected and will perform replicates to improve confidence.

3.4.8 Early analysis shows no AOM-induced recombination, but rapid induction of tumors by DSS

We hypothesized that AOM may produce RaDR mutations in intestinal transit cells that are sloughed off before necropsy. To determine whether this was the case, another cohort of animals were given AOM, DSS and DSS+AOM treatments as described in Figure 3-4A, but all animals were necropsied on day 12, two days after AOM dosing (see Table 3.1). This would provide sufficient time for the AOM to be metabolized and react with DNA, and cells could undergo a full replication cycle to develop the RaDR mutation, but transit cells would not yet be sloughed off.

We did not observe significant induction of mutations at this early timepoint in any intestine segment (Fig 3-10A). One noteworthy observation is that DSS treatment causes colon

tumors within five days of returning to normal water (Fig 3-10B), which is consistent with other studies of $Apc^{Min/+}$ animals treated with DSS [24].

3.4.9 AOM treatment before DSS does not significantly increase mutagenesis

The standard treatment schedule for AOM in combination with DSS is to deliver the AOM first, followed several days later by DSS in drinking water. Therefore, we wished to compare our treatment regimen, where AOM was timed to coincide with proliferation after DSS, to the more traditional model of dosing AOM first. We treated animals as shown in Figure 3-11A (see Tables 3.1 and 3.2 for cohort composition). Animals in this experiment experienced more severe body weight loss and morbidity (Fig 3-11B, C), though it is important to note that a larger number of females were allocated to this experiment than other cohorts (Table 3.1), and females are more sensitive to toxicity from DSS.

We quantified intestinal mutagenicity in terms of total recombinant cell burden as well as crypt foci in non-tumorous tissue. Surprisingly, animals treated with AOM prior to DSS developed fewer recombinant colon crypts as well as a lower proportion of fluorescent tissue in all intestine segments compared to the groups in the main experiment (Fig 3-12A, B. Data for D0, Ctrl, AOM, DSS and DSS+AOM shown for comparison). Indeed, the frequency of converted crypts and overall mutant burden in the AOM-then-DSS animals are much more similar to the animals analyzed for the Day 12 early timepoint (Fig. 3-12C, D. D0 and D12 data shown for comparison). It is important to note that D21, D12 and AOM-then-DSS experiments were not performed in parallel (see Table 3-1). Therefore, comparisons are limited to qualitative descriptions and no firm conclusions can be drawn.

3.4.10 Off-target mutagenesis

In addition to analyses of mutations in intestine tissue, we also collected RaDR data from liver, pancreas, spleen, and thymus tissues to see if DSS or AOM, commonly considered colon-specific treatments, produce mutations in other tissues. There was a small but significant increase in the number of foci in the liver and pancreas of mice that received the combination of DSS followed by AOM (Fig 3-13A, B). The spleen and thymus also appear to be susceptible to increased mutagenesis from AOM treatment (Fig 3-13C, D), but these results are not statistically different from control.

3.5 Discussion

The experiments described in this chapter yielded many unexpected but enlightening results. Although we did not observe an increase in recombination frequency due to inflammation or DNA damage, we uncovered circumstances that increase recombinant cell burden and decrease recombinant cell frequency.

The first experiments described here, dosing *Rag2*$^{-/-}$ mice with *H. hepaticus*, first indicated that infection slightly decreases recombination frequency in the liver and colon, but subsequent image analysis by MATLAB did not show statistically significant difference in results (Fig 3-2). The fact that colon and liver both showed the same trend in decreased recombination frequency is noteworthy because *H. hepaticus* is known to cause both colitis and hepatitis in mice, so both tissues with ambiguously fewer foci were targets of the pathogen [35, 36]. Importantly, however, *H. hepaticus* combines both DNA damage and inflammation into a single treatment, and tumors had not yet begun to develop, so we designed an experiment separating the variables of DNA

damage (AOM) and inflammation (DSS) and applied it to a model of heritable colon cancer. Interestingly, treatment with our model DNA damaging agent AOM also resulted in fewer recombinant crypt foci.

Cairns' immortal strand hypothesis offers one explanation for how both *H. hepaticus* infection and AOM treatment could reduce recombinant crypt foci frequency. Cairns posits that somatic stem cells protect their original DNA strands by selective segregation during mitosis, and that irreversible damage causes the cell to undergo apoptosis as a protective mechanism against mutations [37]. Indeed, a number of studies have evidence supporting a model of selective chromatid segregation [38, 39]. This hypothesis is further supported by studies showing that CDT causes cell cycle arrest and apoptosis via the ATM-dependent intrinsic pathway [7, 9].

There are two important inconsistencies between the immortal strand hypothesis and results of our experiments. First, Cairns suggests that somatic stem cells should be deficient in recombinatorial repair to protect the "immortal strands" from exchange, but the fact that we observe fully fluorescent crypts suggests that not all recombination is inhibited {Cairns 2006}. Second, Cairns posits that dead stem cells are replaced by dedifferentiated daughter cells, but that would entail a RaDR stem cell being replaced with a daughter that also has the RaDR mutation, leaving recombinant crypt frequency unchanged. More work is necessary to determine what happens to colonic stem cells exposed to DNA damage and how the tissue responds. Our data support a model wherein colonic stem cells undergo mutagenic recombination sporadically and crypt foci accumulate with age, and separately, the induction of DNA damage causes crypt stem cells to die without replacement by dedifferentiated daughters.

Complications with the bacteria may have confounded the results of the *H. hepaticus* study. For instance, *H. hepaticus* virulence varies between strains [40], and CDT activity is

necessary for cytotoxicity and DNA damage response activation [9, 36]. If, during culture or passaging of the bacteria, the strain mutated to lose virulence potency, the mutagenic consequences of the CDT toxin may have been diminished. Furthermore, we have seen that the timing of DNA damage in relation to proliferation is a key modulator of recombination frequency, but in this model we know little regarding the kinetics of proliferation and bacteria activity during the 3 months of infection. The gut may enact protective mechanisms, such as modified proliferation kinetics, during infection that cannot be identified at a single late timepoint.

We designed our second set of experiments, treating $Apc^{Min/+}$ (Min) mice with dextran sodium sulfate (DSS) and/or azoxymethane (AOM) with the objective of greater control over experimental variables. A crucial aspect of our experimental design relied on determining when regenerative proliferation peaks following DSS-induced inflammation, having observed synergy when DNA damage occurs during proliferation in the pancreas [29, 30]. We quantified the number of proliferating cells in crypts of each intestine segment one (D8), three (D10) and five (D12) days following the return to normal water after seven days of DSS, and results indicated that proliferation peaked around D10 or D12 (Fig 3-3), which is consistent with other studies [41]. Notably, however, the median numbers of proliferating cells at these times were only one or two increased from untreated animals, so while the increase in proliferation was statistically significant, it was not a large difference. The low variability in colon proliferation activity suggests the colon is less susceptible to perturbations in proliferation as a result of inflammation.

Our two experimental treatments both induced tumors in Min mice, but in different locations. DSS treatment typically produces tumors in the distal colon [23], which is consistent with our results here. Interestingly, however, AOM induced tumors in the proximal and distal

small intestine (duodenum and ileum, respectively). Although AOM is often considered a colon-specific treatment, several studies have shown that it produces methylation adducts in the liver and small intestine, provided the tissue expresses CYP2E1 [26]. The expression of P450 enzymes has not been characterized along the Min small intestine, but P450 expression is known to vary along the gastrointestinal tract [42], so perhaps differential CYP2E1 expression in the duodenum and/or ileum increased the mutagenicity of AOM in those segments.

Proliferation kinetics may also factor into AOM carcinogenicity. Min mice spontaneously develop the majority of polyps in the ileum, suggesting that Wnt dysregulation and hyperproliferation are most pronounced in the ileum, and therefore most susceptible to DNA damage-induced mutations. It is likely that CYP2E1 activity and proliferation kinetics both play a role in AOM tumorigenesis.

While none of these experimental treatments increased recombination frequency in the intestines, we did observe a significant increase in the total burden of recombinant cells in tumorous colon tissue. The most likely mechanism for this observation is that hyperproliferation and progressive genomic instability in tumors produced many opportunities for cells to acquire the RaDR mutation. Indeed, we observed tumors that appear to have acquired the RaDR mutation early on, producing fully or near-fully fluorescent polyps (Fig 3-7). There also appears to be a trend of increasing recombinant cell burden with time post-DSS exposure (e.g. early analysis at D12 and AOM-then-DSS; see Fig 3-12). This result is not surprising, given that we have already shown previously that the majority of RaDR mutant cells in normal tissue derive from clonal expansion of rare recombination events rather than de novo mutations [43, 44].

Finally, these experiments permitted several novel analyses. First, we multiplexed our mutation analyses by performing the Gpt assay on tissue that had been analyzed for sequence

rearrangement mutations. By adding replicates of this assay to our data set, we will be able to confidently comment on multiple types of mutagenicity resulting from AOM and DSS exposures. Additionally, the RaDR mouse permits efficient, cost-effective analysis of off-target tissues as well. Whereas typical laborious mutation assays require careful selection of samples in the interest of time and money, little additional effort is required to analyze many tissues for RaDR mutations. Using the RaDR mouse, we were able to incorporate mutation analyses of many extra-intestinal tissues, including the pancreas, liver, spleen and thymus (Fig 3-13). While we did not anticipate any significant differences in mutations in these off-target tissues, we were intrigued to discover that DSS+AOM increased mutation frequencies in the liver and pancreas, and surprised to discover that AOM-treated lymphoid organs are prone to extremely high proportions of recombinant cells.

In conclusion, the experiments described in this chapter support a model whereby DNA damage in intestinal stem cells promotes apoptosis rather than mutations, and inflammation increases the total burden of mutated cells by clonal expansion.

3.6 Acknowledgements

The work described in this chapter was performed in collaboration with members of several laboratories. The foci counting programs used to quantify *de novo* recombination events were written by Dr. Dushan Wadduwage of Prof. Peter So's laboratory. Dr. Michelle Sukup-Jackson contributed to the experimental design, execution and analysis of the *H. hepaticus* infection study, and Tatiana Levkovich performed *H. hepaticus* gavage. We also thank Glenn Paradis for

training and use of the Koch Institute Flow Cytometry Core. This work was supported in part by the NIH/NIGMS Interdepartmental Biotechnology Training Program (5 T32 GM008334).

3.7 References

1. Rutter, M., et al., *Severity of inflammation is a risk factor for colorectal neoplasia in ulcerative colitis.* Gastroenterology, 2004. **126**(2): p. 451-9.
2. Kim, E.R. and D.K. Chang, *Colorectal cancer in inflammatory bowel disease: the risk, pathogenesis, prevention and diagnosis.* World J Gastroenterol, 2014. **20**(29): p. 9872-81.
3. Lara-Tejero, M. and J.E. Galan, *CdtA, CdtB, and CdtC form a tripartite complex that is required for cytolethal distending toxin activity.* Infect Immun, 2001. **69**(7): p. 4358-65.
4. Nesic, D. and C.E. Stebbins, *Mechanisms of assembly and cellular interactions for the bacterial genotoxin CDT.* PLoS Pathog, 2005. **1**(3): p. e28.
5. Lara-Tejero, M. and J.E. Galan, *A bacterial toxin that controls cell cycle progression as a deoxyribonuclease I-like protein.* Science, 2000. **290**(5490): p. 354-7.
6. Matangkasombut, O., et al., *Cytolethal distending toxin from Aggregatibacter actinomycetemcomitans induces DNA damage, S/G2 cell cycle arrest, and caspase- independent death in a Saccharomyces cerevisiae model.* Infect Immun, 2010. **78**(2): p. 783-92.
7. Jinadasa, R.N., et al., *Cytolethal distending toxin: a conserved bacterial genotoxin that blocks cell cycle progression, leading to apoptosis of a broad range of mammalian cell lineages.* Microbiology, 2011. **157**(Pt 7): p. 1851-75.
8. Cortes-Bratti, X., et al., *The Haemophilus ducreyi cytolethal distending toxin induces cell cycle arrest and apoptosis via the DNA damage checkpoint pathways.* J Biol Chem, 2001. **276**(7): p. 5296-302.
9. Liyanage, N.P., et al., *Helicobacter hepaticus cytolethal distending toxin causes cell death in intestinal epithelial cells via mitochondrial apoptotic pathway.* Helicobacter, 2010. **15**(2): p. 98-107.
10. Erdman, S.E., et al., *CD4+ CD25+ regulatory T lymphocytes inhibit microbially induced colon cancer in Rag2-deficient mice.* Am J Pathol, 2003. **162**(2): p. 691-702.
11. Hassane, D.C., R.B. Lee, and C.L. Pickett, *Campylobacter jejuni cytolethal distending toxin promotes DNA repair responses in normal human cells.* Infect Immun, 2003. **71**(1): p. 541-5.
12. Moser, A.R., H.C. Pitot, and W.F. Dove, *A dominant mutation that predisposes to multiple intestinal neoplasia in the mouse.* Science, 1990. **247**(4940): p. 322-4.
13. Coletta, P.L., et al., *Lymphodepletion in the ApcMin/+ mouse model of intestinal tumorigenesis.* Blood, 2004. **103**(3): p. 1050-8.
14. You, S., et al., *Developmental abnormalities in multiple proliferative tissues of Apc(Min/+) mice.* Int J Exp Pathol, 2006. **87**(3): p. 227-36.
15. Fearnhead, N.S., M.P. Britton, and W.F. Bodmer, *The ABC of APC.* Hum Mol Genet, 2001. **10**(7): p. 721-33.
16. Fodde, R., *The APC gene in colorectal cancer.* Eur J Cancer, 2002. **38**(7): p. 867-71.
17. Rowan, A.J., et al., *APC mutations in sporadic colorectal tumors: A mutational "hotspot" and interdependence of the "two hits".* Proc Natl Acad Sci U S A, 2000. **97**(7): p. 3352-7.
18. Rao, V.P., et al., *Proinflammatory CD4+ CD45RB(hi) lymphocytes promote mammary and intestinal carcinogenesis in Apc(Min/+) mice.* Cancer Res, 2006. **66**(1): p. 57-61.
19. Newman, J.V., et al., *Bacterial infection promotes colon tumorigenesis in Apc(Min/+) mice.* J Infect Dis, 2001. **184**(2): p. 227-30.
20. Erdman, S.E., et al., *CD4+CD25+ regulatory lymphocytes induce regression of intestinal tumors in ApcMin/+ mice.* Cancer Res, 2005. **65**(10): p. 3998-4004.

21. Okayasu, I., et al., *A novel method in the induction of reliable experimental acute and chronic ulcerative colitis in mice.* Gastroenterology, 1990. **98**(3): p. 694-702.
22. Laroui, H., et al., *Dextran sodium sulfate (DSS) induces colitis in mice by forming nano-lipocomplexes with medium-chain-length fatty acids in the colon.* PLoS One, 2012. **7**(3): p. e32084.
23. Chassaing, B., et al., *Dextran sulfate sodium (DSS)-induced colitis in mice.* Curr Protoc Immunol, 2014. **104**: p. Unit 15 25.
24. Tanaka, T., et al., *Dextran sodium sulfate strongly promotes colorectal carcinogenesis in Apc(Min/+) mice: inflammatory stimuli by dextran sodium sulfate results in development of multiple colonic neoplasms.* Int J Cancer, 2006. **118**(1): p. 25-34.
25. Sohn, O.S., et al., *Metabolism of azoxymethane, methylazoxymethanol and N-nitrosodimethylamine by cytochrome P450IIE1.* Carcinogenesis, 1991. **12**(1): p. 127-31.
26. Megaraj, V., et al., *Role of hepatic and intestinal p450 enzymes in the metabolic activation of the colon carcinogen azoxymethane in mice.* Chem Res Toxicol, 2014. **27**(4): p. 656-62.
27. Neufert, C., C. Becker, and M.F. Neurath, *An inducible mouse model of colon carcinogenesis for the analysis of sporadic and inflammation-driven tumor progression.* Nat Protoc, 2007. **2**(8): p. 1998-2004.
28. Corpet, D.E. and F. Pierre, *Point: From animal models to prevention of colon cancer. Systematic review of chemoprevention in min mice and choice of the model system.* Cancer Epidemiol Biomarkers Prev, 2003. **12**(5): p. 391-400.
29. Kiraly, O., et al., *DNA glycosylase activity and cell proliferation are key factors in modulating homologous recombination in vivo.* Carcinogenesis, 2014. **35**(11): p. 2495-502.
30. Kiraly, O., et al., *Inflammation-induced cell proliferation potentiates DNA damage-induced mutations in vivo.* PLoS Genet, 2015. **11**(2): p. e1004901.
31. Ge, Z., et al., *Cytolethal distending toxin is essential for Helicobacter hepaticus colonization in outbred Swiss Webster mice.* Infect Immun, 2005. **73**(6): p. 3559-67.
32. Barker, N., *Adult intestinal stem cells: critical drivers of epithelial homeostasis and regeneration.* Nat Rev Mol Cell Biol, 2014. **15**(1): p. 19-33.
33. Nohmi, T., et al., *A new transgenic mouse mutagenesis test system using Spi- and 6-thioguanine selections.* Environ Mol Mutagen, 1996. **28**(4): p. 465-70.
34. Chawanthayatham, S., et al., *Prenatal exposure of mice to the human liver carcinogen aflatoxin B1 reveals a critical window of susceptibility to genetic change.* Int J Cancer, 2015. **136**(6): p. 1254-62.
35. Fox, J.G., et al., *Helicobacter hepaticus sp. nov., a microaerophilic bacterium isolated from livers and intestinal mucosal scrapings from mice.* J Clin Microbiol, 1994. **32**(5): p. 1238-45.
36. Young, V.B., et al., *In vitro and in vivo characterization of Helicobacter hepaticus cytolethal distending toxin mutants.* Infect Immun, 2004. **72**(5): p. 2521-7.
37. Cairns, J., *Cancer and the immortal strand hypothesis.* Genetics, 2006. **174**(3): p. 1069-72.
38. Potten, C.S., G. Owen, and D. Booth, *Intestinal stem cells protect their genome by selective segregation of template DNA strands.* J Cell Sci, 2002. **115**(Pt 11): p. 2381-8.
39. Karpowicz, P., et al., *Support for the immortal strand hypothesis: neural stem cells partition DNA asymmetrically in vitro.* J Cell Biol, 2005. **170**(5): p. 721-32.

40. Boutin, S.R., et al., *Different Helicobacter hepaticus strains with variable genomic content induce various degrees of hepatitis.* Infect Immun, 2005. **73**(12): p. 8449-52.
41. Owen, K.A., et al., *FAK regulates intestinal epithelial cell survival and proliferation during mucosal wound healing.* PLoS One, 2011. **6**(8): p. e23123.
42. Mitschke, D., et al., *Characterization of cytochrome P450 protein expression along the entire length of the intestine of male and female rats.* Drug Metab Dispos, 2008. **36**(6): p. 1039-45.
43. Wiktor-Brown, D.M., et al., *Integrated one- and two-photon imaging platform reveals clonal expansion as a major driver of mutation load.* Proc Natl Acad Sci U S A, 2008. **105**(30): p. 10314-9.
44. Kimoto, T., et al., *Recombinant cells in the lung increase with age via de novo recombination events and clonal expansion.* Environ Mol Mutagen, 2017. **58**(3): p. 135-145.

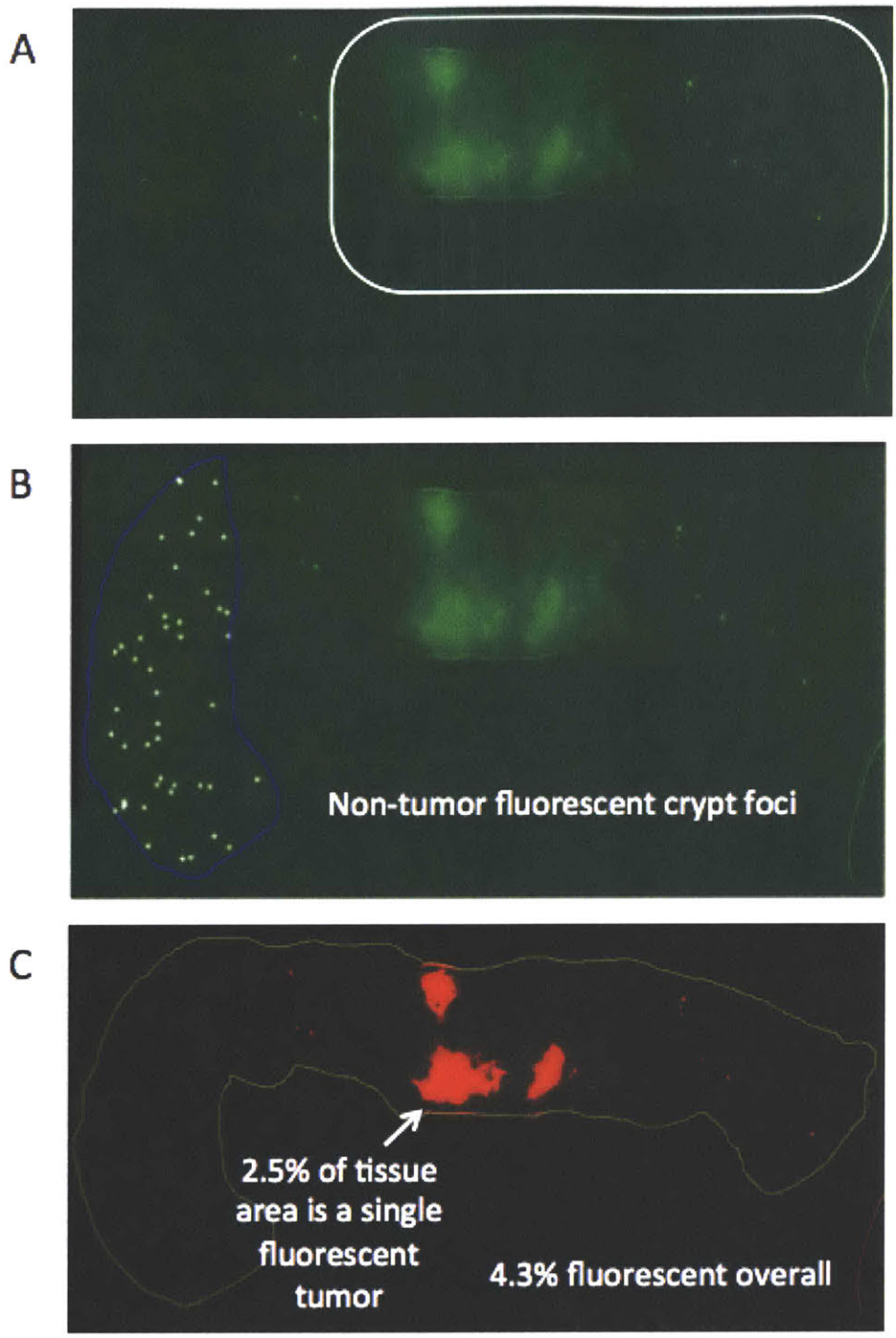

Figure 3-1. Sample quantifications of RaDR mutagenesis. (A) Original colon RaDR image. White box indicates tumor-filled area. (B) Tissue that does not contain tumors can be analyzed for converted crypt foci. (C) Total mutant burden (percent area fluorescent). Note that large red regions correspond to fully (or near-fully) fluorescent tumors.

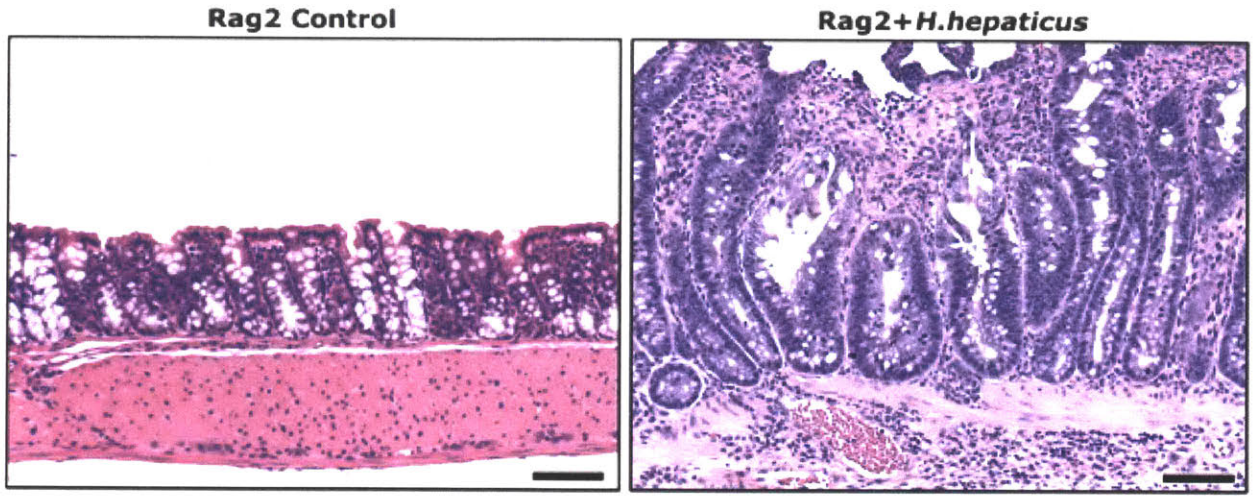

Figure 3-2. *H. hepaticus* infection causes colonic inflammation in *Rag2*$^{-/-}$ mice.

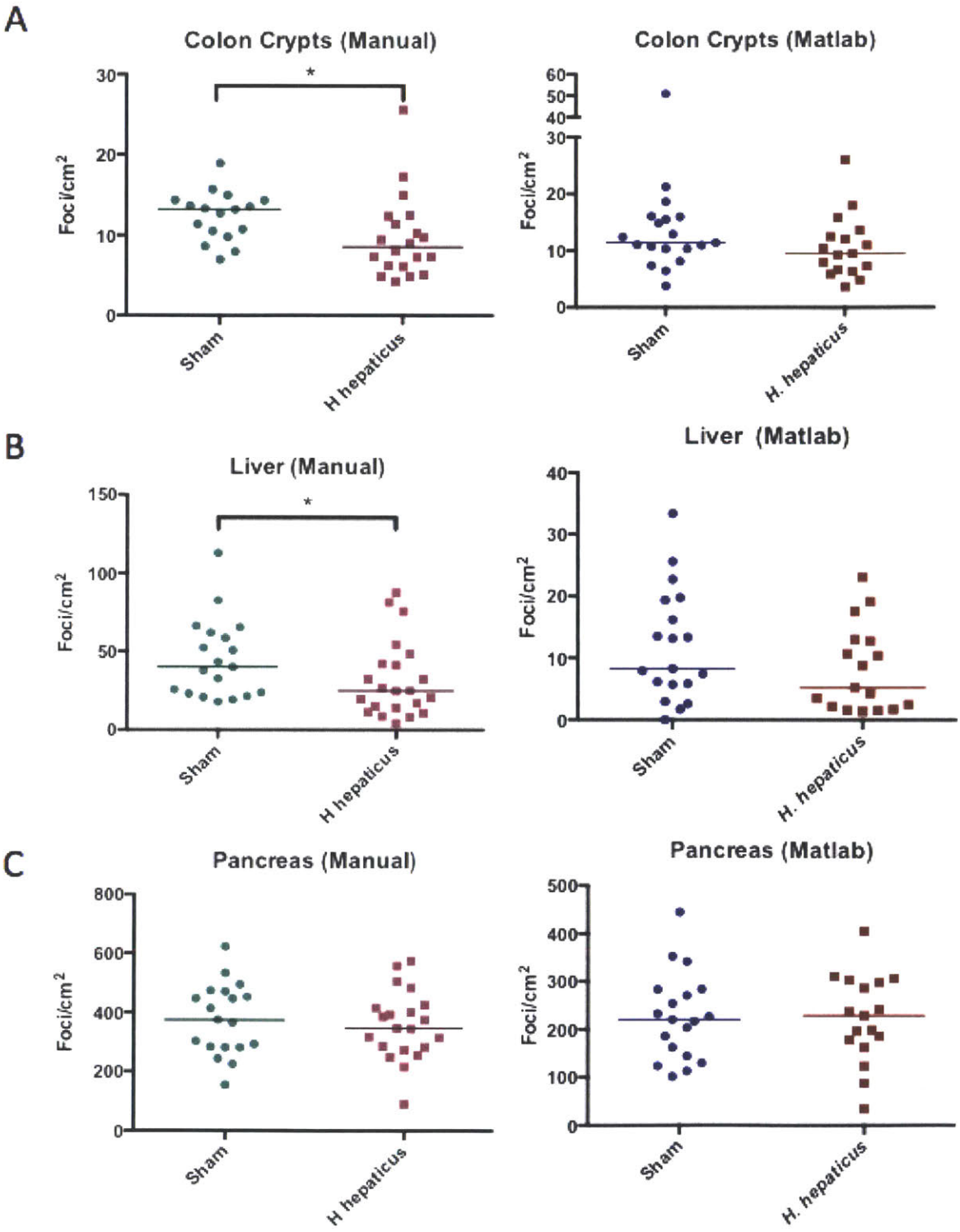

Figure 3-3. RaDR foci in (A) colon crypts, (B) liver, and (C) pancreas tissue from sham- and *H. hepaticus*-infected animals. Charts on the left show results of manual foci counting, charts on the right show results of automated image analysis.

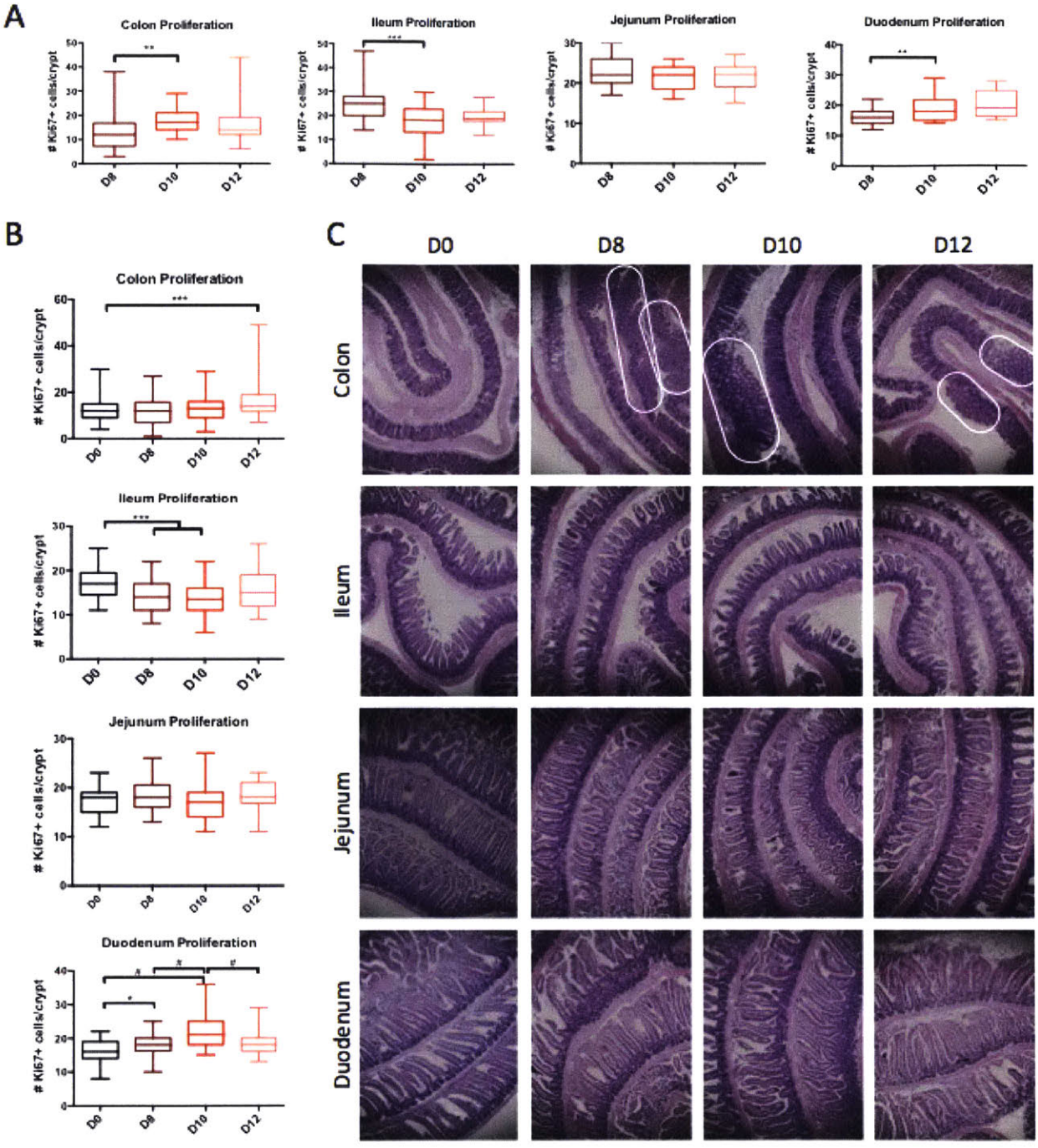

Figure 3-4. Intestine regeneration following 7 days of 1% DSS drinking water. (A) Initial quantification of proliferating cells in DSS recovery crypt cross sections. (B) Quantification of proliferating cells in D0 and DSS recovery crypt cross sections. Boxes indicate quartiles and error bars indicate minima and maxima. (C) H&E sections of D0 and DSS recovery intestines. White ovals indicate colon polyps. Unpaired Student's *t*-test, $^{*}p < 0.05$, $^{**}p < 0.01$, $^{***}p < 0.001$, $^{\#}p < 0.0001$.

Table 3-1 Cohort compositions							
Cohort	**Males**		**Females**		**Total**		**Timing**
	treated	**analyzed**	**treated**	**analyzed**	**treated**	**analyzed**	
DSS recovery pilot	6	2/day			6	6	Separate
D0	3	3	3	3	6	6	Separate
Ctrl	10	10	6	6	16	16	Parallel
AOM	11	10	7	7	18	17	
DSS	11	10	8	6	19	16	
DSS+AOM	12	9	11	6	23	15	
D12 AOM	4	4	1	1	5	5	Parallel
D12 DSS	5	5	1	1	6	6	
D12 DSS+AOM	4	4	4	3	8	7	
AOM-then-DSS	5	3	8	2	13	5	Separate

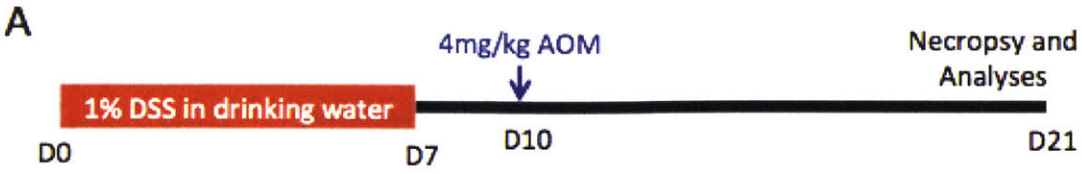

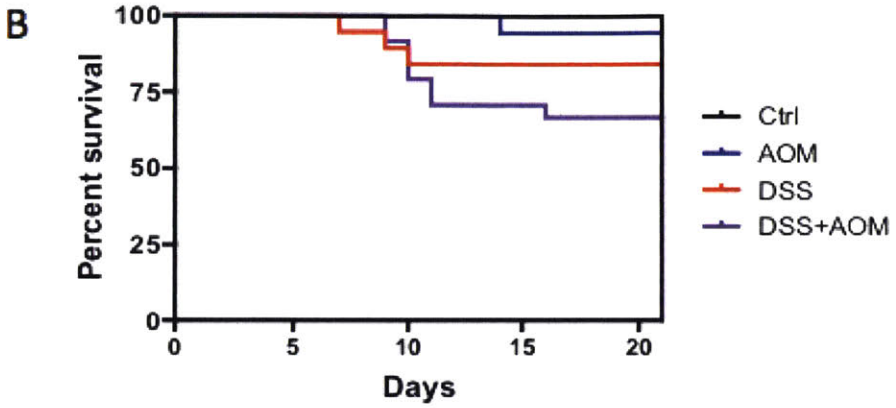

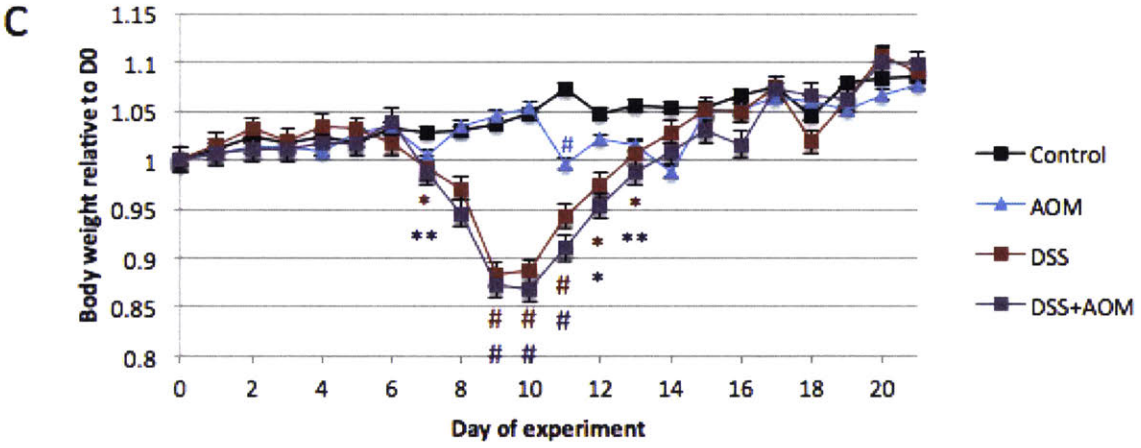

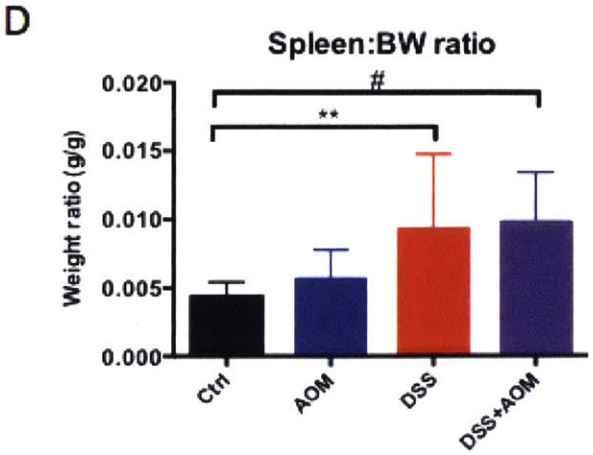

Figure 3-5. Experimental design. (A) Treatment schedule. (B) Kaplan-Meier survival curve. (C) Animal body weight change over the course of the experiment. (D) Ratio of spleen weight to body weight at necropsy. Unpaired Student's *t*-test, $^{*}p < 0.05$, $^{**}p < 0.01$, $^{***}p < 0.001$, $^{\#}p < 0.0001$.

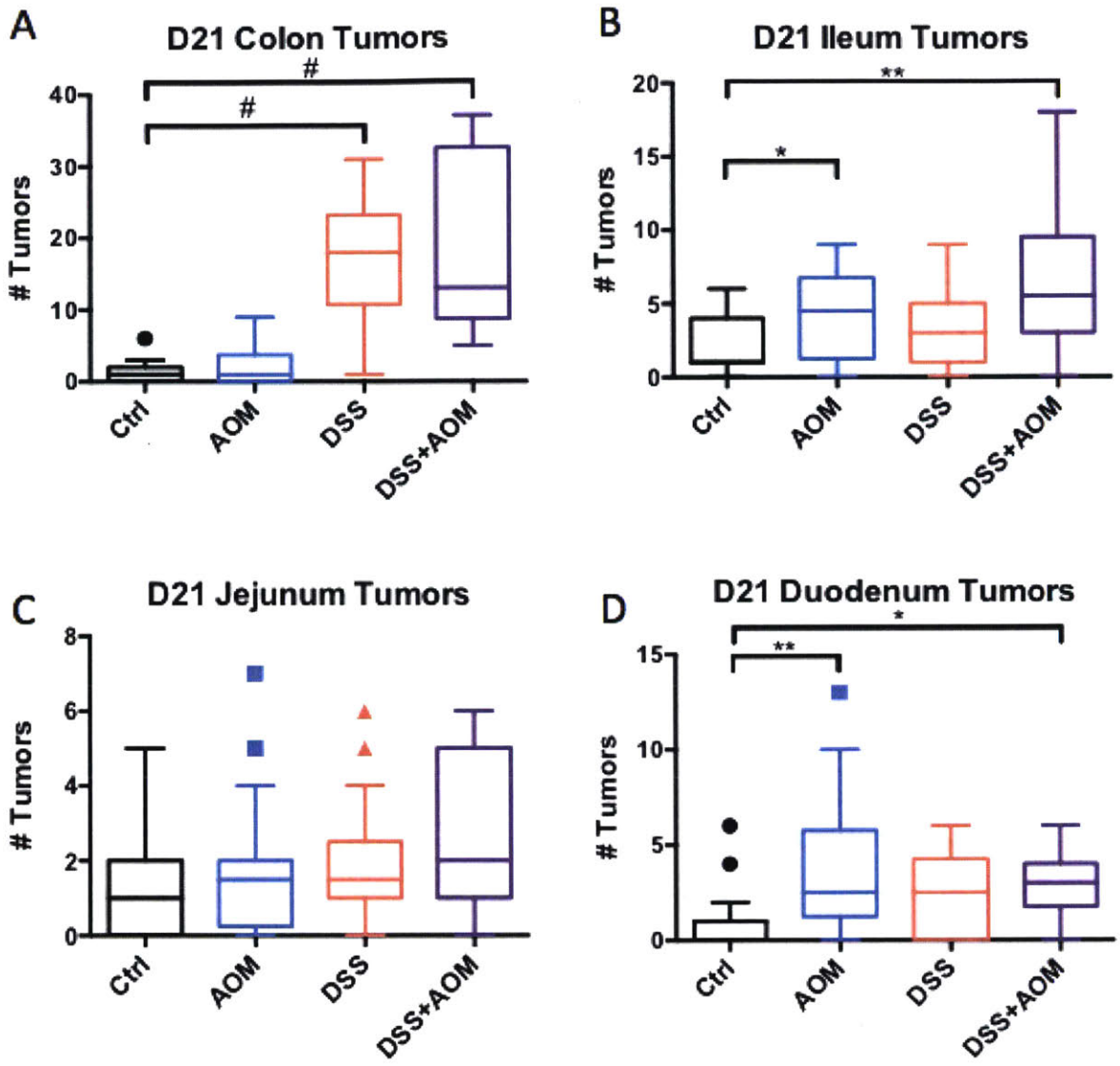

Figure 3-6. Tumor multiplicity in each intestine segment at necropsy. Tukey boxplot. Mann-Whitney *U*-test, $^{*}p < 0.05$, $^{**}p < 0.01$, $^{\#}p < 0.0001$.

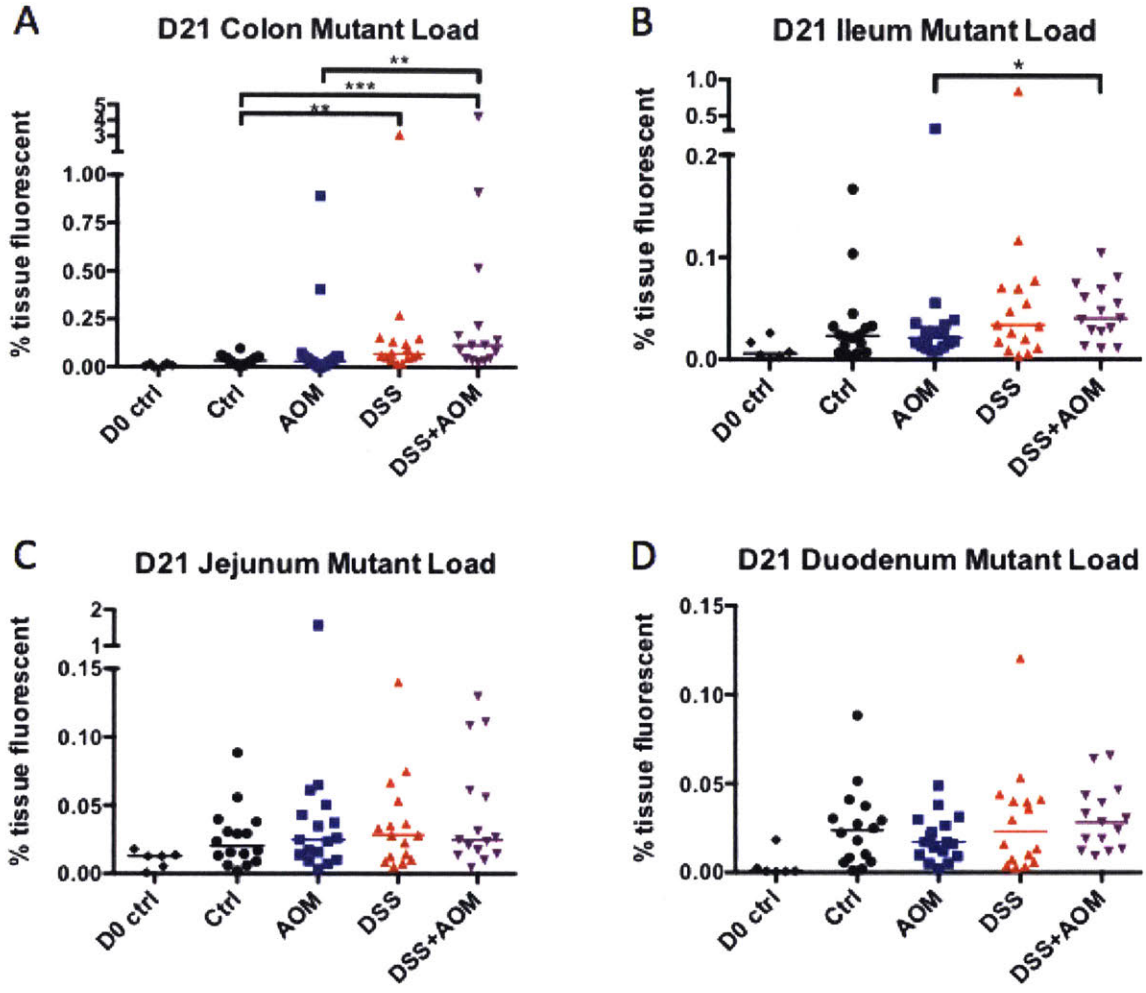

Figure 3-7. Overall burden of recombinant cells in each intestine segment at necropsy. D0 included for reference, not analyzed in parallel. Mann-Whitney *U*-test, $^{*}p < 0.05$, $^{**}p < 0.01$, $^{***}p < 0.001$.

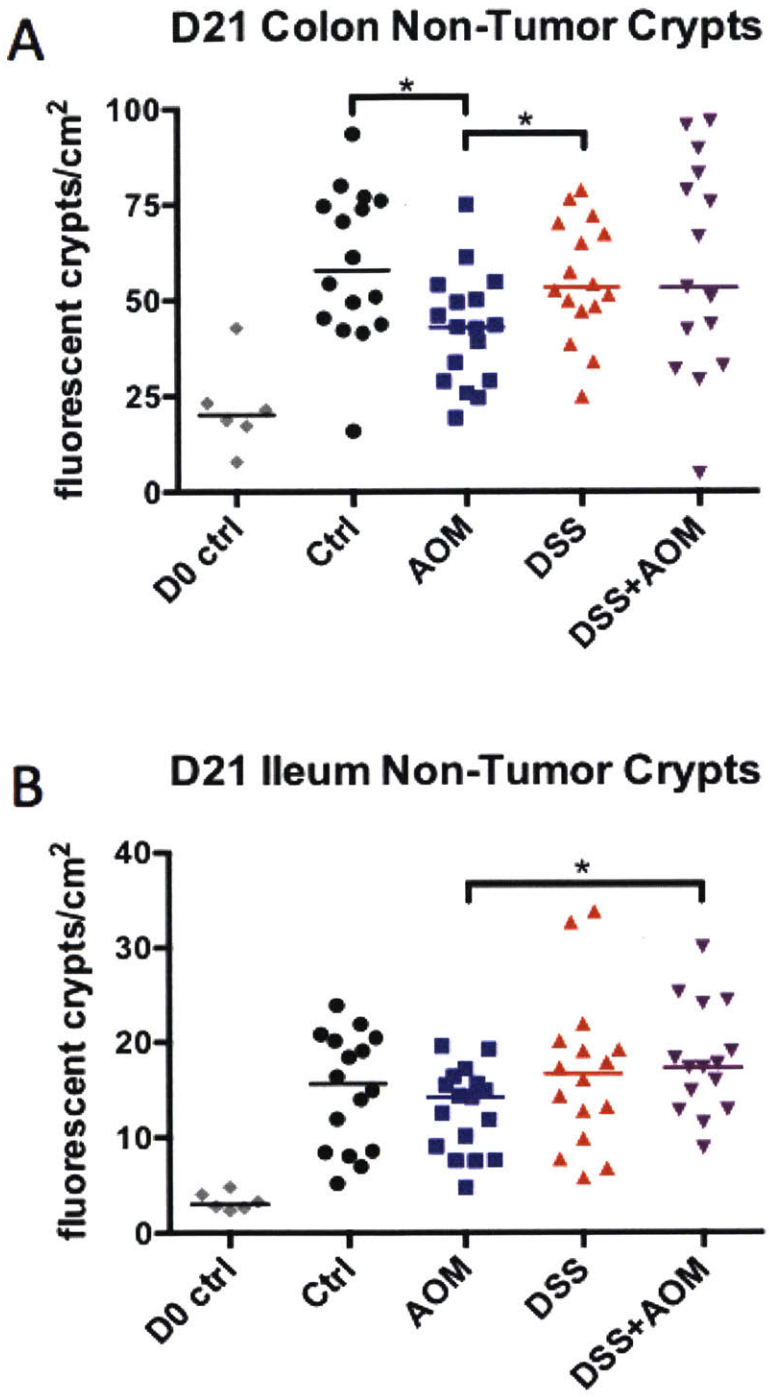

Figure 3-8. Fluorescent crypt foci at necropsy in the (A) colon and (B) ileum. D0 included for reference, not analyzed in parallel. Mann-Whitney *U*-test, $*p < 0.05$.

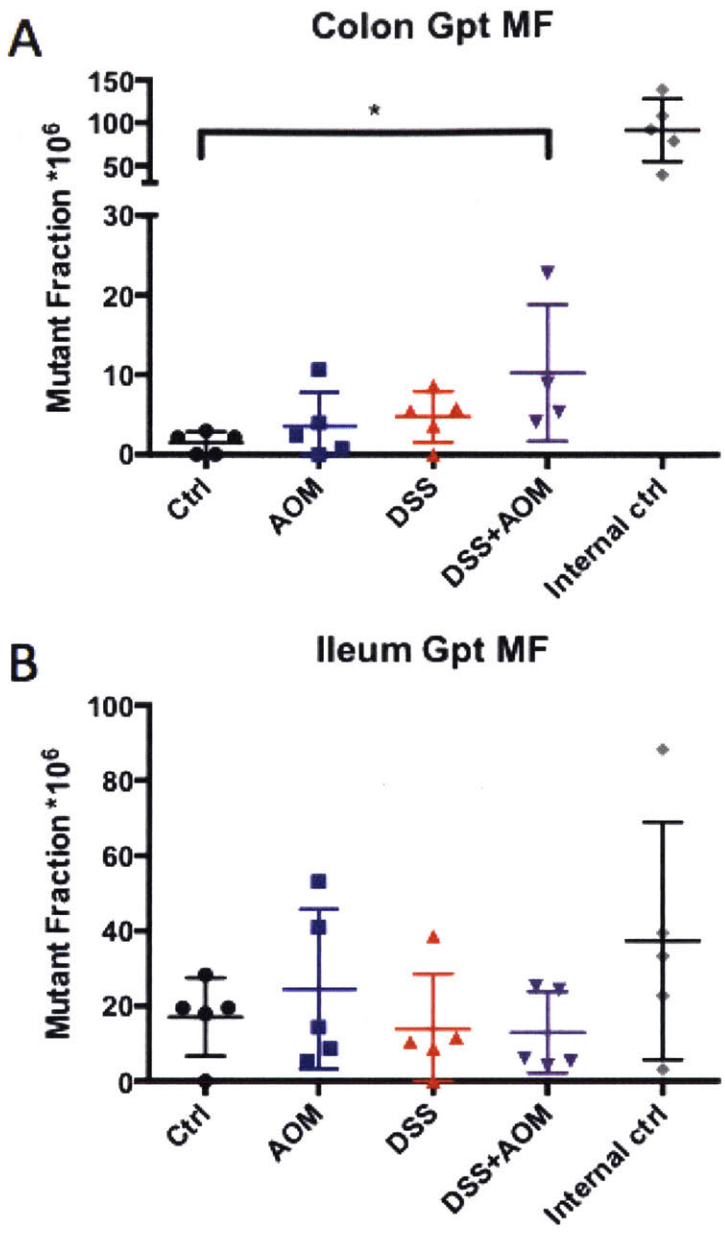

Figure 3-9. Gpt mutant fractions in the (A) colon and (B) ileum. Mann-Whitney *U*-test, $*p < 0.05$.

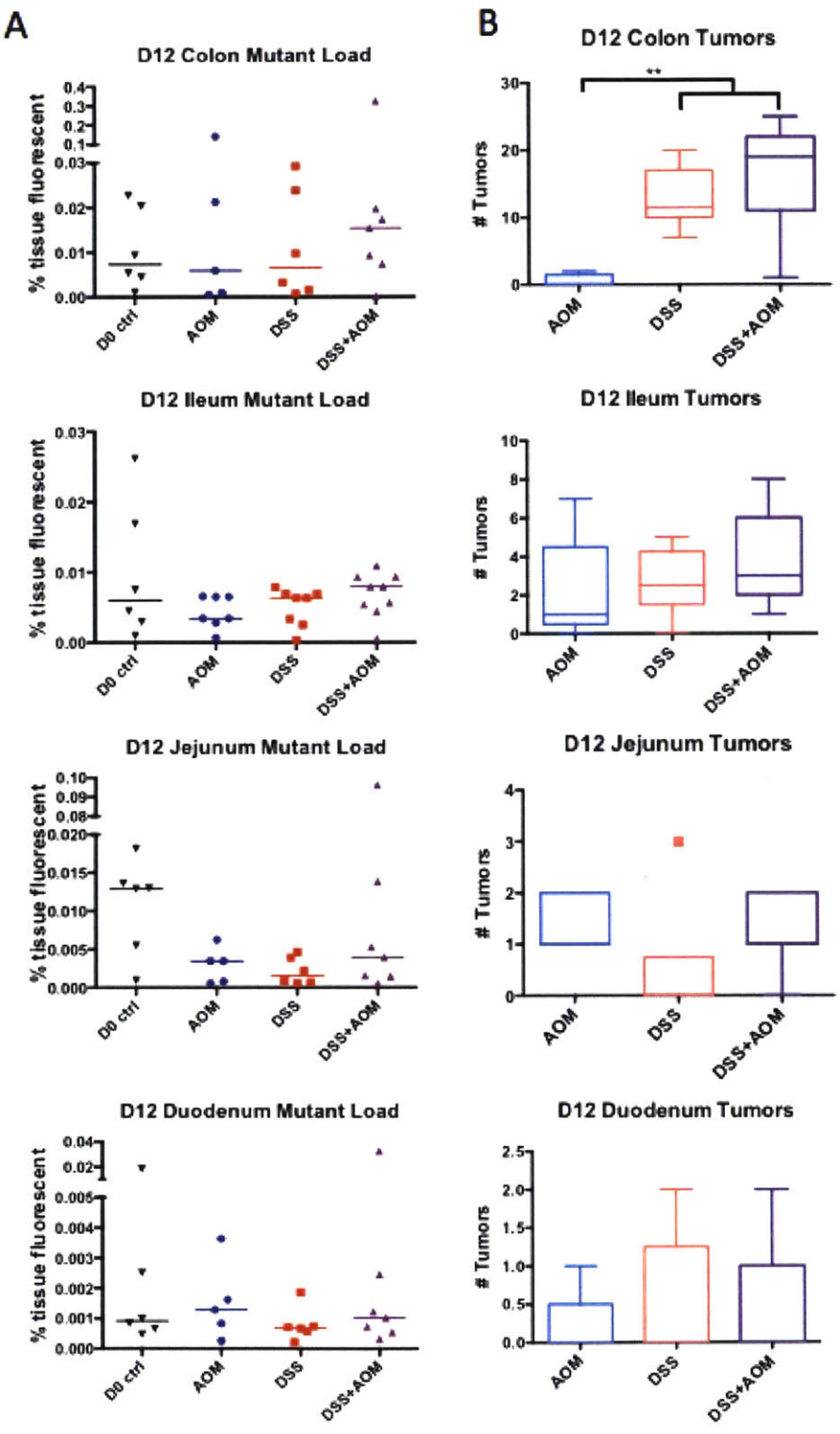

Figure 3-10. (A) Overall mutant burden and (B) tumor multiplicity in each intestine segment on day 12. Tumors represented by Tukey boxplot. D0 included for reference, not analyzed in parallel. Mann-Whitney *U*-test, $^{**}p < 0.01$.

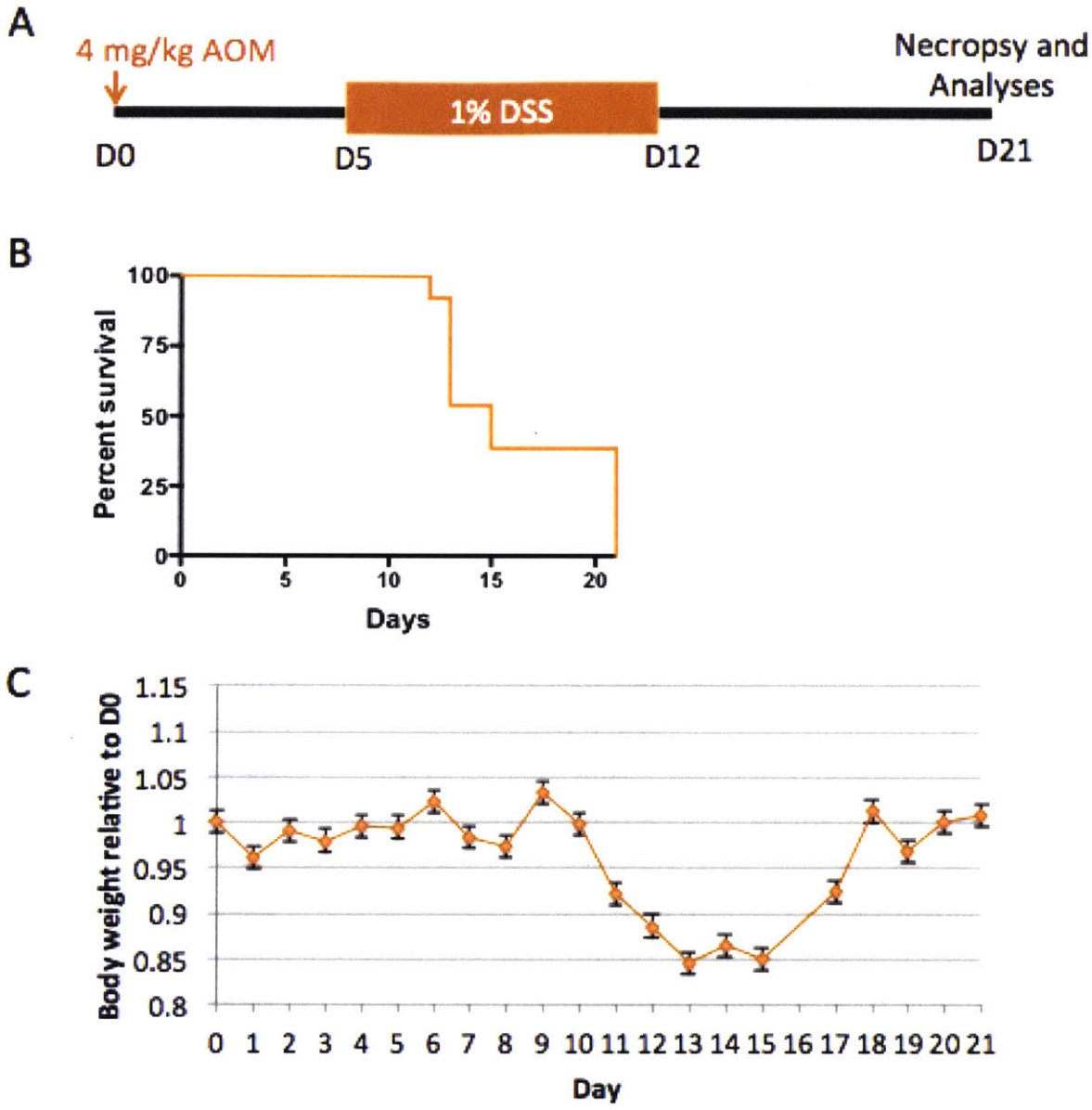

Figure 3-11. (A) treatment schedule for AOM-then-DSS. (B) Kaplan-Meier survival curve. (C) Animal body weight change over the course of the experiment.

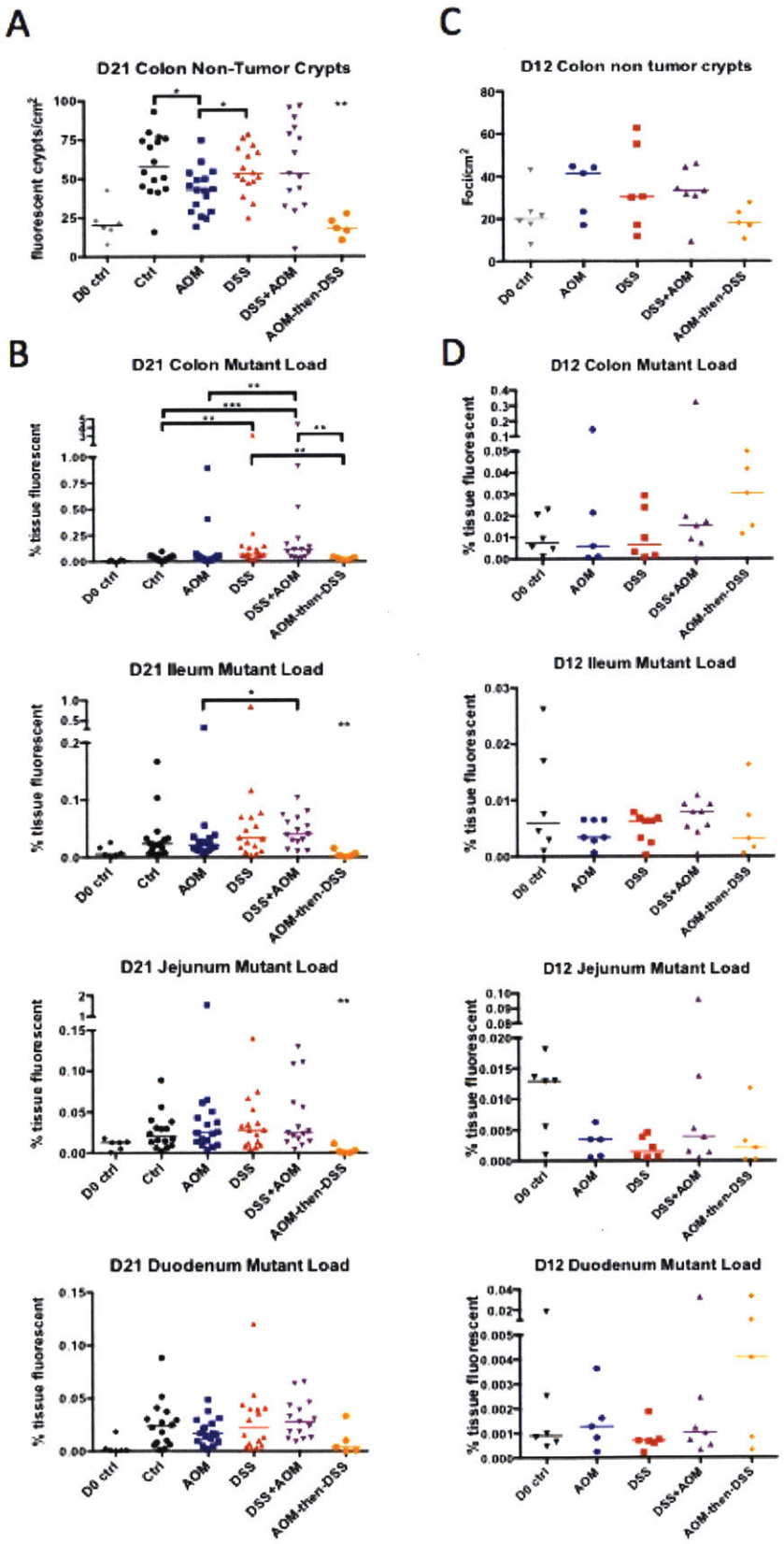

Figure 3-12. Intestine mutations in animals treated with AOM before DSS. (A) Non-tumor colon crypt foci, (B) overall mutant burden. Floating asterisks indicate that the data are significantly different from all groups except D0. For both A and B, D0, Ctrl, AOM, DSS, DSS+AOM included for reference, not analyzed in parallel. (C) and (D) show same AOM-then-DSS data in comparison to D12 AOM, DSS, DSS+AOM results. Mann-Whitney *U*-test, $*p < 0.05$, $**p < 0.01$, $***p < 0.001$.

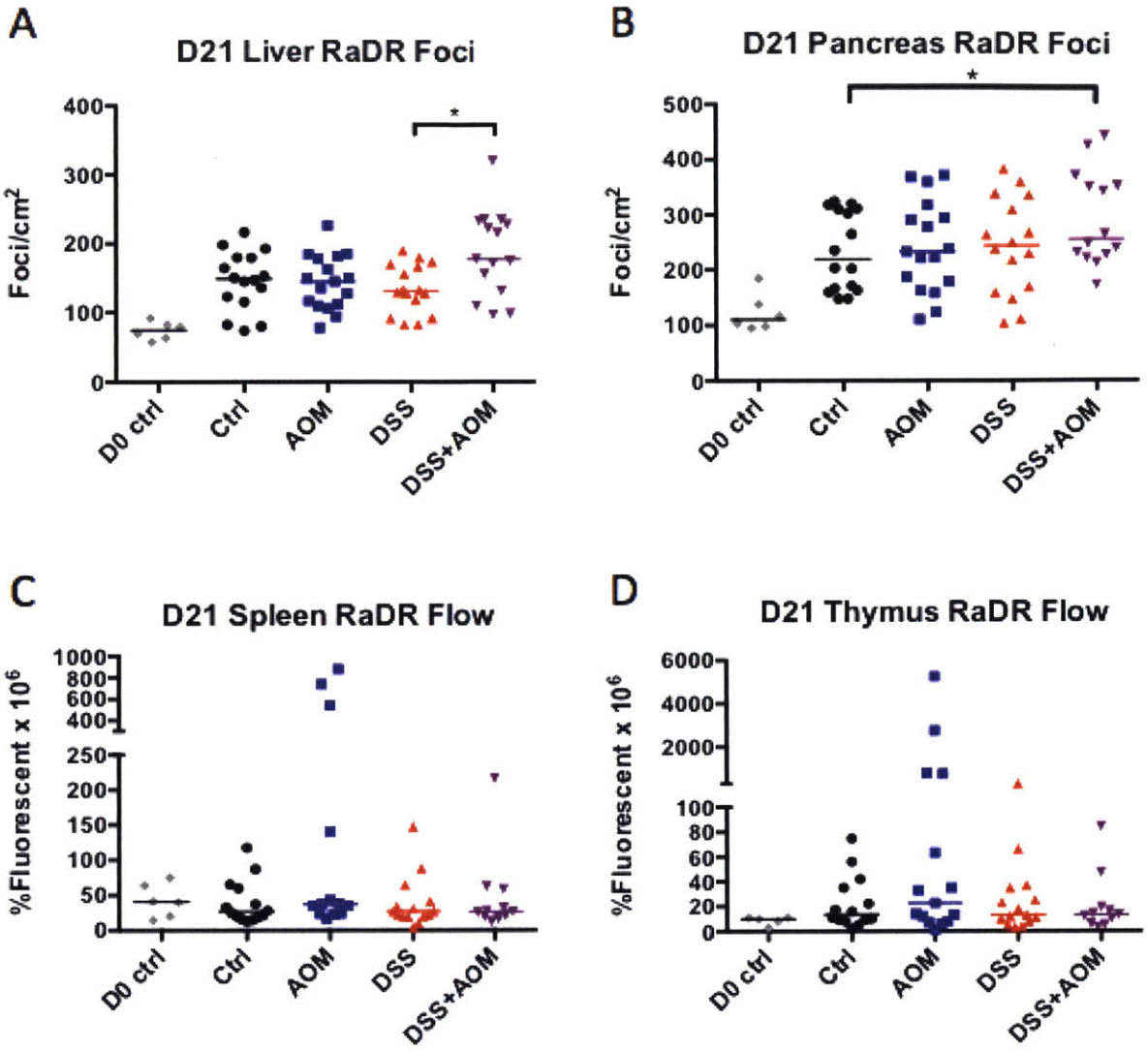

Figure 3-13. RaDR mutations in non-intestinal tissues. (A) Liver RaDR foci density. (B) pancreas RaDR foci density. (C) Spleen RaDR mutant proportion. (D) Thymus RaDR mutant proportion. Mann-Whitney *U*-test, $*p < 0.05$.

Chapter 4

Increased Aag Expression Reduces Spontaneous Sequence Rearrangement Mutations

4.1 Abstract

In order to repair the many types of DNA damage cells may encounter, a network of repair pathways has evolved. One of the most important repair pathways for coping with DNA damage from inflammation is Base Excision Repair (BER), but the intermediates of the BER pathway include abasic sites and strand breaks, which are essentially DNA lesions as well. Importantly, BER intermediates can cause replication forks to break down, and the only way to accurately restore a broken replication fork is with homologous recombination (HR). While HR is mostly error free, it can produce large-scale mutations such as insertions, deletions, translocations and loss of heterozygosity. Thus, BER intermediates during replication can lead to large-scale mutations. To illustrate the relationship between BER intermediates and HR-driven mutations, we crossed animals with increased expression of a BER glycosylase with our RaDR mice and quantified the accumulation of mutations across 10 tissue types. Interestingly, we found that AagTg animals developed fewer RaDR mutations than AagWT, with tissue- and sex-dependent variability. Of the tissues studied, we observed significantly lower frequencies of *de novo* HR events in AagTg pancreata and colons, and lower proportions of mutated cells in the spleen and lungs. Separating the data by animal sex further revealed that the only tissue where AagWT and AagTg females show a significant difference is the pancreas, whereas male animals had

significant differences in the colon, spleen, heart and kidney. Quantifying abasic sites in colon DNA did not reveal a pattern of increased BER intermediates in AagTg animals. Finally, Spearman correlation analyses revealed that mutation frequency (measured by foci) may be correlated between tissues within an animal, but overall mutant proportion (measured by flow cytometry) is not.

4.2 Introduction

In general, Base Excision Repair (BER) DNA repair pathway deals with single-base lesions that do not significantly distort the DNA helix. The first step of BER is removal of the damaged base by one of several DNA glycosylases. The second step is to cut the backbone, which can be accomplished by bifunctional glycosylases or AP endonuclease-1 (APE1). The two ends of the single strand break (SSB) must then be processed to produce a 3'OH (with APE1, Polβ, or PNKP) capable of extension and a 5'PO_4 (with Polβ or PNKP) capable of ligation. The gap is filled in with Polβ, and ligase seals the nick to complete the process. The elements of BER downstream of the glycosylase can also contribute to repair of SSBs.

Importantly, every intermediate of the BER pathway contains a potentially toxic lesion: either an abasic site or a strand break. Normally, the cell is able to complete BER without toxicity, but this is not always the case. If there is a large amount of damage, there may be simply too few of the molecules necessary for repair, such as Polβ, leading to an accumulation of cytotoxic lesions and subsequent apoptosis. Accumulation of BER intermediates can also result in bioenergetic collapse and necrosis due to excessive PARylation of SSBs. Alternatively, if a replication fork encounters a BER intermediate, the fork may break down, creating a one-ended

double strand break (DSB). Thus, while BER is essential for repairing DNA damage during inflammation, this pathway can sometimes do more harm than good by generating toxic intermediates.

Broken replication forks produce toxic DSBs, which require homologous recombination for accurate restoration. Since HR utilizes a homologous region of DNA as a template, this process is mostly error-free as long as the cell identifies the correct sequence in the sister chromatid. However, identification of homology in the homologous chromosome rather than the sister chromatid can lead to loss of heterozygosity, a significant source of tumor suppressor inactivation [1, 2]. Furthermore, a significant portion of the genome has been identified as repetitive or repeat-derived: nearly 10% of the genome consists of Alu repeats [3, 4], and a recent analysis estimates 2/3 of the genome consists of repetitive elements [5]. Thus, there are many opportunities for HR to identify a homologous sequence in the wrong location. Aberrant HR can lead to translocations, deletions, insertions, or sequence rearrangements [6-11].

In order to quantify aberrant HR *in situ*, the Engelward lab developed the RaDR mouse, wherein improper HR within the ubiquitously expressed transgene generates a fluorescent product. Briefly, these transgenic animals contain a direct repeat of truncated EGFP sequences at the Rosa26 locus. The 5' copy of EGFP is truncated within the 5' EGFP coding region, and the 3' copy is likewise truncated at the 3' end of the gene. If a double strand break occurs in one of these repeats, the cell may identify the incorrect EGFP copy as a template for homology-directed repair, producing a full-length EGFP sequence. Here, we crossed RaDR mice with animals expressing different levels of a BER glycosylase to explore the relationship between BER intermediates and HR mutations.

Aag is a monofunctional DNA glycosylase that recognizes and excises a variety of substrates. This enzyme can remove 3-meA, 7-meG, 3-meG, Hx and εA, leaving an abasic site [12]. AagTg animals, which express increased levels of Aag, were created by the Samson laboratory, first reported in 2009 [13] and characterized in 2013 [14]. These animals were generated by pronuclear injection of mouse *Aag* cDNA under a CMV promoter, and were found to express Aag ~2-9 fold higher than AagWT across tissues.

Previously, the Engelward laboratory has observed that knockout of Aag reduces the frequency of sequence rearrangement mutations, likely due to fewer BER intermediates being present at any given time [15]. Further supporting a model whereby BER intermediates promote HR, treating wild type animals with MNU (which creates Aag substrates) caused an increase in sequence rearrangements, but MNU in Aag null animals did not significantly increase these mutations. Thus, we hypothesized that animals expressing an elevated level of Aag (AagTg) would accumulate more RaDR mutations over time than wild type.

4.3 Materials and Methods

4.3.1 *RaDR;AagTg* animals

$RaDR^{R/+}$ and $RaDR^{R/+}$;*AagTg* mice were bred by crossing female 129 $RaDR^{R/R}$ mice with male 129 *AagTg* mice (a generous gift from L.D. Samson). These mice were housed in a barrier facility free of known murine *Helicobacter* species, viruses, *Salmonella* species, *Citrobacter rodentium*, ecto- and endoparasites. Animals were aged with no manipulation for 6 months, at which time they were euthanized by CO_2 according to AVMA guidelines and necropsied with standard procedures. Samples collected and analyzed immediately included: RaDR imaging of

pancreas, liver, colon, and mammary tissues, and RaDR flow cytometry of brain, heart, lung, kidney, thymus, and spleen tissues.

4.3.2 RaDR Necropsy and Tissue Imaging

Animals were euthanized with CO_2 according to AVMA guidelines. Tissues were excised and held on ice in tubes containing PBS (mammary, brain, heart, lung, kidney, thymus, spleen) or PBS with 0.01% trypsin inhibitor (T9008 Sigma-Aldrich or P-1540 Westnet Inc) (pancreas, liver, colon) until use. Intestines were cut open on one side and the lumen was rinsed of fecal matter before placing in PBS + trypsin inhibitor. Mammary, pancreas, liver and colon tissues were compressed to 0.5 mm between coverslips and imaged for EGFP under the 1x objective with the FITC filter of a Nikon 80i fluorescent microscope.

4.3.3 RaDR Image Analysis

RaDR images can be analyzed for the number of *de novo* recombination events by quantifying individual fluorescent foci, or for total burden of recombinant cells by measuring the fluorescent area of the tissue. Both metrics are normalized to tissue area, measured in ImageJ. To quantify fluorescent foci, Dushan Wadduwage of Peter So's laboratory designed MATLAB-based programs that use gradient and intensity features of the image to distinguish individual foci (manuscript under review). The program "FociCounter_3.1" was used to enumerate all foci in pancreas, liver, and mammary tissues, and the program "17.03.27_Crypt counter with GUI" was utilized to enumerate converted colonic crypts. The crypt counting program is trained to recognize crypt foci based on 3-4 researcher-annotated images from the data set, then the program is able to apply those parameters to identify crypt foci in other images. To quantify the

fluorescent area within the tissue, conservative intensity thresholds were set in ImageJ such that background and artifactual fluorescence was excluded, and only brightly fluorescent pixels would be measured. After marking the outline of the tissue, the area of pixels above the threshold intensity were measured as well as the total tissue area.

4.3.4 RaDR Flow Cytometry

Tissues analyzed by flow cytometry were processed after imaging was completed. Briefly, tissues were placed in 5 mL of 2 mg/ml collagenase type V (C9263, Sigma) in HBSS (Life Technologies) in a GentleMACS C tube and mechanically dissociated with the GentleMACS tissue grinder (Miltenyi Biotec). After mechanical disaggregation, the tissues were placed in a 37C incubator for 40 minutes to allow collagenase to degrade connective tissue. Cell suspensions were then triterated 10-15 times and passed through a 70 micron cell strainer into 10 mL of cold media (DMEM + 10% FBS + pen/strep) to halt collagenase digestion. The samples were then centrifuged at 180 x *g* for 10 minutes and supernatant was discarded. The cell pellet was resuspended in 350-500 uL of Opti-MEM reduced serum media (ThermoFisher Scientific) and held on ice until analyzed. The samples were analyzed by a FACScan or FACS Calibur flow cytometer for green fluorescence (530 nm) and red (585 nm) to account for autofluorescence.

4.3.5 Abasic Site Quantification

Abasic sites were quantified from colon DNA with the Dojindo AP-site counting kit (Dojindo Molecular Technologies, Inc, Rockville, MD). Briefly, DNA was extracted from snap-frozen colon tissue by homogenization and extraction with the Roche DNA Isolation kit for cells and tissues (Roche Diagnostics Corporation, Indianapolis, IN). A portion of the extracted DNA was

diluted to 100 μg/mL and abasic sites labeled with a biotin-tagged aldehyde reactive probe. Labeled DNA was bound to a clear 96-well plate, incubated with HRP-conjugated streptavidin, and treated with peroxidase to permit colorimetric detection by optical density at 650 nm.

4.3.6 Statistical Analyses

RaDR foci were quantified as the number of foci per square centimeter of area (foci/cm^2), and RaDR flow cytometry measurements were given as % fluorescent*10^6. Due to the fact that the distribution of EGFP-positive cells in RaDR mice is non-normal across tissues and among individuals, RaDR data sets were compared by Mann-Whitney *U*-test using GraphPad Prism 5. Due to the wide spread of data, some tissues were analyzed a second time after removing outliers (outliers defined as $x < Q1 - (1.5*[Q3-Q1])$ or $x > Q3 + (1.5*[Q3-Q1])$, where Q1 and Q3 represent the first and third quartiles of data in the set, respectively).

4.4 Results

4.4.1 AagTg animals accumulate fewer mutations compared to AagWT in the pancreas, colon, spleen, and lung

We measured recombinant EGFP+ cells in ten tissue types by imaging (colon, pancreas, liver, mammary) or flow cytometry (brain, heart, lung, kidney, thymus, spleen). *De novo* mutations were quantified by automated image analysis in pancreas, liver and mammary tissue. Colon images were similarly analyzed, both for all foci as well as for converted crypts.

There were statistically fewer mutation foci in the pancreata and colon crypts of AagTg animals (Fig 4-1A), and a lower overall proportion of mutated cells in AagTg spleens (Fig 4-1B).

Following removal of statistical outliers (see Materials and Methods), AagTg animals were also found to have a lower proportion of mutated cells in the lung (Fig 4-1B).

4.4.2 AagTg animals have sex-dependent differences in tissue-specific accumulation of mutations

Several studies using AagTg animals have revealed sex-dependent differences in susceptibility to toxicity from DNA methylating agents in the kidney [16], cerebellum [17] and retina (unpublished data). Therefore, we were interested to know whether the accumulation of sequence rearrangement mutations varied by sex of the animal. RaDR foci and flow cytometry data were separated by sex and re-analyzed for significance.

Interestingly, female AagTg animals only showed a significant decrease in mutation accumulation compared to AagWT in the pancreas (Fig 4-2A). In all other tissues, female AagWT and AagTg animals showed similar frequencies or proportions of mutations. In fact, the significant difference in colon crypt and spleen mutations between AagWT and AagTg in sex-pooled data is derived almost entirely from male animals, as the data spread between females was nearly identical in these tissues (Fig 4-2B, C).

By separating data by animal sex, we also discovered that AagTg males develop significantly lower proportions of mutant cells in the heart (Fig 4-2D) as well as the kidney (after removing outliers – see Materials and Methods) (Fig 4-2E), a distinction that was not visible in the sex-pooled data. In both these tissues, AagWT males accumulate a larger proportion of mutant cells compared to both AagTg males as well as AagWT females.

Data for tissue types that did not display statistical differences are presented in Figure 4-3.

4.4.3 Frequency of mutations does not necessarily correlate with frequency of abasic sites

The observed decrease in RaDR mutations in AagTg animals was unexpected, as we had previously shown that BER intermediates promote HR and anticipated that AagTg animals would have more BER intermediates than AagWT. Since our hypothesis was dependent on the assumption that AagTg animals would have more BER intermediates, we first aimed to determine whether this assumption was correct. The Aag glycosylase produces abasic sites, and other BER intermediates are downstream of glycosylase activity, so we utilized a kit to quantify abasic sites in AagWT and AagTg colon tissue, three animals of each sex. We did not observe significant differences in abasic sites between AagWT and AagTg nor between male and female (Fig 4-4). However, this data is from a small sample size, and so we do not posit firm conclusions relating abasic sites to mutations.

4.4.4 Correlation analysis suggests tissue mutation frequency may correlate within an animal, but mutant accumulation does not

Given the wide spread of mutation data between individual animals, we aimed to clarify whether animals that have a large number of recombinant cells in one tissue are also likely to have high levels of mutants cells across other tissues. In collaboration with Duanduan Ma of MIT's BioMicro Center, we calculated Spearmann correlation coefficients for all tissues. Correlation coefficients are listed in Figure 4-5A, and *p*-values for each coefficient are listed in Figure 4-5B. Interestingly, most tissues analyzed for mutation frequency (i.e., foci) correlated significantly, whereas most tissues analyzed for overall mutant proportion (i.e., flow cytometry) did not correlate. Two tissues were exceptions, however: mammary foci did not correlate with other

mutation frequencies, and the mutant proportion of the spleen correlated weakly with pancreas and colon crypt foci.

4.5 Discussion

In this study, we aimed to determine whether increased expression of the Aag glycosylase affects the production of sequence rearrangement mutations. Previous studies have shown that *Aag*$^{-/-}$ animals develop fewer HR-driven mutations, likely due to the presence of fewer BER intermediates. Therefore, we hypothesized that animals expressing elevated levels of Aag would accumulate more sequence rearrangement (RaDR) mutations from the increase in BER intermediates. Surprisingly, counter to our initial hypothesis, AagTg animals accumulated fewer sequence rearrangement mutations overall. The decrease in RaDR mutations in AagTg animals was statistically significant in the pancreas, colon crypts, spleen, and lung after removal of outliers. Separating data by sex of the animal further revealed that AagTg males accumulate fewer mutations than AagWT males in the colon, heart, kidney and spleen, whereas females only appear to have an Aag-dependent decrease in mutations in the pancreas.

Since our initial hypothesis predicted that AagTg animals would have more mutations due to more BER intermediates, we sought to determine whether there was a difference in BER intermediates. We measured abasic sites in the colons of AagWT and AagTg animals, three animals of each sex. We did not observe a significant difference in abasic sites for either genotype or sex, suggesting that AagTg animals do not necessarily have an imbalance in the BER pathway. Previous studies reported that AagTg animals have higher Parp1 activity compared to AagWT [16], suggesting that increased expression of Aag causes upregulation of

downstream factors as well. We hypothesize that since our animals were not treated with a DNA damaging agent, downstream steps of the BER pathway were able to keep up with Aag activity, resulting in improved efficiency and an overall decrease in mutations. Thus, since the BER pathway was not stressed, efficient repair in both AagTg and AagWT animals resulted in similarly low levels of abasic sites.

Importantly, other studies of sequence rearrangement mutations in AagWT and Aag null animals analyzed mutations following alkylation DNA damage [15]. Furthermore, AagTg animals are more sensitive than AagWT to toxicity by alkylating agents [14, 16, 17]. Thus, we predict that treatment with an alkylating agent could reverse the trend observed here, and RaDR;AagTg animals would accumulate more recombinant cells than RaDR;AagWT. This work enables many exciting studies on the Aag-dependent accumulation of recombinant cells following exposures.

The difference in recombinant cell accumulation between male and female kidneys particularly interesting because previous studies with AagTg animals have shown that estrogen is protective against alkylation-induced nephrotoxicity [16]. Our finding that AagWT females accumulate fewer mutated kidney cells than AagWT males is consistent with males being more susceptible to renal damage in a variety of model systems [16, 18-20].

The sex-dependent differences in mutation accumulation indicate that there may be sex-related differences in AagTg expression. The initial characterization of Aag activity across tissues in the AagTg animal did not separate based on sex of the animal. Based on the sex-linked differences in mutation accumulation, it will be of great interest to characterize Aag activity across tissues of both male and female animals. This is especially important for further studies

using these animals, as sex-dependent variations in Aag activity may drive other sex-dependent phenotypes in AagTg mice.

4.6 Conclusions

In this study, we assessed the baseline accumulation of RaDR mutations in AagTg and AagWT mice after six months of age in 10 tissues. Overall, in all cases where there was a difference between AagTg and AagWT, the AagTg animals had developed fewer mutations. Separating data by sex revealed that the differences between AagTg and AagWT mutations is most pronounced in male animals' tissues, whereas AagTg females only had fewer mutations than AagWT in the pancreas. Further studies on these animals will illustrate the source of these Aag-dependent and sex-dependent differences in mutation accumulation. In particular, the activity of Aag should be measured across tissues of male and female AagWT and AagTg animals to clarify results of this and other studies [14, 17]. We also anticipate that measuring RaDR mutations in AagTg, AagWT and Aag null animals following treatment with a DNA-damaging agent will provide a clearer, more complete paradigm linking BER intermediates to HR-derived mutations.

4.7 Acknowledgements

The work described in this chapter was performed in collaboration with members of several laboratories. AagTg animals were a kind gift from Prof. Leona D. Samson. The foci counting programs used to quantify *de novo* recombination events were written by Dr. Dushan Wadduwage of Prof. Peter So's laboratory. Kunal Tangri, an undergraduate in the Engelward

laboratory, assisted in preparation of samples for flow cytometry. Duanduan Ma of the BioMicro Center performed calculations of Spearmann correlation coefficients. We also thank Glenn Paradis for training and use of the Koch Institute Flow Cytometry Core.

4.8 References

1. Gupta, P.K., et al., *High frequency in vivo loss of heterozygosity is primarily a consequence of mitotic recombination.* Cancer Res, 1997. **57**(6): p. 1188-93.
2. Bishop, A.J. and R.H. Schiestl, *Homologous recombination as a mechanism of carcinogenesis.* Biochim Biophys Acta, 2001. **1471**(3): p. M109-21.
3. Kolomietz, E., et al., *The role of Alu repeat clusters as mediators of recurrent chromosomal aberrations in tumors.* Genes Chromosomes Cancer, 2002. **35**(2): p. 97-112.
4. Ohshima, K., et al., *Whole-genome screening indicates a possible burst of formation of processed pseudogenes and Alu repeats by particular L1 subfamilies in ancestral primates.* Genome Biol, 2003. **4**(11): p. R74.
5. de Koning, A.P., et al., *Repetitive elements may comprise over two-thirds of the human genome.* PLoS Genet, 2011. **7**(12): p. e1002384.
6. Furmaga, W.B., et al., *Alu profiling of primary and metastatic nonsmall cell lung cancer.* Exp Mol Pathol, 2003. **74**(3): p. 224-9.
7. Gupta, P.K., et al., *Loss of heterozygosity analysis in a human fibrosarcoma cell line.* Cytogenet Cell Genet, 1997. **76**(3-4): p. 214-8.
8. Pal, J., et al., *Genomic evolution in Barrett's adenocarcinoma cells: critical roles of elevated hsRAD51, homologous recombination and Alu sequences in the genome.* Oncogene, 2011. **30**(33): p. 3585-98.
9. Strout, M.P., et al., *The partial tandem duplication of ALL1 (MLL) is consistently generated by Alu-mediated homologous recombination in acute myeloid leukemia.* Proc Natl Acad Sci U S A, 1998. **95**(5): p. 2390-5.
10. Roy, R., J. Chun, and S.N. Powell, *BRCA1 and BRCA2: different roles in a common pathway of genome protection.* Nat Rev Cancer, 2012. **12**(1): p. 68-78.
11. Gu, W., F. Zhang, and J.R. Lupski, *Mechanisms for human genomic rearrangements.* Pathogenetics, 2008. **1**(1): p. 4.
12. Jacobs, A.L. and P. Schar, *DNA glycosylases: in DNA repair and beyond.* Chromosoma, 2012. **121**(1): p. 1-20.
13. Meira, L.B., et al., *Aag-initiated base excision repair drives alkylation-induced retinal degeneration in mice.* Proc Natl Acad Sci U S A, 2009. **106**(3): p. 888-93.
14. Calvo, J.A., et al., *Aag DNA glycosylase promotes alkylation-induced tissue damage mediated by Parp1.* PLoS Genet, 2013. **9**(4): p. e1003413.
15. Kiraly, O., et al., *DNA glycosylase activity and cell proliferation are key factors in modulating homologous recombination in vivo.* Carcinogenesis, 2014. **35**(11): p. 2495-502.
16. Calvo, J.A., et al., *Parp1 protects against Aag-dependent alkylation-induced nephrotoxicity in a sex-dependent manner.* Oncotarget, 2016. **7**(29): p. 44950-44965.
17. Allocca, M., et al., *PARP inhibitors protect against sex- and AAG-dependent alkylation-induced neural degeneration.* Oncotarget, 2017. **8**(40): p. 68707-68720.
18. Neugarten, J., A. Acharya, and S.R. Silbiger, *Effect of gender on the progression of nondiabetic renal disease: a meta-analysis.* J Am Soc Nephrol, 2000. **11**(2): p. 319-29.
19. Hutchens, M.P., et al., *Estrogen is renoprotective via a nonreceptor-dependent mechanism after cardiac arrest in vivo.* Anesthesiology, 2010. **112**(2): p. 395-405.
20. Tanaka, R., et al., *Protective effect of 17beta-estradiol on ischemic acute kidney injury through the renal sympathetic nervous system.* Eur J Pharmacol, 2012. **683**(1-3): p. 270-5.

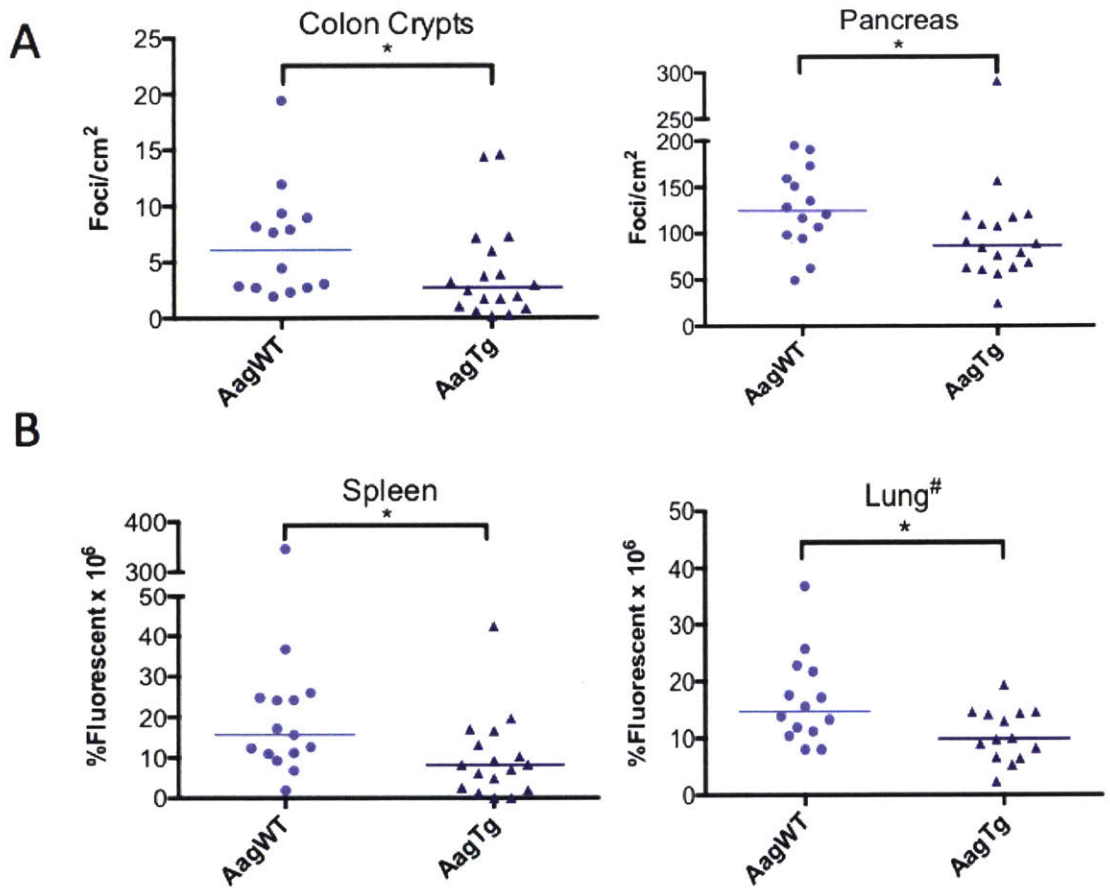

Figure 4-1. AagTg animals accumulate fewer recombinant cells than WT. (A) AagTg animals accumulate fewer recombinant foci than WT in colon crypts and pancreas. (B) AagTg animals accumulate a smaller proportion of recombinant cells than WT in the spleen and lung. Bar indicates median. #Outliers removed (see materials and methods). Mann-Whitney *U*-test, $*p < 0.05$.

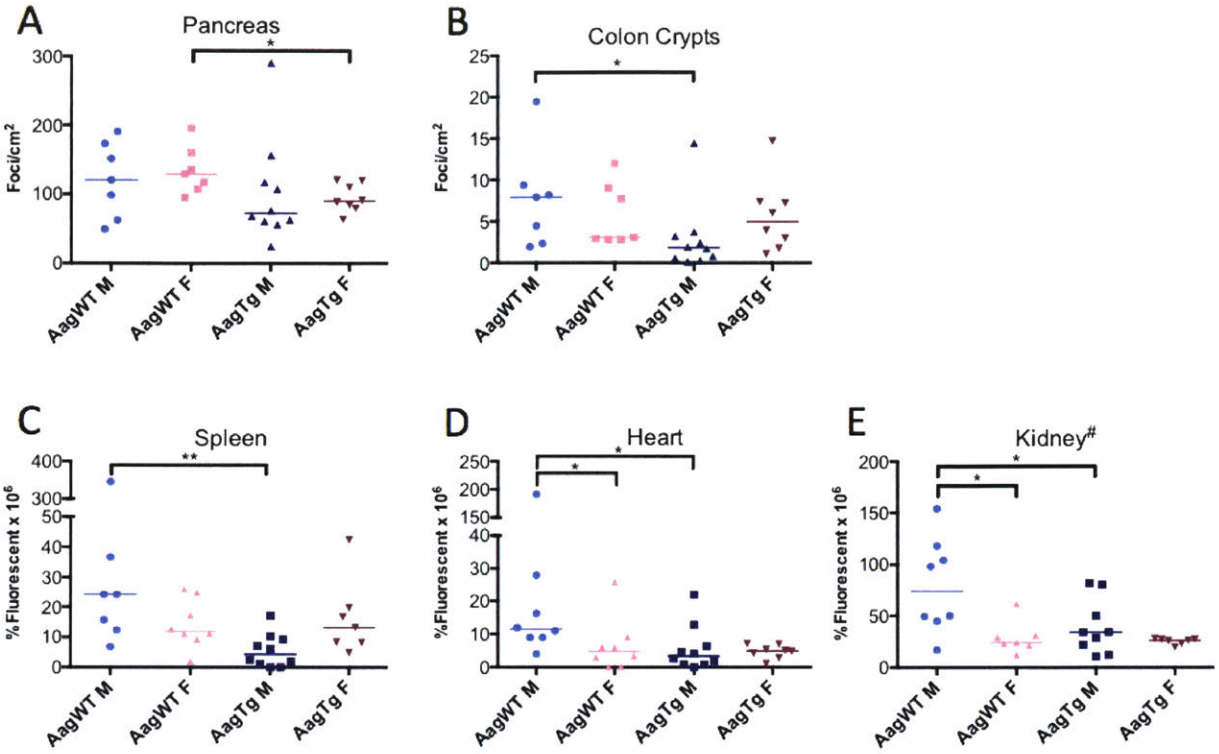

Figure 4-2. Sex-dependent differences in recombinant cell accumulation in the (A) pancreas, (B) colon crypts, (C) spleen, (D) heart, and (E) kidney. Data are the same as in Figure 4.1 but plotted differently. Bar indicates median. #Outliers removed (see materials and methods). Mann-Whitney *U*-test, $*p < 0.05$.

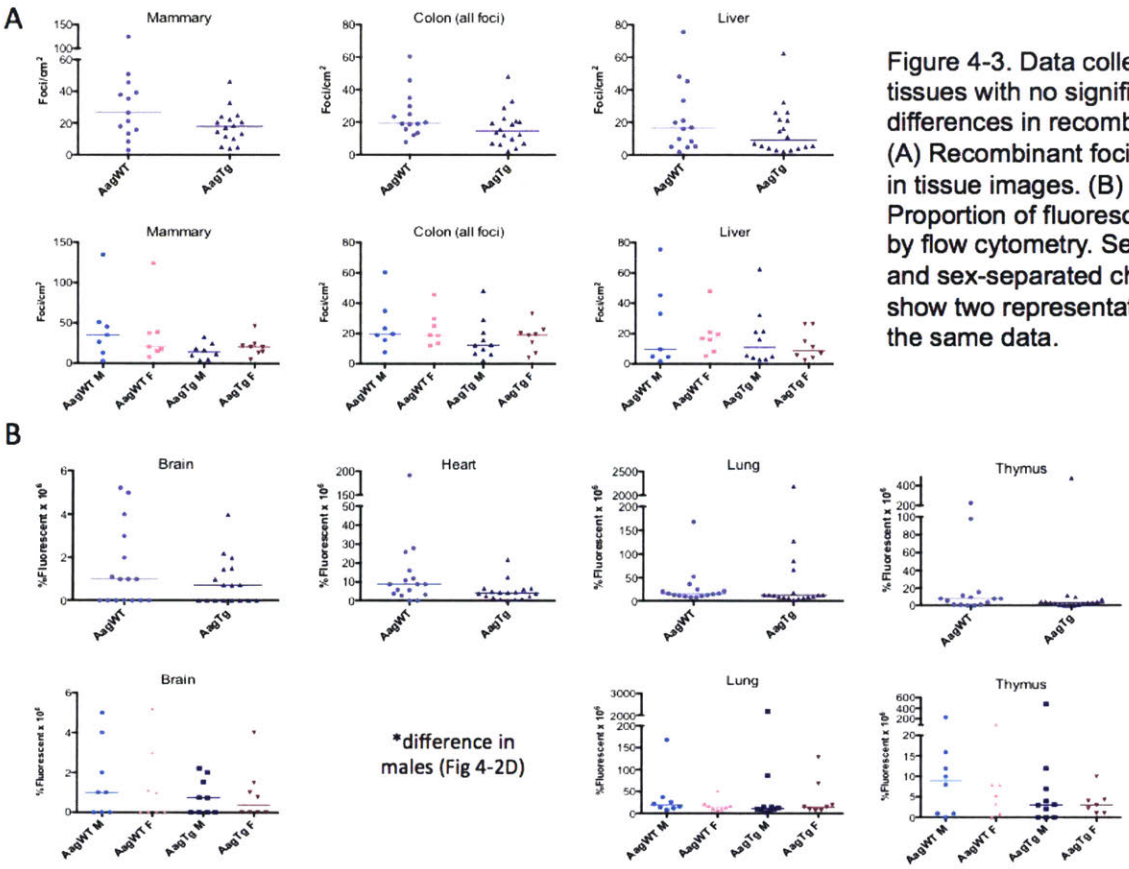

Figure 4-3. Data collected for tissues with no significant differences in recombination. (A) Recombinant foci observed in tissue images. (B) Proportion of fluorescent cells by flow cytometry. Sex-pooled and sex-separated charts show two representations of the same data.

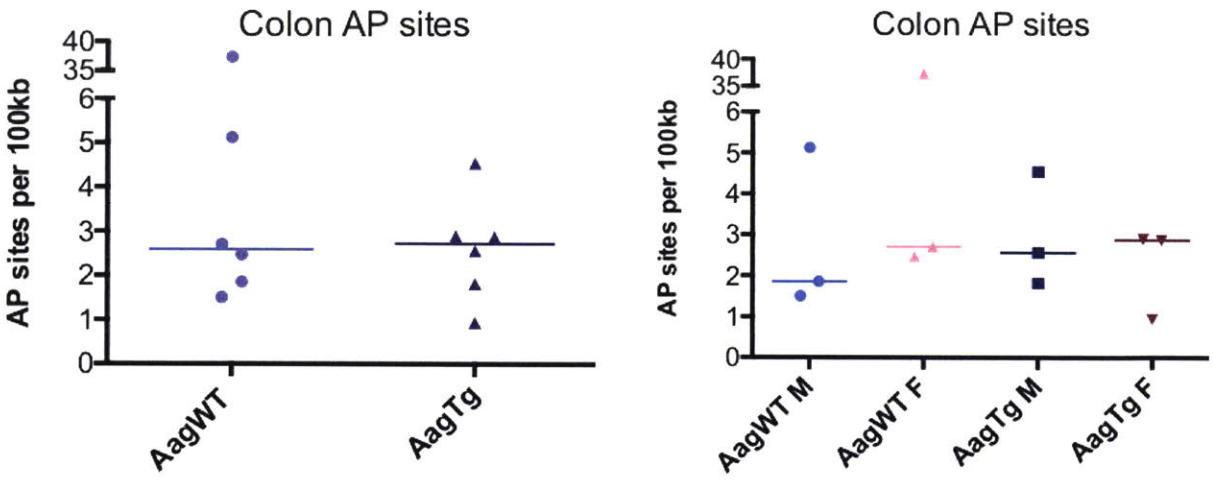

Figure 4-4. Abasic sites in colon DNA. Sex-pooled and sex-separated charts show two representations of the same data.

A

Correlation Coefficients	Pancreas	Colon (All)	Colon (Crypt)	Liver	Mammary	Brain	Heart	Kidney	Lung	Spleen	Thymus
Pancreas	1	0.61	0.66	0.49	0.14	0.03	0.09	0.08	0.14	0.47	0.31
Colon (All)	0.61	1	0.9	0.55	0.28	0.17	0.23	0.05	0.23	0.43	0.29
Colon (Crypt)	0.66	0.9	1	0.47	0.19	0.18	0.3	0.02	0.28	0.54	0.28
Liver	0.49	0.55	0.47	1	0.25	0.29	0.12	0.05	0.09	0.28	0.35
Mammary	0.14	0.28	0.19	0.25	1	0.28	0.21	0.12	0.04	0.05	0.12
Brain	0.03	0.17	0.18	0.29	0.28	1	0.27	0.16	0.04	0.08	0.12
Heart	0.09	0.23	0.3	0.12	0.21	0.27	1	0.6	0.27	0.33	0.4
Kidney	0.08	0.05	0.02	0.05	0.12	0.16	0.6	1	0.09	0.13	0.36
Lung	0.14	0.23	0.28	0.09	0.04	0.04	0.27	0.09	1	0.44	0.14
Spleen	0.47	0.43	0.54	0.28	0.05	0.08	0.33	0.13	0.44	1	0.32
Thymus	0.31	0.29	0.28	0.35	0.12	0.12	0.4	0.36	0.14	0.32	1

B

P values	Pancreas	Colon (All)	Colon (Crypt)	Liver	Mammary	Brain	Heart	Kidney	Lung	Spleen	Thymus
Pancreas	0	0.0001	0	0.0035	0.4509	0.8853	0.6018	0.6526	0.4182	0.0079	0.0896
Colon (All)	0.0001	0	0	0.0007	0.1148	0.3387	0.1915	0.7849	0.183	0.0165	0.1013
Colon (Crypt)	0	0	0	0.0054	0.3004	0.3164	0.0884	0.9031	0.1132	0.0016	0.1203
Liver	0.0035	0.0007	0.0054	0	0.1667	0.0932	0.5091	0.7645	0.6043	0.1313	0.0492
Mammary	0.4509	0.1148	0.3004	0.1667	0	0.1085	0.2435	0.5065	0.8253	0.8108	0.5051
Brain	0.8853	0.3387	0.3164	0.0932	0.1085	0	0.116	0.3599	0.8055	0.6567	0.5254
Heart	0.6018	0.1915	0.0884	0.5091	0.2435	0.116	0	0.0002	0.1213	0.07	0.0243
Kidney	0.6526	0.7849	0.9031	0.7645	0.5065	0.3599	0.0002	0	0.6206	0.4883	0.0403
Lung	0.4182	0.183	0.1132	0.6043	0.8253	0.8055	0.1213	0.6206	0	0.0123	0.4612
Spleen	0.0079	0.0165	0.0016	0.1313	0.8108	0.6567	0.07	0.4883	0.0123	0	0.0799
Thymus	0.0896	0.1013	0.1203	0.0492	0.5051	0.5254	0.0243	0.0403	0.4612	0.0799	0

Figure 4-5. Spearmann correlation coefficients (A) and p-values (B).

Chapter 5

Conclusions and Future Work

The experiments comprising this thesis have revealed a number of notable insights regarding when and how mutations develop. We focused on intestinal inflammation since the relationship between colonic inflammation and cancer is well established and many models exist for studying different aspects of colon carcinogenesis. In addition to uncovering mutation patterns arising from inflammation and DNA damage in the intestine, we also demonstrated the utility of the RaDR mouse for detecting mutations in unexpected "off-target" tissues, providing a more comprehensive view of mutagenicity in whole organisms.

First, we studied the impact of inflammation on the promotion stage of cancer using the $Apc^{Min/+}$ mouse, which contain a cancer-initiating mutation in *Apc* and spontaneously develop intestinal tumors. By blocking inflammation with anti-TNF, we decreased tumor multiplicity as well as overall mutant burden. By exacerbating inflammation with DSS, we increased both tumors and overall mutant burden. In both cases, converted crypt foci were unchanged relative to control. Together, these studies show that inflammation does not contribute significantly to *de novo* sequence rearrangement mutations in colonic crypt stem cells, but it does increase the overall burden of mutant cells through elevated proliferation. The inflammation-associated increase in proliferation correlates with tumor incidence because every division provides cells another opportunity to acquire more potentially oncogenic mutations.

We also incorporated the variable of DNA damage into our studies of inflammation. Our first experiment combined both inflammation and DNA damage in one treatment by infecting $Rag2^{-/-}$ mice with *Helicobacter hepaticus*, a murine pathogen that causes DNA double strand

breaks (DSBs) with its cytolethal distending toxin (CDT) [1]. Initially, we were surprised to discover that this pathogenic infection did not increase mutations, and may have even decreased mutation frequency. Subsequent experiments treating $Apc^{Min/+}$ mice with AOM also showed a decrease in recombinant colon crypts. These similar patterns of decreased crypt foci under conditions of DNA damage, either DSBs from a bacterial toxin or methylation from a chemical carcinogen, lend support to Cairns' immortal strand hypothesis, which suggests that DNA damage induced in a somatic stem cell will cause the cell to preferentially undergo apoptosis rather than risk mutating [2]. Importantly, the immortal strand hypothesis also suggests that when a stem cell dies it is replaced by a dedifferentiated daughter cell [3], but our observations do not support that theory because if a RaDR mutant crypt stem cell were to die, all of its daughter cells necessarily also have the RaDR mutation and the frequency of recombinant crypts would be unchanged. More work is necessary to determine the mechanism of replacing crypt stem cells after apoptosis.

An unexpected and intriguing finding in the work described here is that of increased recombinant foci in $Rag2^{-/-}$ pancreata. Rag2 is thought to be a lymphoid-specific gene [4, 5] and has not been detected in the mouse pancreas [6], so the relationship between Rag2 and recombination in the pancreas is as yet inscrutable. We are preparing to collaborate with Dr. Bert van de Kooij of the Yaffe laboratory to query DSB repair in $Rag2^{-/-}$ cells. Given that *Rag2* is considered lymphoid-specific, any relationship between Rag2 and pancreatic DSB repair will be a novel finding.

Finally, the pattern of fewer recombinant cells in AagTg animals will provide the basis for many interesting studies regarding balance between Base Excision Repair (BER) and homologous recombination (HR). We had previously observed that $Aag^{-/-}$ animals accumulate

fewer recombinant foci compared to WT following treatment with the DNA alkylating agent methylnitrosourea (MNU) [7], and from this we formed our hypothesis that AagTg animals would have more BER intermediates and therefore more recombination events. Here, we show that unchallenged AagTg animals accumulate fewer sequence rearrangement mutations than WT, possibly by more efficient resolution of BER intermediates. This, along with the observation of sex-dependence in mutant cell accumulation, will provide important foundations for upcoming experiments treating *RaDR;Aag*$^{-/-}$, *RaDR;AagWT* and *RaDR;AagTg* with the environmental toxicant *N*-nitrosodimethylamine, a DNA methylating agent.

The work comprising this thesis has provided numerous novel insights to mutagenic recombination and will form the basis for many exciting further studies. Inflammation appears to increase the overall burden of mutant cells by increased proliferation, but we have not separated the variables of inflammation and proliferation to verify whether proliferation is the key to increasing mutant burden. DNA damage decreases the frequency of recombinant crypts, but more work is required to determine what exactly happens to colon stem cells following DNA damage. Studies into the relationship between Rag2 and pancreas DSB repair will provide novel insights to Rag2 activity and lineage specificity. Finally, the tissue- and sex-dependent patterns of decreased RaDR mutant cells in AagTg animals highlights the importance of further characterizing Aag activity across tissues and between sexes in preparation for treatment studies in *Aag*$^{-/-}$, *AagWT* and *AagTg* animals. This thesis presents numerous exciting findings about how organisms develop and accumulate mutations, and provides many opportunities for further discovery.

5.1 References

1. Young, V.B., et al., *In vitro and in vivo characterization of Helicobacter hepaticus cytolethal distending toxin mutants.* Infect Immun, 2004. **72**(5): p. 2521-7.
2. Cairns, J., *Cancer and the immortal strand hypothesis.* Genetics, 2006. **174**(3): p. 1069-72.
3. Cairns, J., *Somatic stem cells and the kinetics of mutagenesis and carcinogenesis.* Proc Natl Acad Sci U S A, 2002. **99**(16): p. 10567-70.
4. Schatz, D.G. and D. Baltimore, *Uncovering the V(D)J recombinase.* Cell, 2004. **116**(2 Suppl): p. S103-6, 2 p following S106.
5. Alt, F.W., et al., *Mechanisms of programmed DNA lesions and genomic instability in the immune system.* Cell, 2013. **152**(3): p. 417-29.
6. Atlas, H.P. *Rag2*. September 1, 2017]; Available from: https://www.proteinatlas.org/ENSG00000175097-RAG2/tissue.
7. Kiraly, O., et al., *DNA glycosylase activity and cell proliferation are key factors in modulating homologous recombination in vivo.* Carcinogenesis, 2014. **35**(11): p. 2495-502.